Synthesis and Characterization of Novel Functionalized Ordered Mesoporous Carbon (OMC) for Resorcinol and Sunset Yellow Removal

A Dissertation

Presented to the

Graduate Faculty of the

University of Louisiana at Lafayette

In Partial Fulfillment of the

Requirements for the Degree

Doctor of Philosophy

Zaki Uddin Ahmad

Spring 2019

ProQuest LLC.
789 East Eisenhower Parkway
P.O. Box 1346
Ann Arbor, MI 48106 – 1346

Synthesis and Characterization of Novel Functionalized Ordered Mesoporous Carbon (OMC) for Resorcinol and Sunset Yellow Removal

Zaki Uddin Ahmad

APPROVED:

Daniel Dianchen Gang, Chair Professor of Civil Engineering	Xiaoduan Sun Professor of Civil Engineering
Mohammad Jamal Khattak Professor of Civil Engineering	William M. Chirdon Associate Professor of Chemical Engineering
Qian Zhang Assistant Professor of Civil Engineering	Srinivasan Ambatipati Senior Chemical Engineer, DynaChem Research Center, LLC (Industry Mentor)
Mary Farmer-Kaiser Dean of the Graduate School	

To my mother:

Because of her I have received more than of my fair share of good fortune

Acknowledgements

First of all, the author would like to express his heartiest gratitude to Almighty Omnipotent God for His graciousness and unlimited kindness and whose blessings are always required for the completion of any good work. Then the author would like to express his humble gratitude to his academic supervisor and dissertation committee chair, Dr. Daniel Dianchen Gang, for his continuous guidance, precious constructive suggestions, encouragement, generous help, and unfailing enthusiasm at every research stage.

The author would like to acknowledge Dr. Xiaoduan Sun, Dr. Mohammad Jamal Khattak, Dr. William M. Chirdon, Dr. Qian Zhang, and Dr. Srinivasan Ambatipati for kindly accepting to be a member of his dissertation committee. The author will always be indebted to them for their guidance in completing this research study.

The author would like to express his gratitude to his previous research partner Bing Chao, who helped him in the beginning phase of research. The author owes a lot to his former group members Grant Adam Besse and Salman Sakib, who have always encouraged him in getting to the end of the tunnel. The author would like to extend special gratitude to Dr. Elman Bashar and Nusrat Jahan, who helped him to settle down in a new city like Lafayette. The author would like to convey special gratitude to Mr. Mark LeBlanc, who has always helped him set up laboratory instrument. Special thanks go to Monjurul Islam Rifat for all the mental support during tough times. Finally, the author would like to thank his current lab partner Qiyu Lian for his support with experimentation.

Special thanks to the family members and beloved ones whose support and unconditional love have always encouraged him to complete this dissertation.

Table of Contents

List of Tables

List of Figures

Chapter 1: Introduction

1.1 Introduction and Background

Rapidly increasing global population and their ever-growing demands are exerting pressure on the natural state of the environment and influencing harmony among environmental variables. Besides the rapid growth of the urban population, unplanned urbanization, industrialization, and agricultural activities, as well as the excessive use of chemicals, have contributed to break this harmony (Gupta, 2009). Water, one of the important elements of natural environment, has been irreversibly degraded for decades by various organic and inorganic contaminants threatening human health and other living organisms as many species are in the spiral of decline (Ceyhan and Baybas, 2001).

Phenols are generally considered to be one of the important organic pollutants discharged into the environment, causing unpleasant odor and taste for drinking water. These phenolic compounds are found in the effluents of various industries, such as oil refineries, petrochemical industries, coal coking operations, pharmaceuticals, resin manufacturing, plastics, paint, paper and pulp, and wood products (Kazemi et al., 2014; Mohammadi et al., 2015). Discharging phenolic compounds in the natural streams without further treatment may cause serious health risks to humans, animals, and aquatic ecosystems (Sun et al., 2015). In addition to this, the presence of phenol in natural waters can lead to the formation of chlorinated phenols during disinfection and oxidation processes (Huang et al., 2009). Phenols have been designated as priority pollutants by the US Environmental Protection Agency (USEPA) and the National Pollutant Release Inventory (NPRI) of Canada (Cordova Villegas et al., 2016). For example, EPA has set a standard permissible limit of 1 ppb in wastewater (USEPA, 1985). According to the Indian standard, phenol contents in drinking water cannot

exceed 2 ppb. The toxicity levels are usually in the range of 9,000-25,000 ppb for both humans and aquatic life (Ahmaruzzaman, 2008).

In addition to this, discharge of colored substances can cause aesthetic issues as well as detrimental effects to biological organisms and ecology (Rêgo et al., 2013). Numerous industries, such as rubber, textiles, cosmetics, plastics, leather, paper, and printing, are the major sources of industrial wastewaters. It has been estimated that each step of textile operation can produce approximately 40 to 65 L kg^{-1} of the product (Mezohegyi et al., 2012). The presence of dyes in textile wastewater is an environmental problem since these dyes are stable to light, heat, and oxidizing agents and are usually non-biodegradable in nature (Kono, 2015). Some of these dyes are mutagenic and carcinogenic, which is the key concern of wastewater treatment process. Further, some of these dyes are xenobiotic in nature and aerobically recalcitrant to biodegradation (Gupta et al., 2013).

Selecting an appropriate method to eradicate different pollutants is essential to remove pollutants and improve the quality of treated water. Different treatment methods have been utilized to remove pollutants from wastewater, which include ion exchange, coagulation-flocculation, chemical precipitation, electrochemical reaction, reverse osmosis, membrane filtration (Vakili et al., 2014). There are several shortcomings associated with these methods, such as high initial cost of installation and operation, generation of excess sludge and subsequent disposal, and low efficiency, which make them inappropriate for small scale industries (Kobya et al., 2005). Adsorption is the most preferred method over other techniques because it is rapid, convenient, and inscrutable to toxic contaminants. It also has low initial costs, producing nontoxic by-products and rather simple in terms of designing and operating the treatment unit (Alver and Metin, 2012).

Activated carbon has attracted much attention as an adsorbent for industrial wastewater treatment due to its high specific surface area, thermal resistance, and chemical affinity towards organic pollutants. But the dominance of micropores (< 2 nm) present in the pore structure limits accessibility of organic pollutants (Dong et al., 2012). Ordered Mesoporous Carbon (OMC), a relatively new member of the carbonaceous family, has attracted substantial attention because of its distinct attributes, such as high BET surface area, narrow pore size distribution, well defined ordered structure, large pore volume, and thermal stability (Ryoo et al., 1999). These special features have promoted research and development for the modification of OMCs with tunable pore sizes (Chao et al., 2017) and improved surface chemistry (Ren et al., 2016), making them a more suitable candidate for adsorption. Traditional nanocasting technique is employed for the synthesis of OMCs that employed the use of a silica template (Ryoo et al., 1999). For example, the successful synthesis of CMK-1, the first ordered mesoporous carbon, was reported by Ryoo et al. (1999) using MCM-48 (cubic *Ia3d*) as a silica template.

1.2 DMADV Approach to Research Study

Design for Six Sigma (DFSS) is a standardized procedure adopted to accomplish a project which is objectively focused on the improvement of an existing system by developing a new procedure. DFSS was applied employing DMADA methodology, which is a six sigma framework that concentrates primarily on the development of a new service, product, or process as opposed to modifying a previously existing one. DMADV stands for Define, Measure, Analyze, Design, and Verify. The five phases of DMADV implemented to establish the research framework are described below:

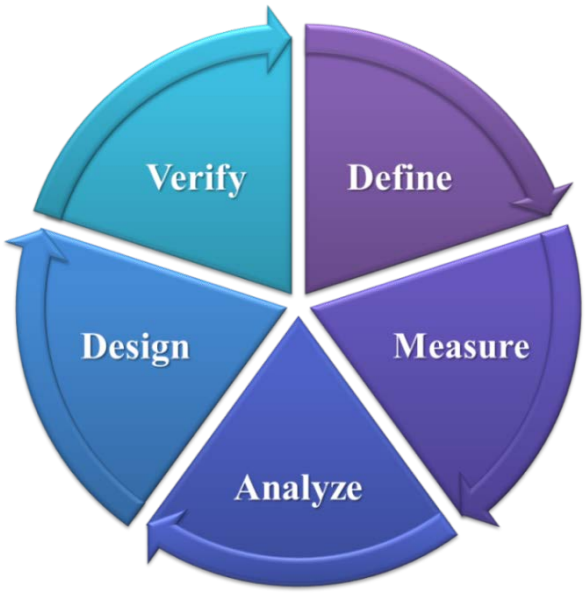

Figure 1.1. Five phases of DMADV process.

1.2.1 Define. The first step during DFSS procedure is to "define" the problem to identify the customer's need. The customer's most important needs are identified in relation to the final deliverable of the project in this stage. The goals of the study were determined based on the needs of the project. Activated carbon has attracted much attention as an adsorbent for the treatment of industrial wastewater. But traditional or commercially available activated carbon has several limitations, such as the large fraction of pores existing as micropore (< 2 nm) and wider pore size distribution. The dominance of micropores in the pore structure makes the large molecules inaccessible to the pore spaces, and subsequent slow adsorption kinetics are observed. All of these disadvantages cause limited adsorption capacity. The main goal of this research was to synthesize and characterize new functionalized ordered mesoporous carbon for alleviating resorcinol and sunset yellow through improved adsorption capacity. Ordered mesoporous carbon (OMC) has been identified as a potential adsorbent with distinct characteristics, such as high BET surface area, narrow pore size distribution, tunable pore size in the mesoporous range (2-50 nm), and

fast adsorption kinetics. All of these properties make OMC an ideal adsorbent for pollutants with large molecules. The main goals of this research initiative were based on the following hypothesis:

1.2.1.1 Hypothesis. The facile synthesis procedure for OMC with varying pore sizes in the range of 3-10 nm where MSU-H ordered mesoporous silica with two dimensional hexagonal structures was utilized as the mesoporous silica template and boric acid was utilized as the pore expansion chemical. Boric acid was co-infiltrated with the carbon precursor into the mesopores of silica. The phase separation of boron from the carbon-silica composite caused the pore expansion during the carbonization process (Lee et al., 2008). In another study carried out by Dai et al. (2009), synthesis of three-dimensional cubic OMCs with tunable pore size distributions employing KIT-6 with cubic *Ia3d* structure as the silica scaffold and boric acid as the pore expanding reagent was reported.

It has been reported that the incorporation of magnetic nanoparticles such as Fe, Ni, Mn, and Co will create specific binding sites whose binding force is favorable to the adsorption process (Phenrat et al., 2009). The interaction between the f-orbitals of Lanthanides and different functional groups can also assist the formation of complexes with organic compounds (Goscianska et al., 2015). Such relationships can be further exploited to synthesize new and innovative materials for abatement of emerging pollutants.

1.2.1.2 Objectives of the study. In order to achieve the goals set for the research study, the following objectives have been established:

1. Modification of ordered mesoporous carbon (OMC) using boric acid as the pore expanding reagent.

2. Introduction of rare earth metals onto the support surface of OMC, such as, cerium and neodymium to introduce surface functionality.
3. Characterize the textual and surface properties of pore size modified OMCs and chemically modified OMCs employing different techniques.
4. Characterize the adsorption performance of all these OMCs to identify the major adsorption mechanism (i.e. physical adsorption or chemisorption) and make comparison with other reported materials in the literature.

1.2.2 Measure. The second step in this procedure is "measure," which focuses on the collection and recording of available data. In this step, CTQs (characteristics that are critical to quality) are identified, which include the critical design parameters, developing the scorecards that will evaluate the design components, and assessment of production process capability and product capability. In this research study, "measure" refers to the "literature review" where the researcher conducted an extensive literature survey by going through all the works published online to make sure that the work was not recurring or being repeated. This stage was even more important for the researcher to collect all the information to have a basic understanding of theories and their applications. This step even helped the researcher to identify those characteristic techniques which can be employed to explore a new insight into the adsorption mechanism.

1.2.3 Analyze. The third step of DMADV is the "analyze" phase that goes hand-in-hand with the measure phase. In this step, the process's inputs are identified that are likely to affect the process outputs or the final products or deliverables. In this step, processes that will be implemented are finalized. In this step of the study, different techniques were identified to characterize the synthesized materials based on the literature survey, such as Nitrogen

Adsorption-Desorption Isotherm, Scanning Electron Microscope (SEM), Transmission Electron Microscope (TEM), Energy Dispersive X-ray Spectroscopy (EDS), Fourier Transform Infrared (FT-IR) Spectra, and X-ray Spectroscopy (XPS). All of these techniques were implemented for to comprehensively characterize materials. The batch adsorption experiment was finalized to measure the adsorption capacity. All the adsorption data were fitted to the available models to reach concluding remarks related to governing adsorption mechanism.

1.2.4 Design. The fourth step of DMADV is "design," which implements the solutions decided in the "analyze" step to satisfy customer needs and specifications. The design step uses newly developed processes to produce the customer's deliverables and makes additional adjustments to the process. The actual success or failure of the study is determined during the stage. In this step of research, actual experimentations were performed and results were collected as the design step.

1.2.5 Verify. The final step of DMADV is the "verification" of the implemented process or steps. This step checks the design to make sure that the process was set up according to plan and conducts trials of the processes to make sure that the results are repetitive. The process is always monitored in this stage. In this step of research, verification was done by comparing the obtained results with the results available in the literature. In the verification stage, the hypothesis of the study was verified through the results of the design step.

Following the DMADV approach, all the research work was conducted and presented in paper format in the following three chapters.

Chapter 2: Adsorptive Removal of Resorcinol on a Novel Ordered Mesoporous Carbon (OMC) Employing COK-19 Silica Scaffold: Kinetics and Equilibrium Study

This work has been published as:

Ahmad, Z.U., Lian, Q., Zappi, M.E., Buchireddy, P.R., Gang, D.D., 2019. "Adsorptive removal of resorcinol on a novel ordered mesoporous carbon (OMC) employing COK-19 silica scaffold: Kinetics and equilibrium study", *Journal of Environmental Sciences*, 75, 307–317. https://doi.org/10.1016/j.jes.2018.04.014.

Abstract

Phenolic compounds and their derivatives have been found in industrial wastewater which poses threats to the natural environment. Ordered mesoporous carbon (OMC) has been identified as an ideal adsorbent possessing high specific surface area and large pore volume to alleviate these pollutants. A novel ordered mesoporous carbon was prepared using COK-19 template with the cubic *Fm3m* structure for the first time. Ordered mesoporous silica COK-19 was synthesized and reported in 2015. Sucrose as the carbon precursor was impregnated into the mesopores of silica and converted to carbon through carbonization process using sulfuric acid as a catalyst. Ordered mesoporous carbon was obtained after the removal of silica framework using hydrofluoric acid. Boric acid was employed for the preparation of OMCs with tunable pore sizes in the range of 6.9-16.6 nm. Several characterization techniques such as nitrogen adsorption-desorption isotherms, transmission electron microscope (TEM), Fourier transform infrared (FT-IR) spectroscopy, Boehm titration and elemental analysis were employed to characterize the OMCs. The pore size analysis and TEM images confirmed that OMC has replicated the mesostructure of the COK-19. Results obtained from adsorption kinetics and isotherms suggest that the Pseudo-second-order model and Langmuir isotherm well described the experimental data.

2.1 Introduction

Since the emergence of modern civilization, the development processes have been stimulated in all branches of industries to meet the growing demands of humans which have left its mark on the natural state of environment. Phenolic compounds and their derivatives are major water pollutants because of their wide usage in industry and agriculture (Mangrulkar et al., 2008; Kumar et al., 2011; Lin and Juang, 2009). These phenolic

compounds are regarded as carcinogenic even at low concentrations (Din et al., 2009; Aghav et al., 2011; Gattrell et al., 1990). For example, Resorcinol (also known as *1,3-dihydroxybenzene*) has been found in industrial effluents such as textile, paper and pulp, petrochemical, petroleum refinery, rubber, pharmaceutical, cosmetics etc. Effluent produced from synthetic coal fuel conversion process contains resorcinol and catechol at a concentration ranging from 1 to 1000 mg/L (Kumar et al., 2003). These compounds are considered as the primary pollutants in the wastewater owing to their high toxicity, higher oxygen demand and low biodegradability (Agarwal and Rani, 2017). The United States Environmental Protection Agency has listed phenolic compounds and their derivatives under priority pollutants list in the Clean Water Act (Duan et al., 2014). As a result, separation of these compounds from water or wastewater has attracted substantial attention.

Diversified technologies, such as coagulation and precipitation, photocatalytic degradation, chemical oxidation, biodegradation, ion exchange and solid-liquid separation technique or adsorption, have been developed and tested over the past few decades for the wastewater treatment. Adsorption has been widely used for the separation of organic pollutants from the aqueous solution owing to the simplicity of design, reliability and convenience of this method (Mukherjee et al., 2007). Numerous studies have been dedicated to the development of adsorption process based on carbonaceous materials. Activated carbon has attracted much attention as an adsorbent for treatment of industrial wastewater due to its high BET surface area, thermal resistance and chemical affinity towards organic pollutants. But the dominance of micropores (< 2 nm) present in the pore structure limits accessibility of organic pollutants with large molecular structure to activated carbon (Zhuang et al., 2009).

In recent years, ordered mesoporous carbon (OMC) has been of vast interest with uniform pore size, higher specific surface area, and large pore volume (Joo et al., 2001; Ryoo et al., 1999; Darmstadt et al., 2002; Kim et al., 2005; Fuertes and Sonia, 2004) since the successful synthesis of OMC was reported (Ryoo et al., 1999). Research development has been achieved in the preparation of OMC with graphitic framework (Kim et al., 2004), pore structures (Joo et al., 2001) and modified surface chemistry (Ren et al., 2016). OMC has been employed for various applications such as adsorption (Guo et al., 2013; Goscianska et al., 2014, 2015, 2017), catalyst support (Chai et al., 2004; Joo et al., 2006; Shon et al., 2016; Xu et al., 2014; Goscianska et al., 2018), hydrogen storage (Fang et al., 2006; Xia et al., 2007), dispersion of non-ionic surfactant (Goscianska and Olejnik, 2018) and CO_2 capture (Liu et al., 2011; Katsoulidis and Kanatzidis, 2011).

Nanocasting technique is traditionally used to fabricate ordered mesoporous carbons (Ryoo et al., 1999, 2001). The hard template method involves the impregnation of an appropriate carbon precursor into the mesopores of silica scaffold followed by thermal polymerization, carbonization, and subsequent removal of silica framework by hydrofluoric acid (HF) or sodium hydroxide (NaOH) (Liang et al., 2008). Since the emergence of numerous mesoporous silica materials, ordered mesoporous carbons with various pore structures and narrow pore size distributions have been synthesized by replicating the structure of mesoporous silica. CMK-1, the first ordered mesoporous carbon, was synthesized by Ryoo et al. (1999) using MCM-48 (cubic *Ia3d*) mesoporous silica as a hard template. After that, ordered mesoporous carbons were synthesized employing mesoporous silica with diverse symmetries, such as SBA-15 (Guo et al., 2013), MCM-48 and KIT-6 (Ryoo et al., 1999; Dai et al., 2009), FDU-12.

The structural characteristics of the OMC, such as the pore size and pore shape, were found to be dependent on the silica template. Distinct limitations exist in the pore size control of OMC materials employing mesoporous silica template which can be ascribed to difficult control of the properties of the silica scaffold (Sayari et al., 1997; Mokaya, 1999). The pore size control of OMC is still limited (Kresge et al., 1992; Lettow et al., 2000; Kim et al., 2001). The synthesis procedure of OMC materials with tunable pore sizes in the range of 2.2-3.3 nm using mesoporous silica template was reported (Lee et al., 2002).

Ordered mesoporous carbon materials possessing larger pore size and specific surface area can be applied in the adsorption process which involves larger molecules and fast mass transfer. Lee et al. (2008) reported the facial synthesis procedure for preparation of OMC materials with tunable pore sizes in the range of 3-10 nm where MSU-H mesoporous silica (2D hexagonal) was employed as the hard template and boric acid was utilized as the pore expanding agent. This method involves the co-infiltration of boric acid with the carbon precursor into the mesopores of silica template. The pore expansion is resulted due to the phase separation of boron from the precursor-silica composite containing sucrose and boric acid. This phase separation takes place during the carbonization process (Lee et al., 2008). In another study, Dai et al. (2009) reported the synthesis of three-dimensional cubic OMCs with tunable pore size distributions employing KIT-6 (cubic *Ia3d*) as the silica scaffold and boric acid as the pore expanding reagent.

The aforementioned rational synthesis pathway was employed in this study to prepare ordered mesoporous carbon with tunable pore sizes using COK-19 as silica template. A new highly ordered mesoporous silica COK-19 was synthesized and reported in 2015 with cubic *Fm3m* structure (Kerkhofs et al., 2015). The aim of this study was to synthesize ordered

mesoporous carbon using COK-19 template modified with boric acid and examine its effectiveness in resorcinol removal from aqueous solution. To the best of our knowledge, this is the first study describing the synthesis of ordered mesoporous carbon employing COK-19 as silica scaffold. **Figure 2.1** illustrates the step by step fabrication process of OMC. The adsorption capacity was studied using batch adsorption method and fitted to Langmuir and Freundlich Adsorption Models. The adsorption kinetics was also studied and fitted to Pseudo-first order kinetic model and Pseudo-second order kinetic model.

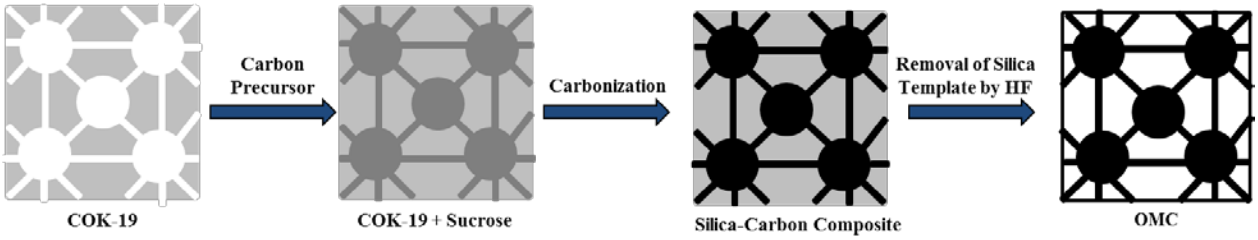

Figure 2.1. Step by step synthesis of OMC.

2.2 Materials and Methods

2.2.1 Chemicals. Triblock copolymer Pluronic F-127 (MW =12600, EO_{106}-PO_{70}-EO_{106}, EO = ethylene oxide, PO = propylene oxide), citric acid monohydrate (ACS reagent, ≥99%), trisodium citrate dihydrate and sodium silicate solution (reagent grade, SiO_2 26.5%) were purchased from Sigma Aldrich. Sucrose (ACS reagent, ≥99.0%), boric acid (ACS reagent, ≥99.5%), sulfuric acid (ACS reagent, 98%) hydrofluoric acid (ACS reagent, 48%) were also purchased from Sigma Aldrich. All chemicals were used as received without any further purification.

2.2.2 Fabrication of COK-19 silica template. The COK-19 was synthesized using Pluronic F-127 triblock copolymer surfactant and sodium silicate solution as the silica source as reported in the literature (Kerkhofs et al., 2015). In a typical synthesis, 2.6 g of Pluronic F-127 was dissolved in 107.5 g of deionized water. To this solution, 3.7 g of citric acid

monohydrate and 2.55 g of trisodium citrate dihydrate were added. This buffered surfactant solution was stirred overnight to dissolve all the components. After that, 10.4 g of sodium silicate solution (26.5% SiO_2) diluted in 30 g of water was added to the buffered F-127 solution at room temperature and the solution was stirred vigorously for 5 min. Precipitation of white solid occurred instantaneously and the milky white suspension was kept under quiescent conditions for aging for 24 hr at 70°C in a constant temperature water bath (Premiere HH-4). Afterwards, the white precipitation was filtered off, washed with deionized water (4,000 mL) and dried in the oven at 105°C overnight. After drying, the resultant solid was calcined at 350°C for 24 hr using a heating rate of 0.5°C/min in a box furnace (Lindberg/Blue M Moldatherm Box Furnace Thermo Scientific). The white COK-19 silica template was stored in the desiccator for the preparation of OMC.

2.2.3 Fabrication of OMCs. COK-19 and sucrose were used as the template and the carbon precursor, respectively. Various amount of boric acid was added to the carbon precursor keeping the amount of sucrose constant. The carbon replicas are designated as OMC-B-*a*, where B stands for boric acid and *a* stands for the molar ratio of sucrose to boric acid. In a typical synthesis of OMC-B-*2*, 0.54 g of boric acid (99.8% wt.), 1.50 g of sucrose (99.5% wt.) and 15 drops of H_2SO_4 were dissolved in 15 mL of distilled water. After adding 2 g of COK-19, the mixture was heated at 100°C for 6 hr and subsequently at 160°C for another 12 hr. The resulting composite was impregnated again with an aqueous solution of 0.18 g of boric acid, 0.50 g of sucrose, 10 drops of H_2SO_4 and 10 mL of distilled water. Afterwards, the mixture was heated at 100°C for 6 hr and 160°C for another 12 hr. The composite was carbonized at 700°C for 8 hr under nitrogen flow. Finally, the material was

obtained by the removal of silica template using 48% HF solution at room temperature. The obtained material was labeled as OMC-B-2.

2.2.4 Characterization. Nitrogen sorption isotherms were recorded on Micromeritics ASAP 2020 (Accelerated Surface Area and Porosimetry System). Specific surface areas of the samples were calculated using the BET (Brunauer-Emmett-Teller) Equation, while pore size distribution (PSD) curves were calculated by the BJH (Barrett-Joyner-Halenda) Method using the adsorption branch. Prior to measurement, OMC was degassed at 300°C for 6 hr under reduced pressure. The total pore volume was obtained from the amount adsorbed at a relative pressure (P/P_0) of 0.99, where P and P_0 are equilibrium and saturation pressure of adsorbate.

TEM images were obtained using a Hitachi 7600 Transmission Electron Microscope (Hitachi America Ltd., Tarrytown, New York). The acceleration voltage used was 100 kV. The samples were prepared by dispersing large number of particles in ethanol with an ultrasonic bath for 45 min and a few drops of the resulting suspension were placed on a 400 mesh Cu grid.

Fourier transform infrared (FT-IR) spectra was obtained in a transmission mode from KBr pellets at room temperature on a Jasco 4700 spectrometer with a resolution of 4 cm^{-1}, using 32 scans per spectrum in the region of 400-4000 cm^{-1}. The mass ratio of sample to KBr was kept constant at 1:100.

Element composition analysis was obtained using Elementar vario MICRO Cube CHNS elemental analyzer. Sulfanilic acid was used as a standard for reference. Combustion and reduction tube temperatures were set at 1150°C and 850°C, respectively. TCD-Detector temperature was maintained at 60°C and the flow of helium to the detector was 200 mL/min.

The content of oxygen containing functional groups on the surface of mesoporous carbon was determined by the Boehm method (Boehm, 1994). Different bases such as $NaHCO_3$, Na_2CO_3, and NaOH were used. 10 mg of OMCs were added to 40 mL of the 0.05 mol/L acid and 0.05 mol/L basic solutions in flask. The flasks were sealed and shaken for 24 hr at 250 rpm at room temperature of 25°C. The samples were filtered using 0.45 μm filter papers. Then 5 mL of the filtrate was transferred to 50 mL beaker using pipette. HCl and NaOH solutions with concentration of 0.05 mol/L were then used to neutralize the filtrate. The number of acidic functional groups was calculated following the assumption that NaOH neutralizes all acidic groups and HCl reacts with basic groups.

2.2.5 Batch adsorption study. Batch adsorption experiments were conducted to evaluate the adsorption capacity of resorcinol onto the OMCs. For that purpose, 100 mL of resorcinol solution with a concentration of 10 mg/L at pH value of 6.1 was placed in 250 mL conical flasks for both control (without OMC labeled as blank) and experimental (with OMC and adsorbate) conditions. All the samples were placed in an E24 incubator shaker (New Brunswick Scientific). The adsorption studies were conducted at room temperature of 25°C and the shaking speed was maintained at 275 rpm. After 24 hr, the conical flasks were removed from the shaker and the solution was filtered using 0.45 μm glass filter paper. The blank solution was used as a reference to establish the initial concentration for the solutions containing OMCs. The concentration of resorcinol was determined using a UV-visible spectrophotometer (Cary 50 Varian) set at a wavelength of 500 nm. The amount of resorcinol adsorbed by OMCs was determined by subtracting the final concentration from the initial concentration using the following formula:

$$\boldsymbol{Q_e = \frac{(C_o - C_e) \times V}{M}} \qquad \textbf{(2.1)}$$

Where, Q_e (mg/g) is the adsorption capacity of the adsorbent at equilibrium, C_0 (mg/L) is the initial concentration of resorcinol in the solution, C_e (mg/L) is the final concentration of resorcinol in the treated solution, V (L) is the volume of the solution taken, and M (g) is the weight of the adsorbent OMC. All the experiments were carried out in duplicates and the average values were reported.

2.2.6 Regeneration study. The regeneration potential of synthesized OMCs was evaluated following batch adsorption method (El-Naas et al., 2010). An amount of 0.10 g of spent OMC was placed in 100 mL of 95% ethanol and stirred for 2 hr. The regenerated OMC was washed with distilled water and dried in an oven at 105°C overnight. This procedure was repeated for four cycles. The adsorption capacity was calculated by the following formula:

$$\boldsymbol{Q_{r,i} = \frac{(C_{o,i} - C_{e,i}) \times V_i}{M_i}} \quad \textbf{(2.2)}$$

Where, Q_r (mg/g) is the adsorption capacity of regenerated OMC; the subscript i represents the regeneration cycle number; $C_{0,i}$ (mg/L) and $C_{e,i}$ (mg/L) are the initial and final concentration of resorcinol, respectively; V_i (L) is the volume of solution; and M_i (g) is the mass of OMC used in that cycle. The regeneration efficiency (%RE) of each cycle was calculated as follows:

$$\boldsymbol{RE = \frac{Q_r}{Q_e} \times 100\%} \quad \textbf{(2.3)}$$

Where, Q_e (mg/g) is the adsorption capacity of virgin OMC.

2.3 Results and Discussion

2.3.1 Adsorbent characterizations.

2.3.1.1 N_2 Adsorption-desorption isotherm and TEM image. The N_2 adsorption-desorption isotherms of COK-19 behave like representative type IV curves with a sharp capillary condensation step in the relative pressure range of 0.65-0.75 as shown in **Figure**

2.2(a). The COK-19 capillary condensation step is located in the smaller relative pressure range that can be interpreted to narrow pore size distribution, which is confirmed by the pore size distribution as depicted in **Figure 2.2(b)**. Nitrogen adsorption-desorption isotherms and the corresponding pore size distributions of prepared OMCs are shown in **Figure 2.3**. All OMCs had type IV isotherms with H2 type hysteresis loops indicating the presence of mesopore framework with a uniform size as shown in **Figure 2.3(a)** (Thommes et al., 2015). With the increasing boron content, distinct steps appear in the adsorption-desorption curves at a relative pressure (P/P_0) of 0.45 to 0.95. The sharp capillary condensation step occurs at a relative pressure of $P/P_0 = 0.65$ due to rapid nitrogen adsorption within the mesopores of OMC-B-0. The gradual shifting of the position of the sharp step in the isotherm to higher relative pressure can be attributed to increased boron content. This phenomenon indicates that the pore size increases in systematic manner depicting the effects of boron content which was in line with the results obtained from pore size distribution curves as shown in **Figure 2.3(b)**. Similar observations were reported in literature (Lee et al., 2008; Chao et al., 2017).

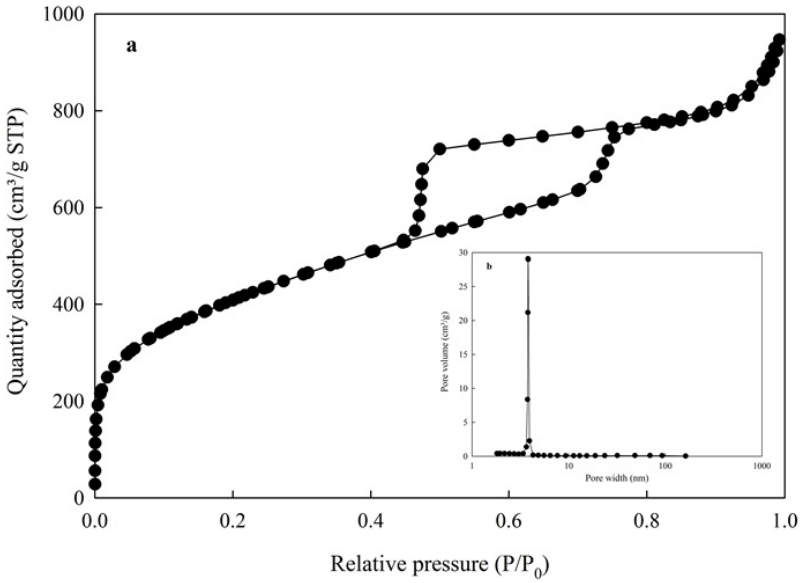

Figure 2.2. (a) N_2 adsorption-desorption isotherm of COK-19 (b) Corresponding pore size distribution.

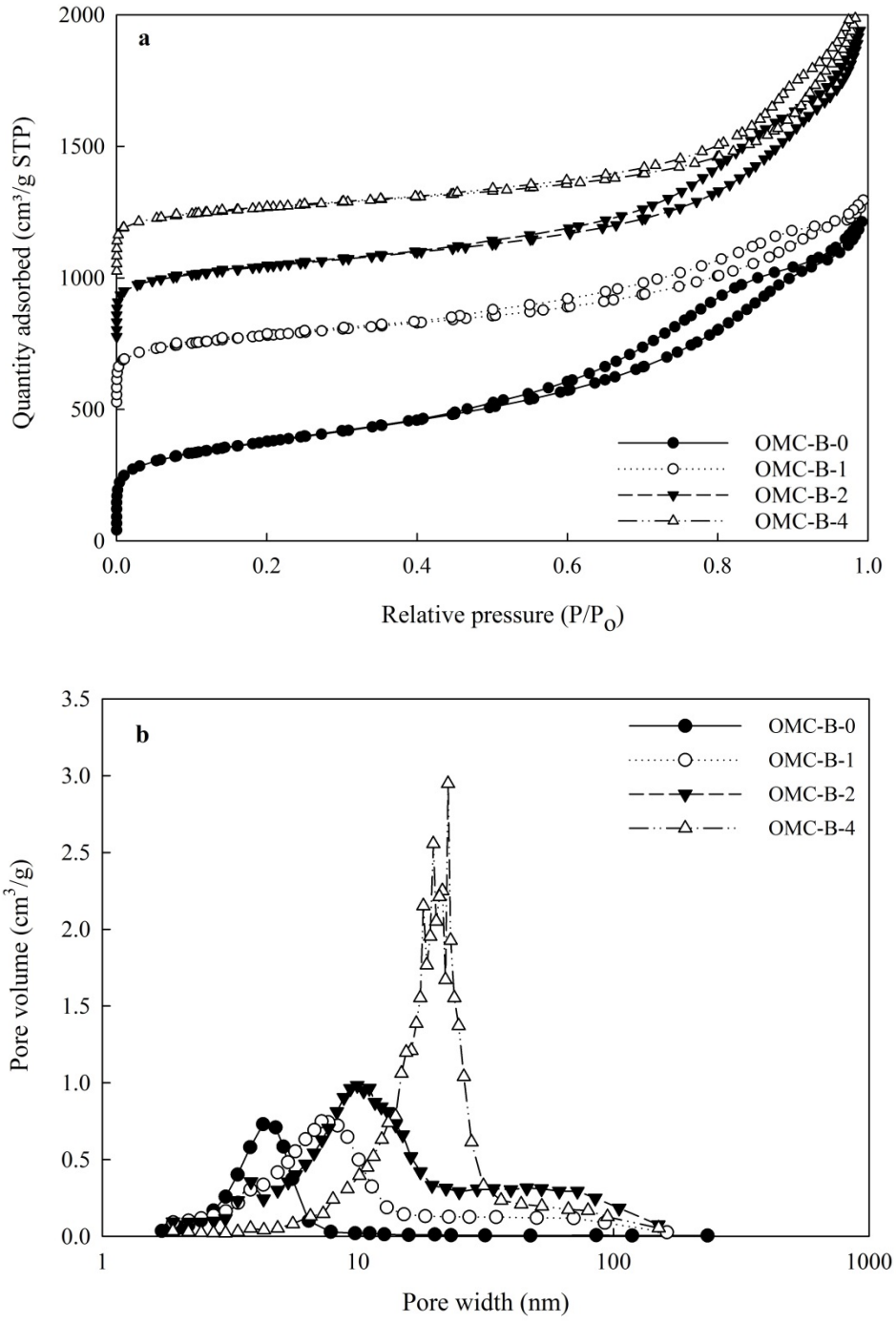

Figure 2.3. (a) N_2 adsorption-desorption isotherm of OMCs. The sorption isotherms for the OMC-B-1, OMC-B-2, and OMC-B-4 have been vertically shifted by 500, 750, and 1000 cm^3/g, respectively and (b) their corresponding pore size distribution.

The detailed textual parameters of the COK-19 and OMCs are summarized in **Table 2.1**. These data confirmed the positive effects of boric acid addition for pore enlargement. As the molar ratio of boric acid to sucrose gradually increased from 0 to 4, the pore sizes increased from 6.9 to 16.6 nm and the pore volumes also increased from 1.71 to 1.98 cm^3/g. All the pore size distribution curves showed the gradual shifting of average diameter from 6.9 nm to 7.1, 10.3, 16.6 nm without significant loss of mesostructural order. OMC-B-4 demonstrated a relatively wider pore size distribution curve centered around 16.6 nm, which may be ascribed to structural collapse due to inadequate framework support (Dai et al., 2009).

Table 2.1. Textual parameters of COK-19 and OMC-B-*a*.

Sample	BET surface area (m^2/g)	Average pore size (nm)	Total pore volume (cm^3/g)
COK-19	1481.15 ± 56	6.1 ± 0.02	1.14 ± 0.02
OMC-B-0	1014.3 ± 26	6.9 ± 0.2	1.71 ± 0.01
OMC-B-1	1310.96 ± 124	7.1 ± 0.2	1.78 ± 0.01
OMC-B-2	1126.35 ± 69	10.3 ± 0.2	1.82 ± 0.12
OMC-B-4	1029.35 ± 42	16.6 ± 0.3	1.98 ± 0.05

Figure 2.4 shows the TEM images of COK-19 and OMC-B-*a* materials. All the images reveal an ordered arrangement of mesopores. For OMC-B-4, the carbon rods were small in diameter to support the structural framework of OMC resulting in breakdown of pores and consequent decrease of specific surface area (Dai et al., 2009). The OMC-B-*a* materials synthesized with the addition of boric acid have a higher tendency to structural breakdown compared to the OMC prepared with the no addition of boric acid. The pore collapse can be attributed to insufficient support provided by the graphitic framework. But OMC-B-1 and OMC-B-2 showed ordered structure, except for OMC-B-4.

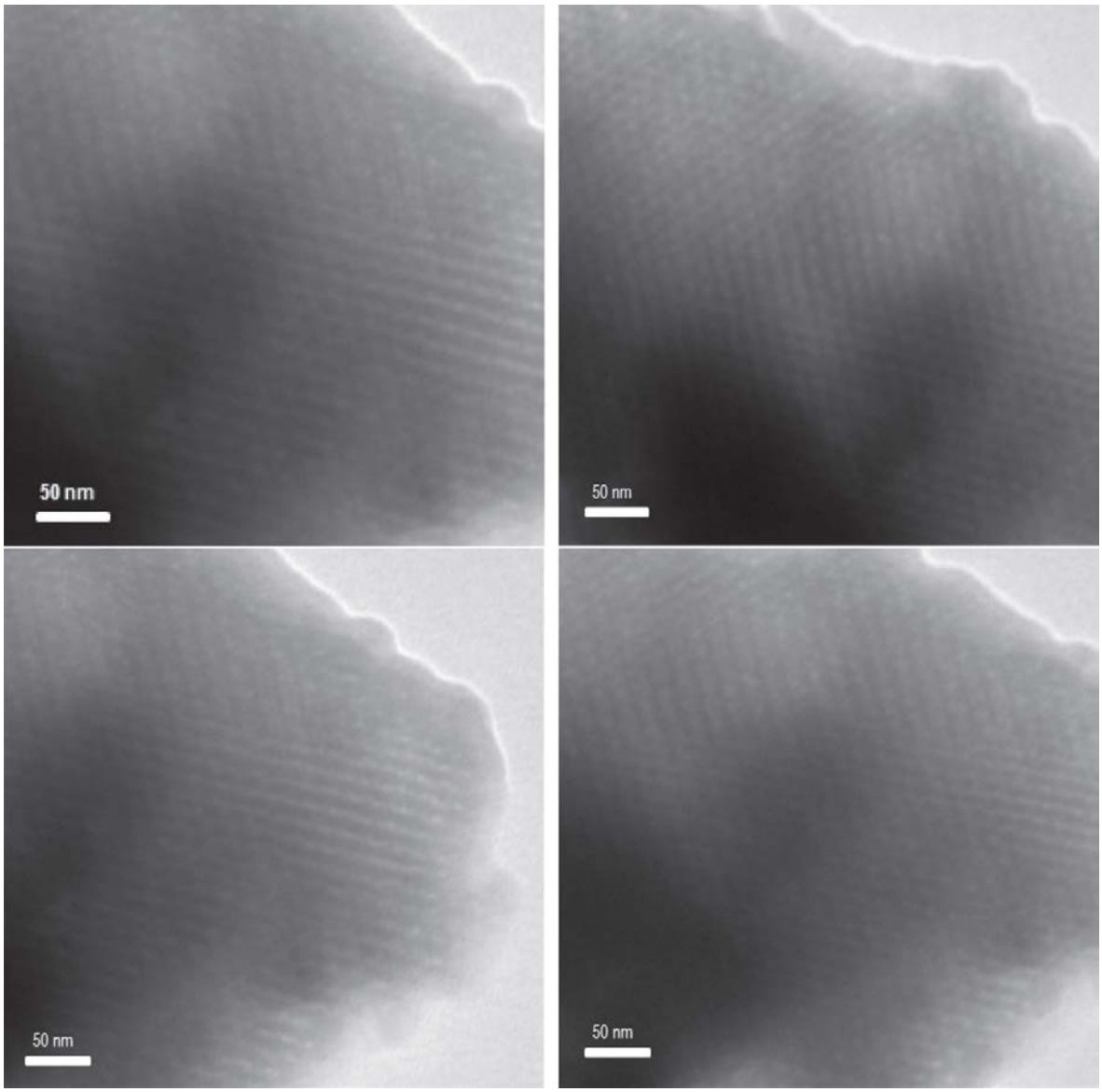

Figure 2.4. Transmission electron microscope (TEM) images of (a) COK-19 (b) OMC-B-0 (c) OMC-B-1 (d) OMC-B-2.

2.3.1.2 FT-IR analysis. To identify the functional groups present on the OMCs, FT-IR spectrum of the OMC-B-0, OMC-B-1, OMC-B-2, and OMC-B-4 were obtained. **Figure 2.5** shows the FT-IR spectra of the prepared OMCs. Results obtained from FT-IR analysis reveal that the addition of boric acid did not change the type of functional groups present on the OMCs. The peaks observed around 3438-3691 cm^{-1} could be assigned to –OH stretching because these groups usually appear as a very wide and strong band for –OH stretching (Shen et al., 2008). The peaks observed around 1510 cm^{-1} could be related to C=O stretching in the carboxylic groups (O–C=O) (Guo et al., 2013; Shou et al., 2016). A peak observed at 2351 cm^{-1} could be ascribed to S–H functional group due to the presence of sulfuric acid that acted as a catalyst in the synthesis process. A peak observed at 1394 cm^{-1} could be associated to C–H group (Cansado et al., 2012; Swiatkowski et al., 2004). The small peak observed around 1624 cm^{-1} was attributed to C=C or carbonyl (C=O) groups (Wang et al., 2010).

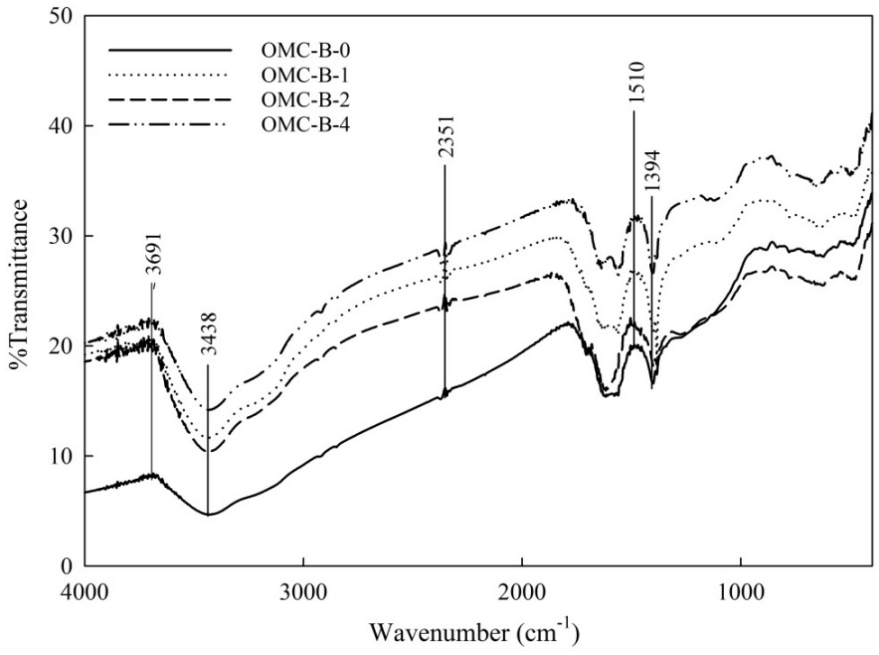

Figure 2.5. Fourier transform infrared (FT-IR) spectra of OMCs.

2.3.1.3 Elemental analysis and Boehm titration. Results of elemental analysis and Boehm titration of prepared OMCs are represented in **Table 2.2** and **Table 2.3,** respectively. The elemental analysis indicated that carbon was the dominant element, followed by oxygen. Sulfur present on the OMC could be due to the addition of sulfuric acid in the fabrication process. The carboxylic group increases from 0.64 to 0.92 mmol/g with the increment in the amount of boric acid. The results were consistent with the FT-IR analysis where the C=O stretching group was originated from the carboxylic function group. The peak observed for –OH functional group was from phenolic group. The increased oxygen content for prepared OMCs obtained from elemental analysis was also found to be consistent with the increased amount of carboxylic group as presented in **Table 2.2**. Kim et al. (2005) reported similar observations.

Table 2.2. Results of elemental analysis of OMC-B-0 to OMC-B-4.

Sample	%C	%O	%H	%N	%S
OMC-B-0	82.46±0.9	13.94±0.9	2.35±0.1	0.70±0.1	0.55±0.04
OMC-B-1	75.66±0.4	20.21±1.2	2.58±0.1	0.71±0.1	0.84±0.02
OMC-B-2	73.54±0.7	22.71±0.8	2.65±0.15	0.53±0.1	0.58±0.08
OMC-B-4	69.74±0.5	25.89±0.8	2.78±0.1	0.50±0.1	1.08±0.08

Table 2.3. Results of Boehm titration of OMC-B-0 to OMC-B-4.

Sample	Phenolic (mmol/g)	Lactonic (mmol/g)	Carboxylic (mmol/g)	Total acidic (mmol/g)
OMC-B-0	0.065±0.001	0.016±0.001	0.64±0.02	0.721
OMC-B-1	0.007±0.001	0.084±0.001	0.72±0.02	0.811
OMC-B-2	0.084±0.001	0.042±0.001	0.82±0.02	0.946
OMC-B-4	0.058±0.001	0.054±0.001	0.92±0.02	1.052

2.3.2 Adsorption behavior.

2.3.2.1 Adsorption kinetics. The time dependence of resorcinol adsorption onto ordered mesoporous carbon was investigated to determine the time required to reach equilibrium. Sufficient contact time is of importance for maximum resorcinol adsorption onto prepared OMCs. The results are shown in the **Figure 2.6**. From the **Figure 2.6**, it is evident that a contact time of 24 hr was required to achieve equilibrium for adsorption process. The analyzed data revealed that the initial rapid adsorption rate decreased as the adsorption process attained equilibrium. The higher concentration gradient between the adsorbent and the adsorbate in the solution, higher number of available adsorption sites on the adsorbent, strong affinity between adsorbent and adsorbate and greater driving force for mass transfer can be attributed for this rapid initial adsorption (Kumar et al., 2003; Konggidinata et al., 2017a).

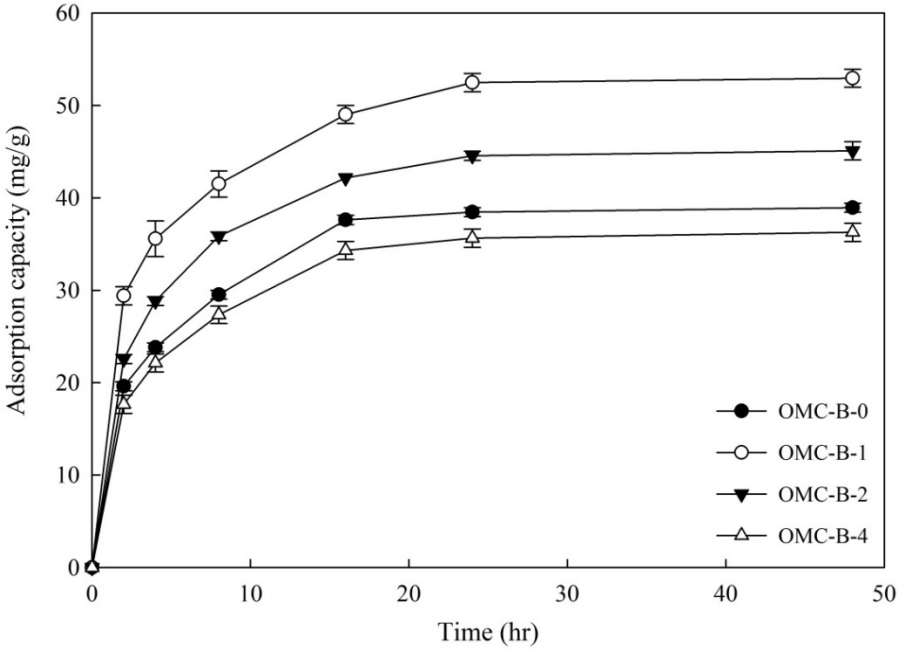

Figure 2.6. Influence of contact time on resorcinol adsorption (C_0: 10 mg/L, temperature 25°C, pH 6.1, adsorbent dosage 0.1 g/L).

2.3.2.2 Adsorption kinetics models. To investigate the possible adsorption mechanism of resorcinol onto the ordered mesoporous carbon, the Pseudo-first order Model and Pseudo-second-order model were used. The Lagergren- first-order kinetic model is the most popular kinetics equation. The model is expressed by the following Eq. (4) (Lagergren, 1898; Sari et al., 2007):

$$\boldsymbol{ln(q_e - q_t) = ln(q_e) - k_1 t} \quad \textbf{(2.4)}$$

Where, q_e (mg/g) is the amount of resorcinol adsorbed at equilibrium, q_t (mg/g) is the amount of resorcinol adsorbed by the adsorbent at time t (hr), k_1 (hr^{-1}) is the rate constant of the Pseudo-first-order reaction.

The Pseudo-second-order kinetic model equation (Dursun and Kalayci, 2005) is expressed as follows:

$$\frac{t}{q_t} = \frac{1}{k_2 q_e^2} + \frac{t}{q_e} \quad \textbf{(2.5)}$$

where, q_t (mg/g) is the amount of resorcinol adsorbed by the adsorbent at any at time t (hr), qe (mg/g) is the amount of resorcinol adsorbed at equilibrium, k_2 (g/mg/hr) is the rate constant of the Pseudo-second-order reaction.

The fitting plots using the Pseudo-first-order and Pseudo-second-order equations are shown in the **Figure 2.7**. The value of k_1 was calculated from the plot of $ln(q_e-q_t)$ versus t as shown in **Figure 2.7(a)**. Similarly, the value of k_2 was calculated from the linear plot of t/q_t versus t as shown in **Figure 2.7(b)**. The kinetic parameters acquired from fitting results are summarized in **Table 2.4**. The higher correlation coefficients of 0.999 indicate that the Pseudo-second-order kinetics was being followed in the adsorption process of resorcinol onto ordered mesoporous carbon implying that the resorcinol adsorption was closer to chemisorption (Chen et al., 2011). Additionally, the adsorption capacity acquired from

Pseudo-second-order equation fitting results was found to be closer to the experimental value meaning that these experimental observations followed Pseudo-second-order equation very well. Similar observations were reported for adsorption of phenols onto chitin (Dursun and Kalayci, 2005).

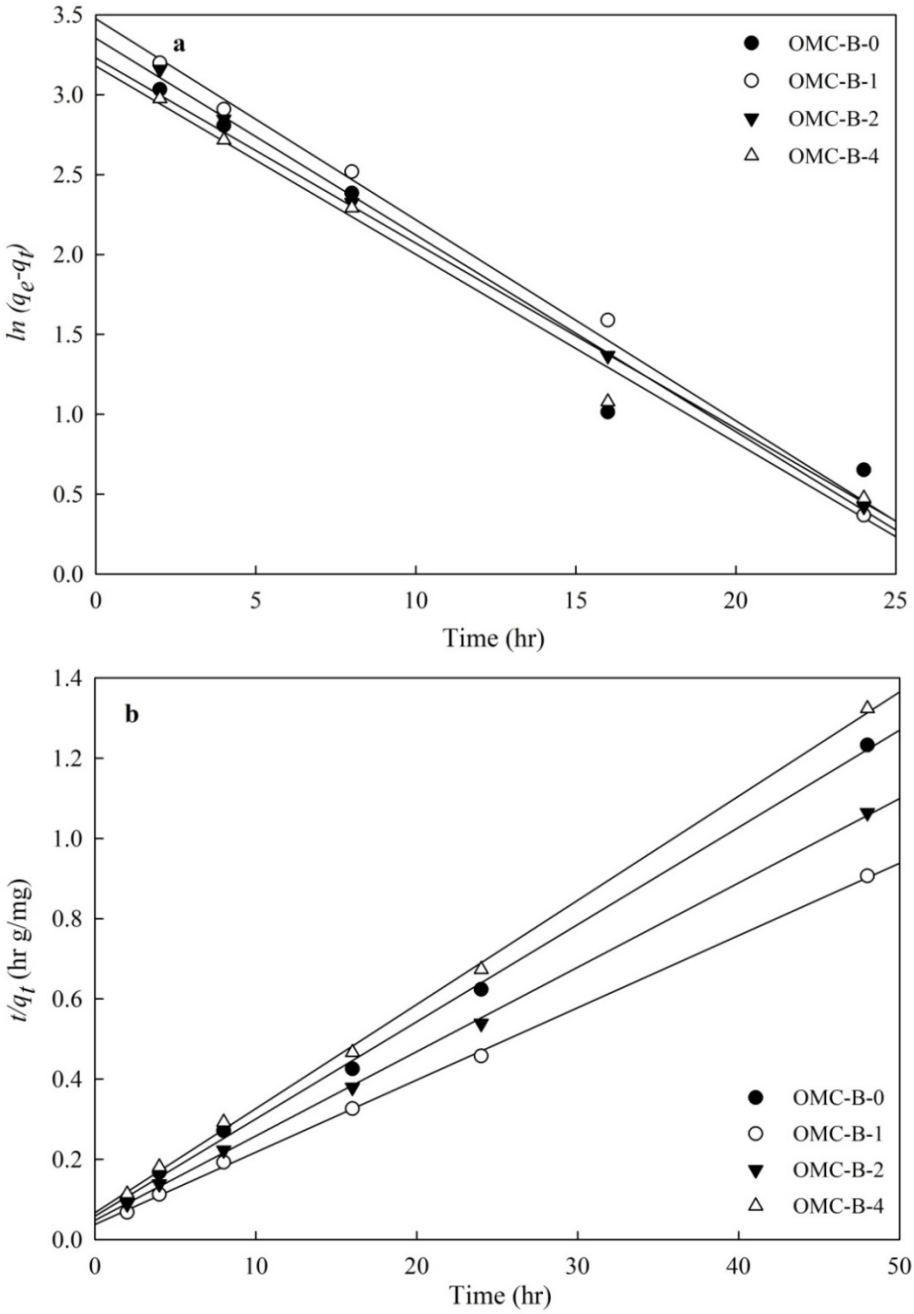

Figure 2.7. Linearized form of (a) Pseudo-first-order kinetic plot and (b) Pseudo-second-order kinetic plot for resorcinol adsorption onto OMCs (C_0 10 mg/L, temperature 25°C, pH 6.1, adsorbent dosage 0.1 g/L).

Table 2.4. Coefficients of Pseudo-first-order and Pseudo-second-order kinetic models for resorcinol adsorption onto OMCs.

Adsorbent	$q_{e(exp)}$ (mg/g)	Pseudo-first-order model			Pseudo-second-order model		
		$q_{e(cal)}$ (mg/g)	k_1 (hr^{-1})	R^2	$q_{e(cal)}$ (mg/g)	k_2 (g/mg/hr)	R^2
OMC-B-0	38.46	25.29	0.1160	0.9610	42.92	0.0080	0.9991
OMC-B-1	52.48	32.31	0.1258	0.9942	56.50	0.0070	0.9995
OMC-B-2	44.55	29.92	0.1253	0.9981	48.78	0.0075	0.9995
OMC-B-4	35.64	24.72	0.1186	0.9827	39.68	0.0080	0.9989

2.3.2.3 Adsorption isotherms. To examine the efficiency of prepared OMC materials, the equilibrium adsorption of resorcinol as a function of equilibrium concentration was studied. **Figure 2.8** shows the equilibrium adsorption isotherms of resorcinol onto ordered mesoporous carbon modified with boric acid. The amounts of adsorbed resorcinol onto the surface of ordered mesoporous carbon increase in the following sequence: OMC-B-1 > OMC-B-2 > OMC-B-4 > OMC-B-0. The reduction in adsorption capacities observed for OMC-B-0 and OMC-B-4 could be due to the decrease in specific surface area (Chao et al., 2017).

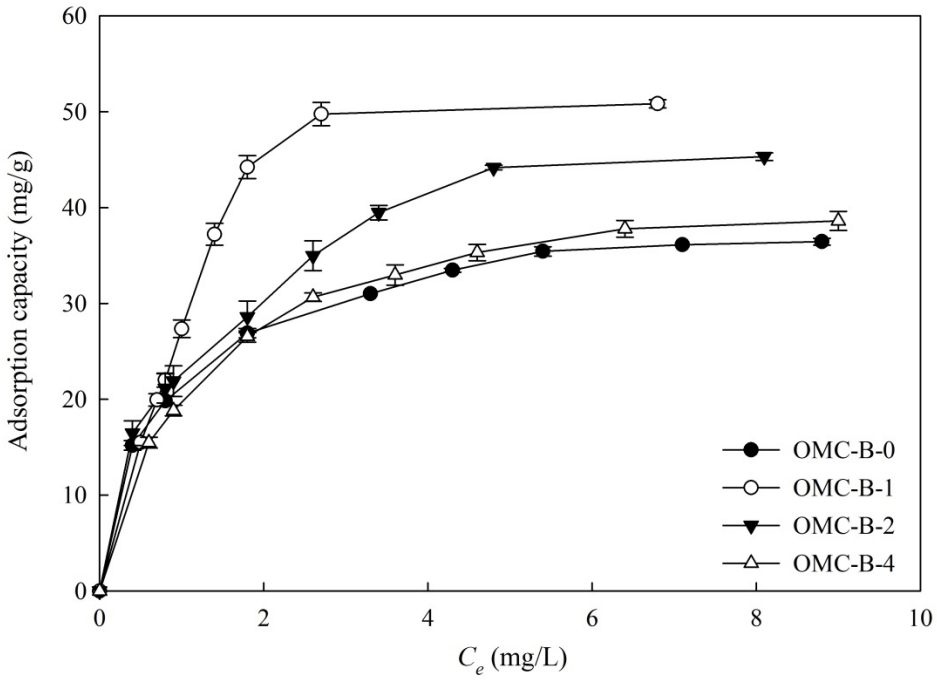

Figure 2.8. Adsorption isotherms of resorcinol onto ordered mesoporous carbon (C_0: 10 mg/L, temperature 25°C, pH 6.1, contact time 24 hr).

The adsorption isotherm describes the mechanism of interaction between adsorbate and adsorbent, and reveals the adsorption capacity of the adsorbent. The equilibrium data were analyzed and fitted by Langmuir and Freundlich isotherm models. The Langmuir isotherm model assumes uniform adsorption energies and monolayer adsorption of adsorbates onto the homogenous surface of the adsorbent with a finite number of identical sites (Chutia et al., 2009). The Langmuir adsorption isotherm is expressed by the following linearized equation (Belhamdi et al., 2016):

$$\frac{C_e}{Q_e} = \frac{1}{Q_{max}K_L} + \frac{C_e}{Q_{max}} \quad \textbf{(2.6)}$$

Where, Q_{max} (mg/g) is the maximum adsorption capacity, C_e (mg/L) is the equilibrium concentration in the solution, Q_e (mg/g) is the equilibrium adsorption amount and K_L (L/mg) is the Langmuir adsorption constant. A linearized plot was obtained when

C_e/Q_e was plotted against Ce over the entire concentration range as shown in the **Figure 2.9(a)**. The calculated Q_{max}, K_L and correlation coefficients are presented in **Table 2.5**. The adsorption capacity of resorcinol onto ordered mesoporous carbon was found to be 39.8 mg/g, 63.3 mg/g, 52.4 mg/g, and 43.9 mg/g for OMC-B-0, OMC-B-1, OMC-B-2, OMC-B-4, respectively. OMC-B-1 has the highest adsorption capacity.

Freundlich adsorption isotherm is empirical in nature and assumes adsorption of adsorbates onto the heterogeneous adsorbent surface with no restriction to the formation of a monolayer. The mathematical expression representing Freundlich adsorption is expressed by the following equation (Sari et al., 2007; Freundlich, 1907):

$$\boldsymbol{lnQ_e = lnK_F + \frac{1}{n} lnC_e} \qquad \textbf{(2.7)}$$

Where, Q_e (mg/g) is the amount of resorcinol adsorbed at equilibrium, C_e (mg/L) is the equilibrium concentration of resorcinol. K_F and n are the Freundlich constants where n describes the efficiency of adsorption process and K_F is defined as an adsorption coefficient representing the amount of adsorbate adsorbed on the adsorbent at unit equilibrium concentration. The values of K_F and 1/n are calculated from the intercept and slope of the plot of lnQ_e vs. lnC_e as shown in **Figure 2.9(b)**. For resorcinol adsorption on the surface of OMC, the values of K_F and n are listed in **Table 2.5**. K_F (mg/g (L/mg)1/n) was found to be 24.42, 32.23, 25.61, and 24.05 for OMC-B-0, OMC-B-1, OMC-B-2, OMC-B-4, respectively. n values obtained from fitting the experimental data were 4.99, 3.28, 3.26 and 4.27 for OMC-B-0, OMC-B-1, OMC-B-2, OMC-B-4, respectively. Based on the n values calculated, it can be concluded that all ordered mesoporous carbon modified with boric acid are effective for resorcinol adsorption. Similar experimental observations were stated by Mckay et al. (1980).

Table 2.5. Summary of parameters calculated from fitting the results of adsorption isotherm of resorcinol onto OMCs.

Adsorbent	Langmuir			Freundlich			
	Q_{max} (mg/g)	K_L (L/mg)	R^2	K_F (mg/g (L/mg)$^{1/n}$)	*n*	*1/n*	R^2
OMC-B-0	39.8	1.27	0.9989	24.42	4.99	0.200	0.9509
OMC-B-1	63.3	0.81	0.9683	32.23	3.28	0.305	0.8246
OMC-B-2	52.4	0.85	0.9935	25.61	3.26	0.306	0.9463
OMC-B-4	43.9	0.87	0.9995	24.05	4.27	0.234	0.9518

Surface heterogeneity or non-ideal adsorption on heterogeneous surface is indicated by the value of 1/*n* varying from 0 to 1. The value of 1/*n* closer to zero is an indication of increased surface heterogeneity. The values of 1/*n* ranges from 0.2 to 0.3 for resorcinol adsorption onto the surface of ordered mesoporous carbon reflecting a normal Langmuir isotherm (Fytianos et al., 2000).

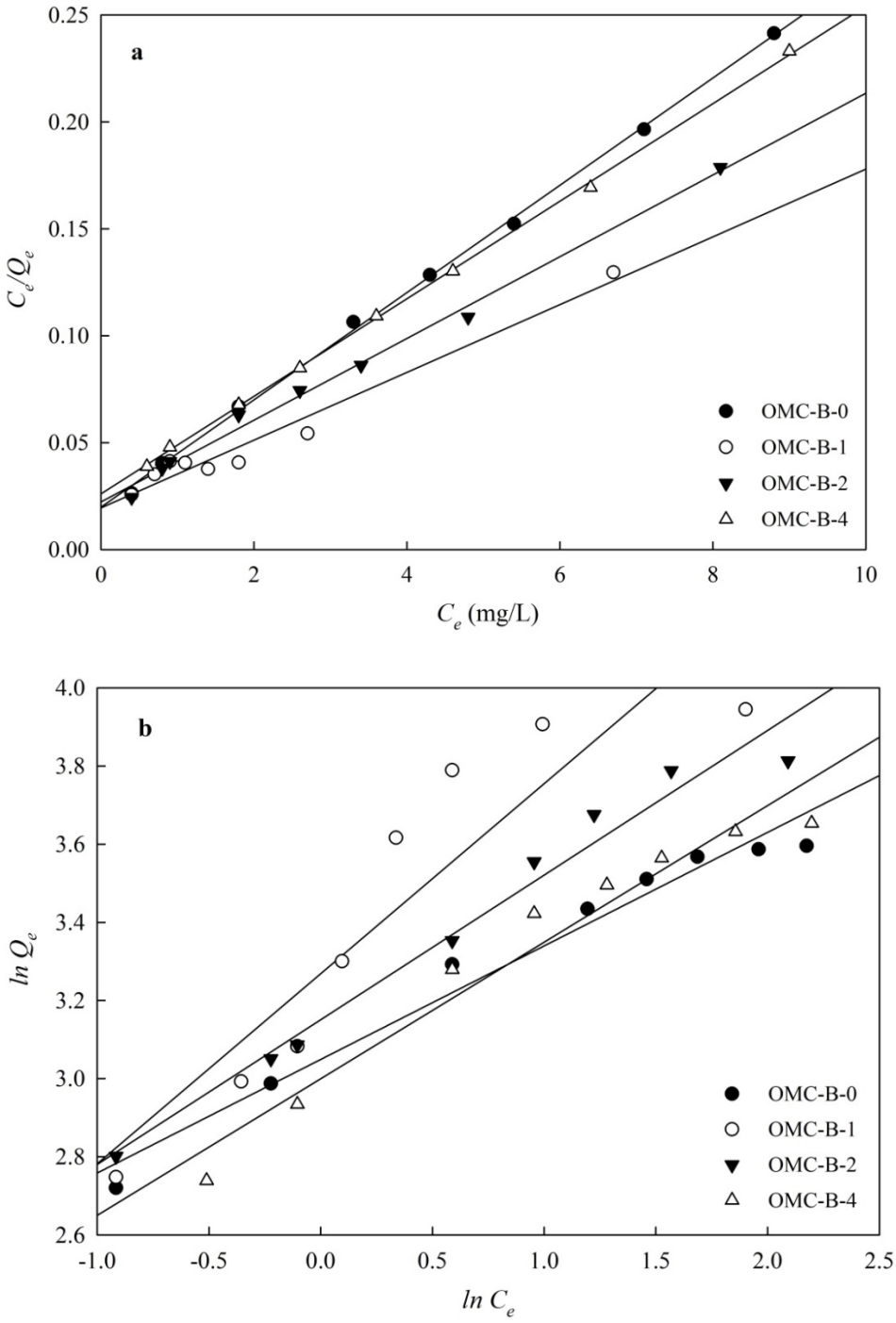

Figure 2.9. Linearized form of (a) Langmuir and (b) Freundlich isotherms for resorcinol adsorption onto OMCs (C_0: 10 mg/L, temperature 25°C, pH 6.1, contact time 24 hr).

The adsorption of resorcinol on the modified OMCs may be attributable to the presence of functions groups found on the surface of OMCs through the formation of hydrogens bonds (Lee et al., 1999; Lu et al., 2005). Oxygen containing surface function group, specifically carboxylic groups can adsorb organic compounds through hydrogen bonding (Sun et al., 2005). The presence of these oxygen containing functional groups was discernible in the FT-IR spectra which was further confirmed by the results of Boehm titration. Besides, hydroxyl group of resorcinol also contributed to the formation of organic-complex with the oxygen containing functional groups (Arafat et al., 1999). The higher adsorption capacities of OMCs can be also attributed to the higher BET surface areas. It can be concluded that the adsorption process was a complex one which was controlled by both textual parameters and surface chemistry. Similar observations were reported by Bashkova et al. (2003).

A comparison of the adsorption capacities of resorcinol onto various adsorbents reported in the literature is presented in **Table 2.6**. OMC materials prepared in this study showed better adsorption capacity compared to commercially available granular activated carbon.

Table 2.6. Comparisons of resorcinol adsorption capacity for various adsorbents.

Adsorbent	Q_e (mg/g)	Conditions	Reference
OMC-B-0[a]	39.8	25°C, C_0 10 mg/L	This study
OMC-B-1[a]	63.3		
OMC-B-2[a]	52.4		
OMC-B-4[a]	43.9		
GAC[b]	36	25°C, C_0 5 mg/L	Chao et al. (2017)
OMC-0[b]	36.5		
OMC-1[b]	40		
OMC-2[b]	64		
OMC-4[b]	44		
CTAB/NaOH/fly ash composite[a]	500	30°C, C_0 50-300 mg/L	Agarwal and Rani, 2017
HJ-1[a]	128.2	20°C, C_0 200-1200 mg/L	Huang et al. (2009)
Activated Carbon Cloth (ACC)[a]	232.3	C_0 7.6×10^{-4} mol/L	Bayram et al. (2009)
Multi-walled Carbon Nanotubes[a]	48	C_0 50-500 mg/L	Liao et al. (2008)
TiO_2[a]	7.87	25°C, C_0 10-150 mg/L	Arana et al. (2007)
TiO_2-H_2O_2[a]	7.61		

Note: *Superscript a: maximum adsorption capacity calculated from Langmuir model. b: equilibrium adsorption capacity.*

2.3.2.4 Regeneration study. To have further insight into the potential application of novel OMC, the regeneration and reuse of the OMCs were performed. **Figure 2.10** shows the

regeneration efficiencies of used OMCs over the four successive adsorption-desorption cycles. It was found that after three regeneration cycles; the maximum regeneration efficiency was in the range of 66%-75%. The highest regeneration efficiency was obtained for OMC-B-1 after the third cycle, suggesting the potential use and regeneration of OMC-B-1. After fourth cycle, the regeneration efficiency of used OMCs was around 40%.

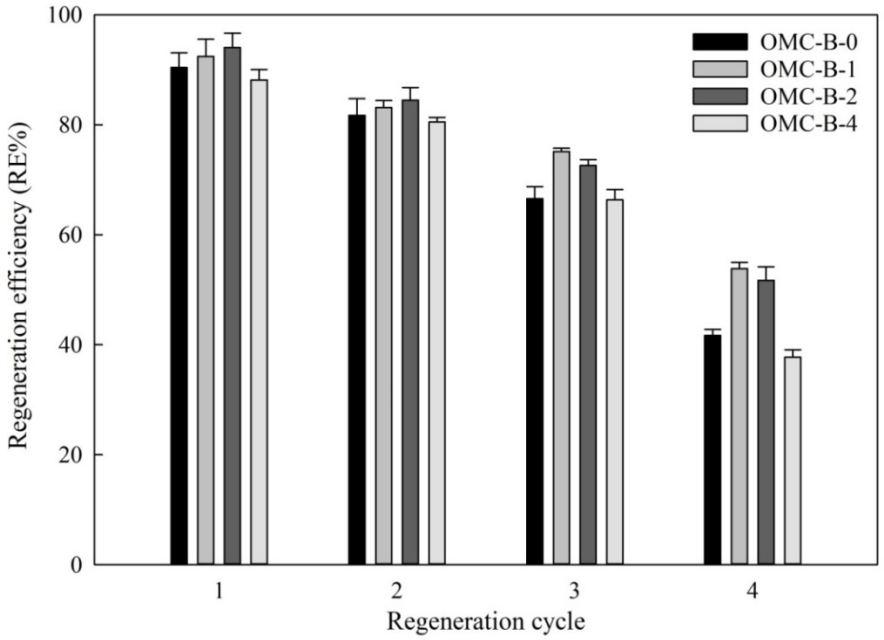

Figure 2.10. Regeneration efficiency from batch experiments for four cycles of regeneration of OMCs.

2.4 Conclusion

In this present work, a novel order mesoporous carbon was successfully synthesized by the hard template method using COK-19 silica scaffold for the first time. OMCs modified with boric acid as the pore enlargement reagent have showed tailored pore size ranging from 6.9 to 16.6 nm. The removal of resorcinol from synthetic wastewater onto ordered mesoporous carbons was studied using batch adsorption technique. The adsorption capacities of different ordered mesoporous adsorbents decrease in the following order: OMC-B-1 (63.3

mg/g) > OMC-B-2 (52.4 mg/g) > OMC-B-4 (43.9 mg/g) > OMC-B-0 (39.8 mg/g). Adsorption kinetics and adsorption isotherms for resorcinol adsorption were also evaluated. The adsorption kinetics was found to follow the Pseudo-Second-Order Kinetic Model. The results revealed that Langmuir model was found to be more suitable to describe the adsorption of resorcinol onto ordered mesoporous carbon. OMC-B-1 has the highest adsorption capacity which can be attributed to higher specific surface area and the presence of carboxylic group. The pore size enlargement technique using boric acid as the reagent can be considered as an efficient method for improved adsorption capacity of OMCs. The characterization techniques employed and batch adsorption study suggests that adsorption process was controlled by porosity characteristics of carbon materials and modified surface chemistry simultaneously. The synthesized OMC suggests it scientific and technological importance as an adsorbent for future modification.

Acknowledgements

This work was supported by the University of Louisiana at Lafayette and Louisiana Board of Regents (*LEQSF(2015-16)-ENH-TR-32* and *LEQSF(2016-17)-RD-C-15*). Assistance and support provided by all the staff of the Energy Institute of Louisiana is also acknowledged in this research.

Chapter 3: Adsorptive Removal of Resorcinol onto Surface Modified Ordered Mesoporous Carbon (OMC): Kinetics and Equilibrium Study

This work has been published as:

Ahmad, Z.U., Lian, Q., Zappi, M.E., Buchireddy, P.R., Gang, D.D., 2019. "Adsorptive Removal of Resorcinol onto Surface Modified Ordered Mesoporous Carbon: Kinetics and Equilibrium Study", *Environmental Progress and Sustainable Energy*, 38 (S1), S386–S397. https://doi.org/10.1002/ep.13070.

Abstract

Ordered Mesoporous Carbon (OMC), a new member of carbonaceous family, has been able to attract substantial attention due to its unique attributes which are high BET surface area, narrow pore size distribution, large pore volume and thermal stability. A novel ordered mesoporous carbon was synthesized using COK-19 silica template for the first time and doped with cerium (III) chloride for the removal of resorcinol from aqueous solution. Traditional multistage technique was employed for the synthesis of OMC. Nitrogen Adsorption-Desorption Isotherms, Scanning Electron Microscope (SEM), Transmission Electron Microscope (TEM), Fourier Transformed Infrared Spectroscopy (FTIR), Energy Dispersive X-ray Spectroscopy (EDS) were employed to characterize the modified OMCs. Adsorption behavior of resorcinol was studied using batch adsorption method. Results from adsorption kinetics and isotherms suggest that Pseudo-Second-Order Model and Langmuir Isotherm well described the experimental data. The adsorption capacities of ordered mesoporous adsorbents decrease in the following order: OMC-5Ce (61 mg g^{-1}) > OMC-3Ce (54 mg g^{-1}) > OMC-1Ce (46 mg g^{-1}) > OMC-0.5Ce (39.4 mg g^{-1}) > OMC (34.5 mg g^{-1}). Adsorption capacity increased by 76.8% with increasing cerium content from 0 to 5%.

3.1 Introduction

Phenols and their derivatives are widely used and identified in the effluents of a number of industries such as oil refineries, paper, textile, synthetic rubber, petrochemical units, and pharmaceutical and steel industries (Bilgili, 2006; Dąbrowski et al., 2005). Phenolic compounds are considered as pollutants of substantial threat to the environment. Because of the high toxicity, higher oxygen demand (theoretically 2.4 mg O_2 mg^{-1} phenol) and low biodegradability (Ku and Lee, 2000; Lin and Juang, 2009), phenols and their

derivatives have been listed as one of the primary pollutants by the United States Environmental Protection Agency (USEPA). Even trace amount of phenolic compounds can potentially have severe impacts on living system since they are known as carcinogenic (Kumar et al., 2003). Therefore, it is necessary to remove these phenolic compounds from industrial wastewater before discharging to the natural stream. Diversified technologies, such as coagulation and precipitation, photocatalytic degradation, chemical oxidation, biodegradation, ion exchange and solid-liquid separation technique or adsorption (Lin and Juang, 2009), have been developed and tested over the past few decades for the treatment of wastewater. Adsorption has been widely used for the separation of organic pollutants from the aqueous solution owing to the simplicity of design, reliability and convenience of this method (Choi et al., 2016). Numerous studies have been dedicated to the development of the adsorption process based on carbonaceous materials. Activated carbon has attracted much attention as an adsorbent for treatment of industrial wastewater due to high BET surface area, thermal resistance and chemical affinity towards organic pollutants. But the dominance of micropores (<2 nm) present in the pore structure limits accessibility of organic pollutants (Dong et al., 2012).

It is preferred that adsorbents have a well-defined mesoporous structure (2-50 nm) for the efficient removal of organic pollutants. Ordered Mesoporous Carbons (OMCs), a new member of the carbonaceous family, have been able to attract substantial attention because of its distinct attributes, such as high BET surface area, narrow pore size distribution, well defined ordered structure, large pore volume, and thermal stability (Joo et al., 2001; Ryoo et al., 1999; Kim et al., 2005, Fuertes and Alvarez, 2004), which promoted research development for the modification of OMCs with tunable pore sizes (Kim et al., 2004) and

improved surface chemistry (Ren et al., 2016), making them more suitable candidate for applications such as adsorption (Guo et al., 2013; Goscianska et al., 2014; Goscianska et al., 2015; Ahmad et al., 2019), catalyst support (Chai et al., 2004; Joo et al., 2006; Shon et al., 2016; Xu et al., 2014), CO_2 capture (Liu et al., 2011; Katsoulidis et al., 2011), and hydrogen storage (Fang et al., 2006; Xia and Mokaya, 2007). Traditionally nanocasting technique is employed for the synthesis of OMCs (Ryoo et al., 1999; Ryoo et al., 2001). The successful synthesis of first ordered mesoporous carbon, CMK-1, was reported by Ryoo et al. (1999) using MCM-48 (cubic *Ia3d*) silica template. After that, diverse mesoporous silica templates were used to synthesize ordered mesoporous carbons, for example, SBA-15 (2D hexagonal *p6mm*) (Chao et al., 2016; Shou et al., 2016), KIT-6 (cubic *Ia3d*) (Dai et al., 2009), and FDU-12 (cubic *Fm3m*) (Xu et al., 2014).

Two factors affecting the adsorption efficiency of OMCs are the interaction between the adsorbate and the adsorbent, including electrostatic, hydrogen bonding, acid-base interaction, and textual parameters of the adsorbent such as BET surface area, pore size, and volume (Ahmad et al., 2018). For instance, ordered mesoporous carbon functionalized by 4-acetophenone oxime was found to be a promising adsorbent for Uranium(VI) (Tian et al., 2011). Magnetic dual-pore mesoporous carbon was synthesized by chemical modification followed by the reduction of $Fe(NO_3)_3$ under inert conditions (Dong et al., 2012). The adsorption capacity of OMC can be increased by incorporating metal nanoparticles onto the surface of OMCs (Jaroniec, 2008). It has been reported that the interaction between the f-orbitals of Lanthanides and different functional groups can assist the formation of complexes with organic compounds (Goscianska et al., 2014). Therefore, the incorporation of lanthanide ions provides a means to concentrate on the surface of adsorbents (Ökte and Yilmaz, 2009a;

Ökte and Yilmaz, 2009b). The main objective of this research work was to synthesize ordered mesoporous carbons modified with cerium using COK-19 silica template and study their effectiveness for resorcinol removal from aqueous solution. Surface modified OMCs were characterized using different techniques and the adsorption behavior of resorcinol was studied using batch adsorption methods under varying conditions.

3.2 Materials and Methods

3.2.1 Chemicals. Triblock copolymer Pluronic F-127 (M_w = 12600, EO_{106}-PO_{70}-EO_{106}, EO = ethylene oxide, PO = propylene oxide), citric acid monohydrate (ACS reagent, ≥99%), trisodium citrate dihydrate and sodium silicate solution (reagent grade, SiO_2 26.5%), sucrose (ACS reagent, ≥99.0%), sulfuric acid (ACS reagent, 98%) hydrofluoric acid (ACS reagent, 48%) were purchased from Sigma Aldrich. Cerium(III) chloride ($CeCl_3$ Anhydrous, 99.5%, Alfa Aesar™) was purchased from Fisher Scientific. All chemicals were used as received without any further purification.

3.2.2 Synthesis of COK-19 template. The COK-19 was synthesized using Pluronic F-127 triblock copolymer surfactant and sodium silicate solution as the silica source. In a typical synthesis, 2.6 g of Pluronic F-127 was dissolved in 107.5 g of deionized water. To this solution, 3.7 g of citric acid monohydrate and 2.55 g of trisodium citrate dihydrate were added. This buffered surfactant solution was stirred overnight to dissolve all the components. After that, 10.4 g of sodium silicate solution (26.5% SiO_2) diluted in 30 g of water was added to the buffered F-127 solution at room temperature and the solution was stirred vigorously for 5 min. Precipitation of white solid occurred instantaneously and the milky white suspension was kept under quiescent conditions for aging for 24 hr at 70 ºC in a constant temperature water bath (Premiere HH-4). The white precipitation was then filtered off,

washed with deionized water (4,000 mL) and dried in the oven at 105 ºC overnight. The resultant solid was calcined at 350 ºC for 24 hr using a heating rate of 0.5 ºC/minute in a box furnace (Lindberg/Blue M Moldatherm Box Furnace Thermo Scientific). The white COK-19 silica template was stored in the desiccator for the preparation of OMC.

3.2.3 Synthesis of Ordered Mesoporous Carbon. Ordered Mesoporous Carbon (OMC) was prepared via hard template method using sucrose as the carbon precursor and COK-19 as the silica scaffold. Typically, 1.5 g of sucrose ($C_{12}H_{22}O_{11}$) and 15 drops of sulfuric acid (H_2SO_4) were dissolved in 15 mL of water. 2.0 g of COK-19 was then added to the solution and stirred for 2-3 hrs. The mixture was heated at 100 °C for 6 hr and subsequently at 160 °C for an additional 6 hr. The resulting composite was impregnated again with an aqueous solution of 0.5 g sucrose mixed with 10 drops of a solution sulfuric acid dissolved in 10 mL of water. After the second heat treatment at 100 °C and 160 °C respectively, the composite was carbonized at 700 °C for 8 hr under a nitrogen flow of 100 mL min^{-1}. Afterwards, the silica template was removed using approximately 50 mL of HF solution at room temperature. The product obtained was filtered and washed with 4,000 mL of DI water to obtain final OMC.

3.2.4 Sample modification. Incipient wetness method was employed to impregnate ordered mesoporous carbon with an aqueous solution of Cerium(III) Chloride ($CeCl_3$) in accurately calculated amount to obtain 0.5, 1, 3, 5 wt% metal loading. The samples were successively dried at 100 °C for 5 hr and heated in nitrogen for 3 hr at 400 °C. The samples obtained were denoted as OMC-0.5Ce, OMC-1Ce, OMC-3Ce, OMC-5Ce, respectively. The step by step synthesis procedure of OMC is shown in **Figure 3.1**.

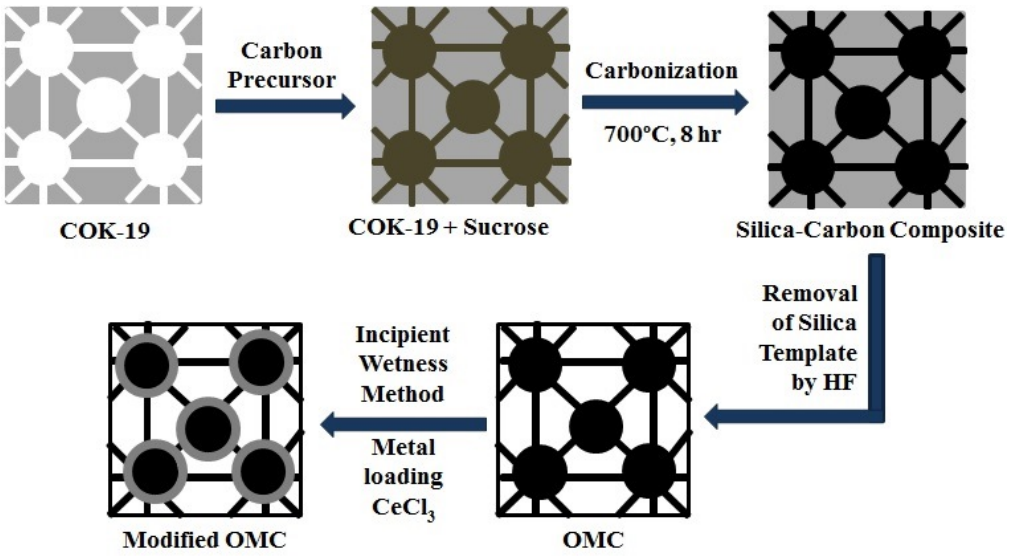

Figure 3.1. Step by step synthesis of OMC.

3.2.5 Characterization. Nitrogen sorption isotherms were recorded on Micromeritics ASAP 2020 (Accelerated Surface Area and Porosimetry System). Specific surface areas of the samples were calculated using the BET (Brunauer-Emmett-Teller) equation, while pore size distribution (PSD) curves were calculated by the BJH (Barrett-Joyner-Halenda) method using the adsorption branch. Prior to measurement, OMC was degassed at 300 °C for 6 hr under reduced pressure. The total pore volume was obtained from the amount adsorbed at a relative pressure (P/P0) of 0.99, where P and P0 are equilibrium and saturation pressure of adsorbate.

Fourier Transform Infrared (FT-IR) spectra was obtained in a transmission mode from KBr pellets at room temperature on a Jasco 4700 spectrometer with a resolution of 4 cm-1, using 32 scans per spectrum in the region of 400-4000 cm^{-1}. The mass ratio of sample to KBr was constant at 1:100.

Energy dispersive X-ray Spectroscopy (EDS) was used to determine the elemental composition of prepared OMCs. EDS measurements were conducted on a JEOL 6300 Field

Emission Scanning Electron Microscope (JEOL Ltd., Tokyo, Japan) using imaging techniques at 15 kV. SEM images were also obtained using the same instrument and operating conditions. The OMC samples were sputter coated with 20 nm of gold.

TEM images were obtained using a Hitachi 7600 Transmission Electron Microscopy (Hitachi America Ltd., Tarrytown, New York). The acceleration voltage used was 100 kV. The samples were prepared by dispersing a large number of particles in ethanol with an ultrasonic bath for 45 min and a few drops of the resulting suspension were placed on a 400 mesh Cu grid.

3.2.6 Batch adsorption study. Batch adsorption experiments were conducted to evaluate the adsorption capacity of resorcinol onto the OMCs. For that purpose, 100 mL of resorcinol solution with a concentration of 20 mg L^{-1} at pH value of 6.5 was placed in 250 mL conical flasks for both control (without OMC labeled as blank) and experimental (with OMCs and adsorbate) conditions. All the samples were placed in an E24 incubator shaker (New Brunswick Scientific). The adsorption studies were conducted at room temperature of 25 °C and the shaking speed was maintained at 250 rpm. After 24 hr, the conical flasks were removed from the shaker and the solution was filtered using 0.45 μm glass filter paper. The blank solution was used as a reference to establish the initial concentration for the solutions containing OMCs. The concentration of resorcinol was determined using a Cary 50 UV-visible spectrophotometer (Varian) set at a wavelength of 500 nm. The amount of resorcinol adsorbed by OMCs was determined by subtracting the final concentration from the initial concentration using the following formula:

$$\boldsymbol{Q_e = \frac{(C_o - C_e) \times V}{M}} \qquad \textbf{(3.1)}$$

Where Q_e is the adsorption capacity (mg g^{-1}) of the adsorbent at equilibrium, C_o is the initial concentration of resorcinol in the solution (mg L^{-1}), C_e is the final concentration of resorcinol in the treated solution (mg L^{-1}), V is the volume of the solution taken (L), and M is the weight of the adsorbent OMC (g).

3.2.7 Adsorption isotherm models. The Langmuir Isotherm Model is established based on the assumption that the maximum adsorption capacity corresponds to a formation of a saturated monolayer of adsorbates onto the homogenous surface of the adsorbent with a finite number of identical sites and also with a constant energy. The model also assumes that there is no interaction between adsorbed molecules (Belhamdi et al., 2016). The linearized form of Langmuir adsorption isotherm is expressed by the following equation (Yang et al., 2015):

$$\frac{C_e}{Q_e} = \frac{1}{Q_{max}K_L} + \frac{C_e}{Q_{max}} \quad \textbf{(3.2)}$$

Where q_e is the equilibrium adsorption amount on the OMC (mg g^{-1}), C_e is the equilibrium concentration in the solution (mg L^{-1}), q_{max} is the maximum adsorption capacity (mg g^{-1}), and K_L is the Langmuir adsorption constant related to affinity of the binding sites (L mg^{-1}). The values of q_{max} and K_L are calculated from the slopes ($1/q_{max}$) and intercept ($1/q_{max}K_L$) of the linear plot of C_e/q_e vs. C_e.

The main characteristic of the Langmuir Isotherm Model is the dimensionless separation factor, R_L, which indicates the nature of adsorption and can be defined by the following equation (Liu et al., 2010):

$$R_L = \frac{1}{1+K_L C_e} \quad \textbf{(3.3)}$$

$R_L > 1$, $R_L = 1$, $R_L = 0$, and $0 < R_L < 1$ indicates that adsorption is unfavorable, linear, irreversible, and favorable, respectively.

The Freundlich Isotherm Model is based on heterogeneous adsorbent surface with the interaction between adsorbed molecules (Sari et al., 2007). The linearized form of Freundlich Isotherm Model is expressed as follows (Soto et al., 2011):

$$\boldsymbol{lnQ_e = lnK_F + \frac{1}{n} lnC_e} \quad \textbf{(3.4)}$$

Where q_e is the equilibrium adsorption amount on the OMC (mg g^{-1}), Ce is the equilibrium concentration in the solution (mg L^{-1}), K_F is the Freundlich adsorption isotherm constant [(mg g^{-1})(L mg^{-1})1/n], and n describes the efficiency of the adsorption process. The Freundlich constants can be calculated from the slope ($1/n$) and intercept (lnK_F) of the linear plot of lnq_e vs. lnC_e.

Dubinin-Radushkevich (D-R) Model is also widely used to have a better understanding of adsorption process which does not assume a homogeneous surface or constant adsorption potential. The linearized form of D-R Model can be expressed by the following equation (Konggidinata et al., 2017a):

$$\boldsymbol{lnq_e = lnq_m - \beta\varepsilon^2} \quad \textbf{(3.5)}$$

Where β is a constant related to the mean energy of adsorption (mol^2 J^{-2}), qm is the theoretical adsorption capacity (mg g^{-1}), and ε is the Polanyi potential (J mol^{-1}) that is related to the equilibrium concentration and is expressed as follows:

$$\boldsymbol{\varepsilon = RTln\left(1 + \frac{1}{C_e}\right)} \quad \textbf{(3.6)}$$

Where R and T are the universal gas constant (8.314 J mol^{-1} K^{-1}) and absolute temperature (K), respectively. The adsorption free energy, E (J mol^{-1}) can be calculated using the constant β which indicates that one molecule of adsorbate is transferred to the surface of adsorbent from the solution and can be calculated using the following equation:

$$\boldsymbol{E = \frac{1}{\sqrt{2\beta}}} \quad \textbf{(3.7)}$$

Where the magnitude of E indicates the adsorption mechanism. E < 8 kJ mol^{-1} indicates physical adsorption is dominating, whereas 8 kJ mol^{-1} < E < 16 kJ mol^{-1} and E > 16 kJ mol^{-1} suggest ion exchange and diffusion, respectively (Kaveeshwar et al., 2018).

3.2.8 Adsorption kinetic models. Four kinetic models, namely Pseudo-First-Order, Pseudo-Second-Order, Elovich and Intra-particle Diffusion Model were selected in this study to have better insight and describe the adsorption process.

The Linearized Pseudo-First-Order Kinetic Model can be expressed in the following linear form (Aydin et al., 2008):

$$\boldsymbol{ln(q_e - q_t) = ln(q_e) - k_1 t} \quad \textbf{(3.8)}$$

Where q_e (mg g^{-1}) is the amount of resorcinol adsorbed at equilibrium, qt (mg g^{-1}) is the amount of resorcinol adsorbed by the adsorbent at time t, k_1 (hr^{-1}) is the rate constant of the Pseudo-First-Order reaction. The k_1 values are calculated from the plot of ln(q_e−q_t) vs. t.

The Pseudo-Second-Order Kinetic Model Equation is expressed as follows (Ghaedi et al., 2015):

$$\boldsymbol{\frac{t}{q_t} = \frac{1}{k_2 q_e^2} + \frac{t}{q_e}} \quad \textbf{(3.9)}$$

Where q_t (mg g^{-1}) is the amount of resorcinol adsorbed by the adsorbent at time t, q_e (mg g^{-1}) is the amount of resorcinol adsorbed at equilibrium, k_2 (g mg^{-1} hr^{-1}) is the rate constant of the Pseudo-Second-Order reaction. The values of k_2 and q_e were calculated from the slope and intercept of the t/q_t vs. t plot.

The Elovich equation is useful in chemisorption process which involves valence forces through sharing or exchange between the adsorbate and the adsorbent (Wu et al.,

2009). The removal efficiency decreases with time because of the coverage of active sites (Aharoni and Tompkins, 1970). The Elovich Model is generally expressed as:

$$\frac{d_{qt}}{dt} = \alpha \exp(-\beta q_t) \quad \textbf{(3.10)}$$

Where q_t is the amount of resorcinol adsorbed onto the OMC at time t (mg g^{-1}), α is the initial sorption (mg g^{-1} hr^{-1}), and β is the desorption constant (g mg^{-1}). Assuming $\alpha\beta t >> 1$ and boundary conditions of: $q_t = 0$ at $t = 0$ and $q_t = q_t$ at $t = t$, the Elovich equation can be simplified into:

$$q_t = \beta \ln(\alpha\beta) + \beta lnt \quad \textbf{(3.11)}$$

The constants α and β are obtained from the slope and intercept of the linear plot q_t vs. lnt.

Intra-particle Diffusion Model is used to compute the rate controlling step, while Pseudo-First-Order, Pseudo-Second-Order, and Elovich models are used to compute the rate constant. The Weber-Morris Intra-Particle Diffusion Model Equation is shown as below (Weber and Morris, 1964):

$$q_t = K_{diff} t^{1/2} + I \quad \textbf{(3.12)}$$

Where q_t (mg g^{-1}) is the amount of adsorbate adsorbed on the adsorbent at time t, k_{diff} is the intra-particle diffusion rate constant (mg g^{-1} $hr^{-1/2}$) and I is a constant that is proportional to the boundary layer thickness; i.e. the value of I increases with increase in the boundary layer thickness. If the line passes through the origin, then intra-particle diffusion is the limiting step, otherwise it is not only the rate determining factor due to the effects of boundary layer diffusion (Adebisi et al., 2017).

3.4 Results and Discussion

3.4.1 Characterization of adsorbents. The N_2 adsorption-desorption isotherm of COK-19 behave like the representative type IV curve, with a sharp capillary condensation step in the relative pressure range of 0.65-0.75 as shown in **Figure 3.2(a)**. The COK-19 capillary condensation step is located in the smaller relative pressure that can be translated to narrow pore size distribution which is confirmed by the pore size distribution as shown in **Figure 3.2(b)**. The mesoporous characteristics of synthesized OMCs are confirmed by the nitrogen adsorption-desorption isotherm and the corresponding pore size distribution in **Figure 3.3** and **Figure 3.4**, respectively. All the OMCs exhibit type IV isotherm with H2 hysteresis loops demonstrating the presence of mesopores having a uniform distribution of pore size as shown in **Figure 3.3**. Narrow pore size distributions are centered on 6.9-7.2 nm for all synthesized OMCs as presented in **Figure 3.4**.

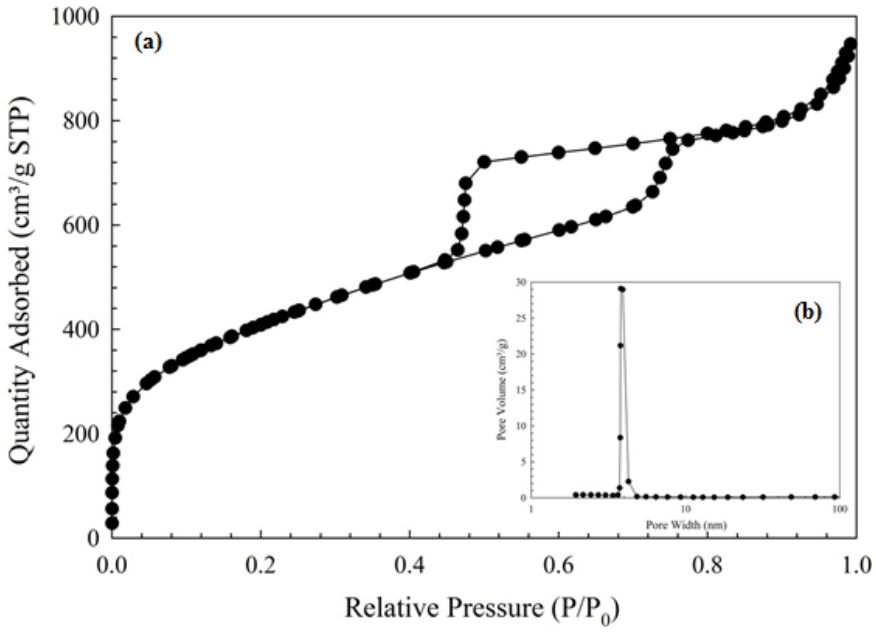

Figure 3.2. (a) Nitrogen adsorption-desorption isotherm of COK-19 (b) corresponding pore size distribution.

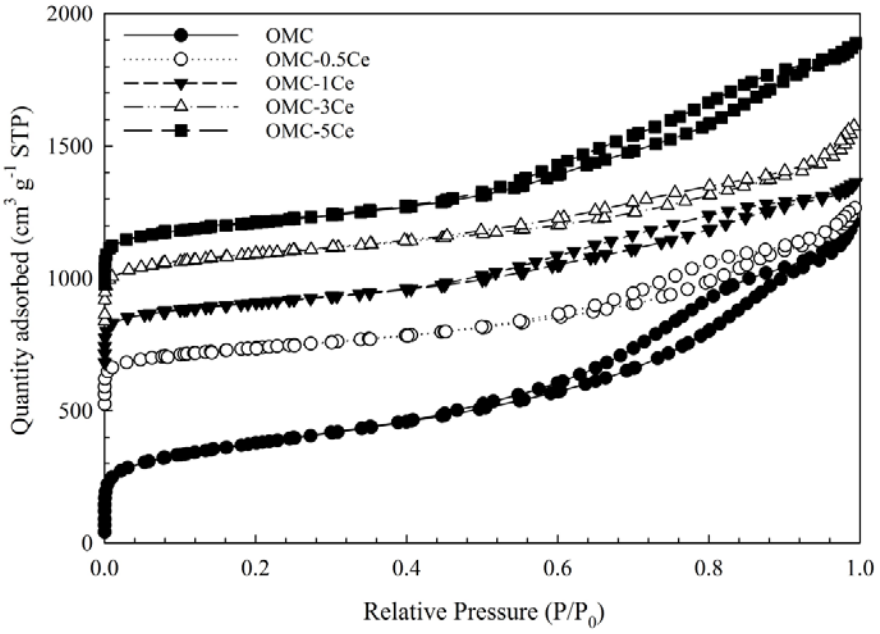

Figure 3.3. N_2 adsorption-desorption isotherms of OMCs. The sorption isotherms for the OMC-0.5Ce, OMC-1Ce, OMC-3Ce, and OMC-5Ce have been offset by 500, 650, 800, and 950 cm^3 g^{-1}, respectively.

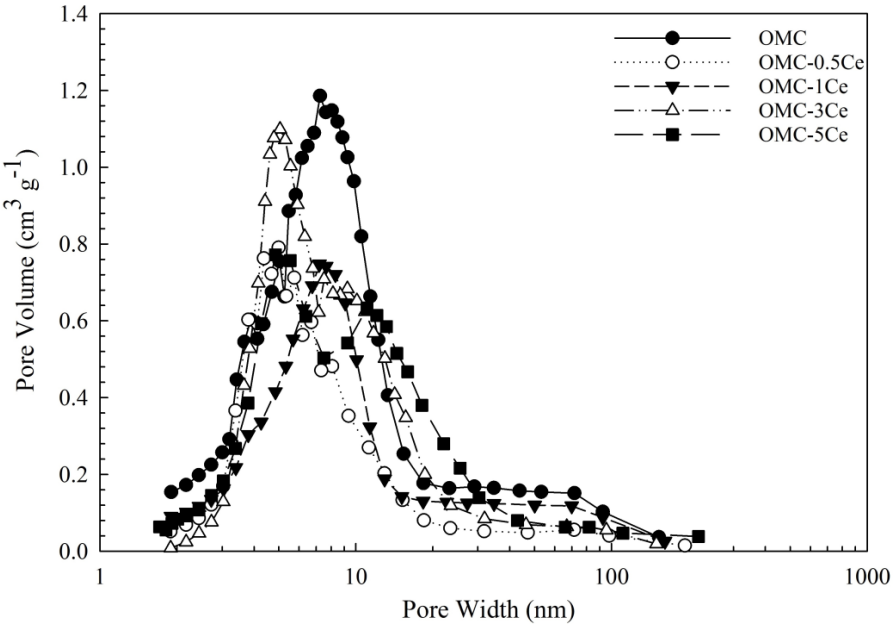

Figure 3.4. Pore size distribution of OMCs.

The corresponding textual parameters of the modified OMCs are summarized in **Table 3.1**. The parent OMC shows the largest BET surface area of 1014.31 $m^2 g^{-1}$, with pore size of 6.9 nm and pore volume of 1.71 $cm^3 g^{-1}$. Modification with cerium(III) chloride causes to decrease BET surface area and pore volume. The highest decrease in BET surface area was observed for OMC-5Ce which was 932.46 $cm^3 g^{-1}$. The change in BET surface area for OMC-5Ce was 8% in comparison to that of the parent OMC. This phenomenon is attributed to the pore blocking, from the interaction between $CeCl_3$ and carbon structure, and subsequent pore collapse. The increased amount of $CeCl_3$ nanoparticle introduced on the support surface caused a small increase in pore size, from 7.05 nm for OMC-0.5Ce, to 7.21 nm for OMC-5Ce.

Table 3.1. Textual parameters of parent OMC and modified OMCs.

Sample	BET Surface Area ($m^2 g^{-1}$)	Total pore volume ($cm^3 g^{-1}$)	Pore size (nm)
OMC	1014.31	1.71	6.91
OMC-0.5Ce	1002.62	1.65	7.05
OMC-1Ce	993.40	1.63	7.12
OMC-3Ce	957.76	1.48	7.18
OMC-5Ce	932.46	1.44	7.21

The parent OMC showed broad particle size distribution with the mean diameter of 11.18 μm. After doping with 1, 3, and 5% of cerium, the particle sizes increased. The mean diameter was found to be 40.6 μm, 46.52 μm, and 52.5 μm, respectively with broader particle size distribution.

The surface morphology of synthesized OMCs was revealed by the SEM micrographs as shown in **Figure 3.5(a)-(c)**. The modification produces smooth surfaces with reduced

number of cracks on the carbon surfaces, as the metal concentration increases from 0.5% to 5%. These observations were in line with the decrease in BET surface area and pore volume (Goscianska et al., 2014). TEM micrographs of modified OMCs are shown in **Figure 3.6(a)-(b)**. OMC synthesized using COK-19 silica template by the hard template was found to have ordered structure, the same as the modified OMCs. As the cerium content increased form 0.5% to 5%, more cerium was deposited on the OMC surface and cavities were further clogged, resulting in smooth surfaces. The decrease in BET surface area can also be attributed to this phenomenon (Goscianska et al., 2014).

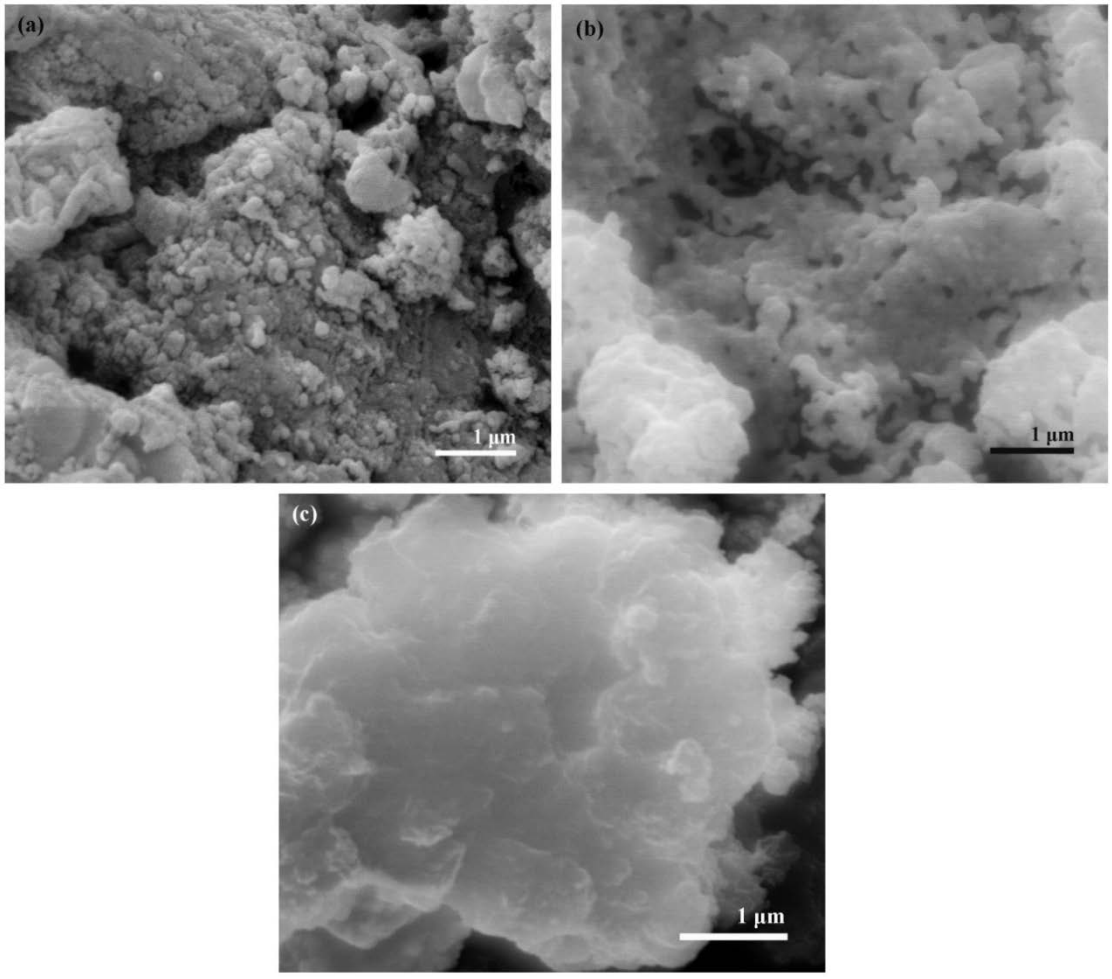

Figure 3.5. SEM micrographs of (a) OMC (b) OMC-1Ce (c) OMC-5Ce.

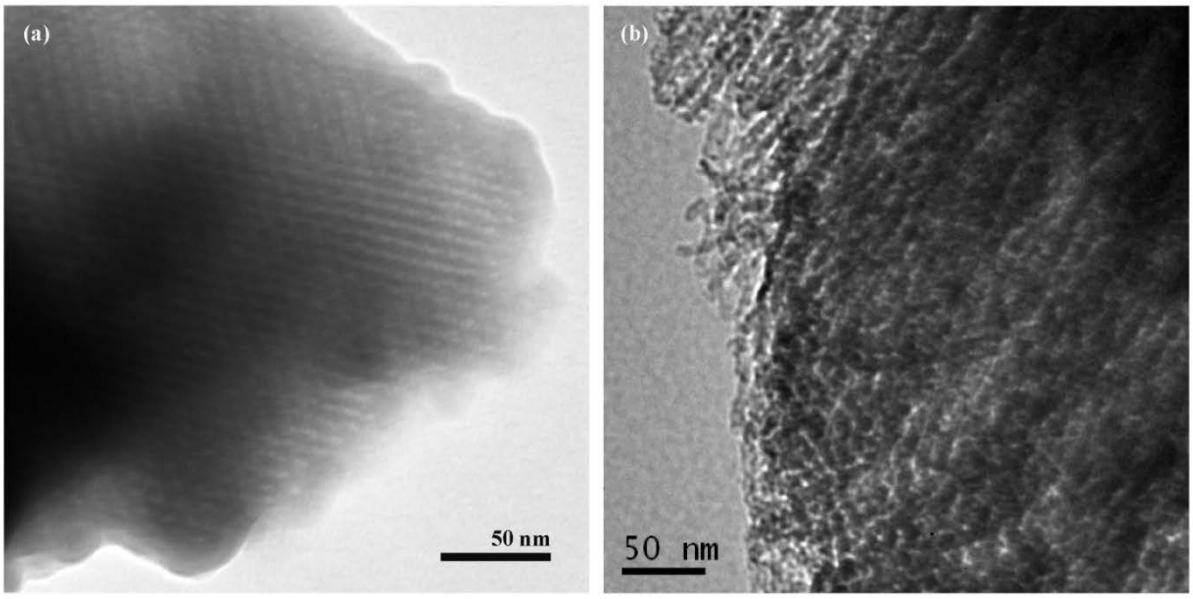

Figure 3.6. TEM micrographs of (a) OMC (b) OMC-1Ce.

To identify the functional groups present on the synthesized OMCs, FT-IR spectra of the OMC, OMC-0.5Ce, OMC-1Ce, OMC-3Ce, and OMC-5Ce were acquired as depicted in **Figure 3.7**. FT-IR spectra reveal that the modification of OMC affects the type of functional groups present on the OMCs. It is observed that broad peak around 3400-3700 cm^{-1} is associated to the surface-adsorbed water and hydroxyl groups (Soler-Illia et al., 2002). The decrease in the intensities of these bands in the FT-IR spectra of modified OMCs can be attributed to the increasing amount of induced cerium onto the surface of OMC. The band around 1295 cm^{-1} is the characteristic band for Ce–O bond. The incorporation of cerium is partially responsible for the depletion of surface-adsorbed water and hydroxyl groups in the modified OMCs (Xiao et al., 2006). A small peak observed at 2346 cm^{-1} could be credited to S–H function group due to the addition of sulfuric acid in the synthesis procedure that acted as a catalyst (Chao et al., 2016). The peaks around 1620 cm^{-1} could be assigned to C=O stretching in the carboxylic groups (O-C=O) (Shou et al., 2016). The small peak observed

around 1402 cm^{-1} corresponds to C–H group (Swiatkowski et al., 2004; Cansado et al., 2012).

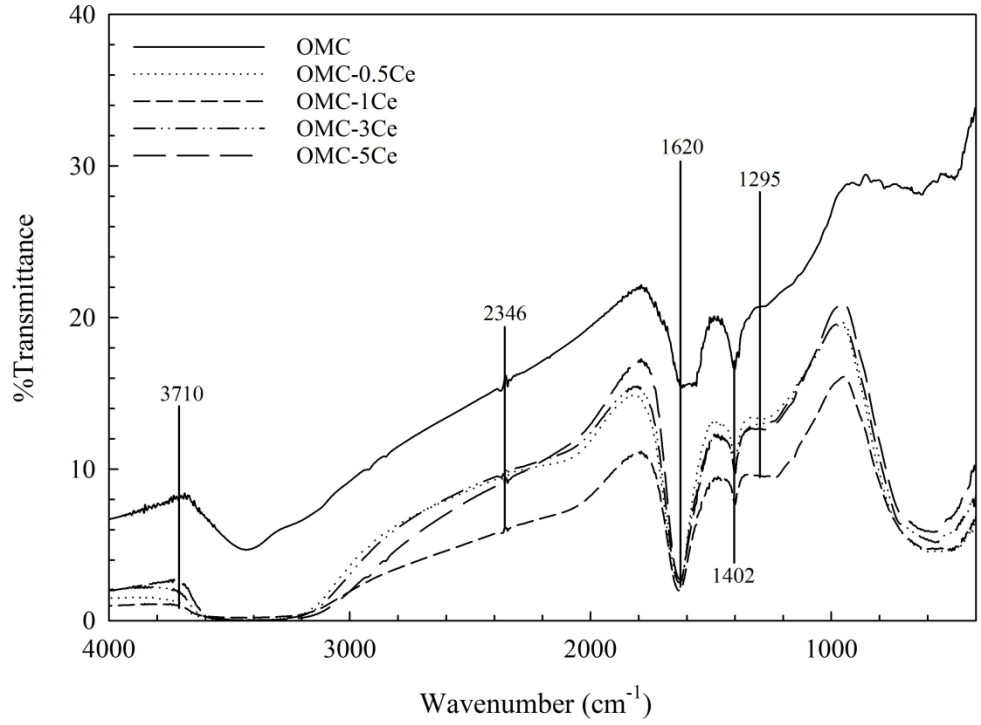

Figure 3.7. FT-IR Spectra of synthesized OMCs.

The results of elemental analysis are given in **Table 3.2**. The analysis showed that the carbon was the dominant element, followed by cerium. The metal content of 0.5%, 1%, 3% and 5% cerium doped on the OMC caused an increase of cerium from 7.992%, 12.214%, 20.416% to 24.097%. This was also confirmed by the EDS spectra as shown in **Figure 3.8**. The presence of Ce–O was further confirmed by the increased content of oxygen. Combined with the EDS map scanning as shown in **Figure 3.9,** it was found that Ce ions were distributed on the OMC support surface.

Table 3.2. Results of Elemental Analysis of OMCs.

Sample	%C	%O	%S	%Cl	%Ce
OMC-0.5Ce	85.994	0.732	0.521	4.761	7.992
OMC-1Ce	80.576	1.648	0.404	5.158	12.214
OMC-3Ce	63.329	3.339	0.512	12.405	20.416
OMC-5Ce	54.188	5.648	0.147	15.920	24.097

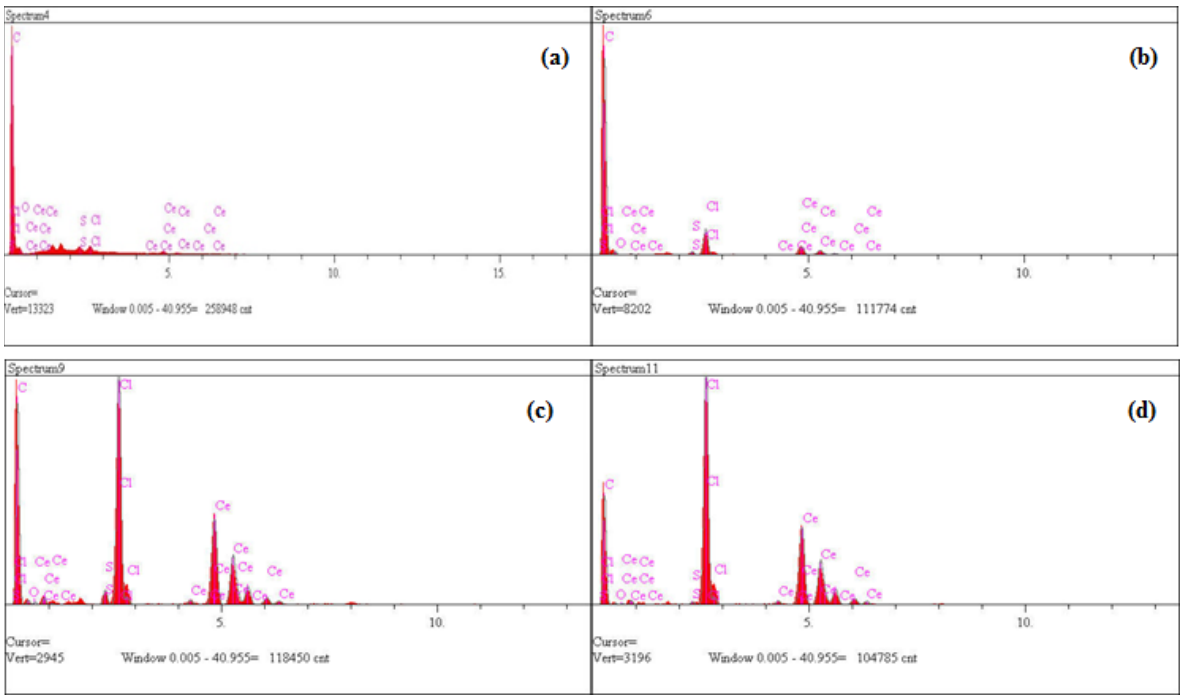

Figure 3.8. Elemental composition of modified OMC samples with cerium(III) chloride (a) OMC-0.5Ce (b) OMC-1Ce (c) OMC-3Ce (d) OMC-5Ce.

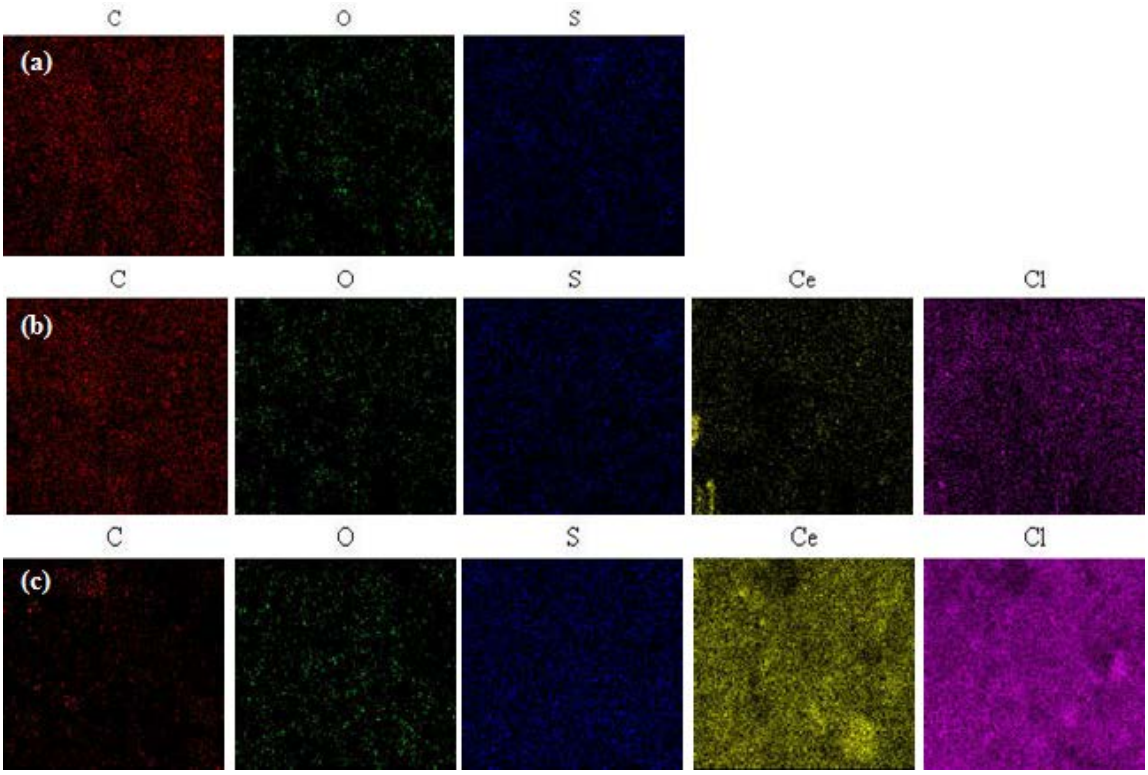

Figure 3.9. EDS scanning maps of (a) OMC (b) OMC-1Ce (c) OMC-5Ce.

3.4.2 Adsorption behavior.

3.4.2.1 Effects of cerium loading on removal efficiency. **Figure 3.10** shows the effects of doped cerium onto the surface of OMCs for resorcinol removal efficiency. The resorcinol removal efficiency is enhanced from 0 to 5 wt% Ce loading. The highest removal efficiency was obtained for 5 wt% cerium loading, caused by the increased cerium loading. Then, a slight reduction in the removal efficiency for 7.5 wt% cerium loading is found, followed by a dramatic decrease in the removal efficiency for 10 wt% cerium modified OMC. This can be explained by a decreased BET surface area at high Ce loading (718.26 m^2 g^{-1} and 486.16 m^2 g^{-1} for OMC-7.5Ce and OMC-10Ce, respectively).

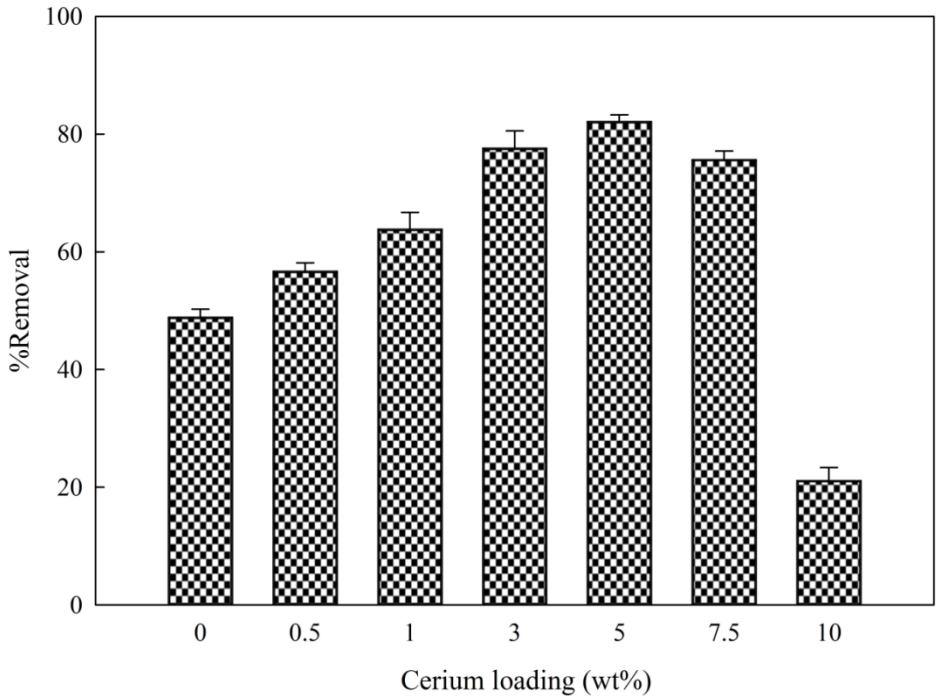

Figure 3.10. Effects of cerium loading on resorcinol removal.

3.4.2.2 Effect of adsorbent dosage. In the adsorption process, the amount of adsorbent or dosage of the adsorbent plays an important role. In order to evaluate the effects of adsorbent dosage (in grams of adsorbent per one liter of solution) on resorcinol removal, various amounts of cerium modified OMCs in the range of 0.1 to 0.75 g L^{-1} were contacted with the aqueous solution with an initial concentration of 20 mg L^{-1}. The effect of adsorbent dosage on the percentage removal of resorcinol after a contact period of 24 hr is shown in **Figure 3.11**. It was found that the final concentration of resorcinol decreased with an increase in the adsorbent dosage. This could be explained by the fact that the increased adsorbent dosage at a fixed initial concentration of resorcinol provided more available adsorption sites and therefore the removal was enhanced. Therefore, an adsorbent dosage of 0.5 to 0.6 g L^{-1} can be considered as optimum dosage for the cerium modified OMCs to remove resorcinol from synthetic wastewater.

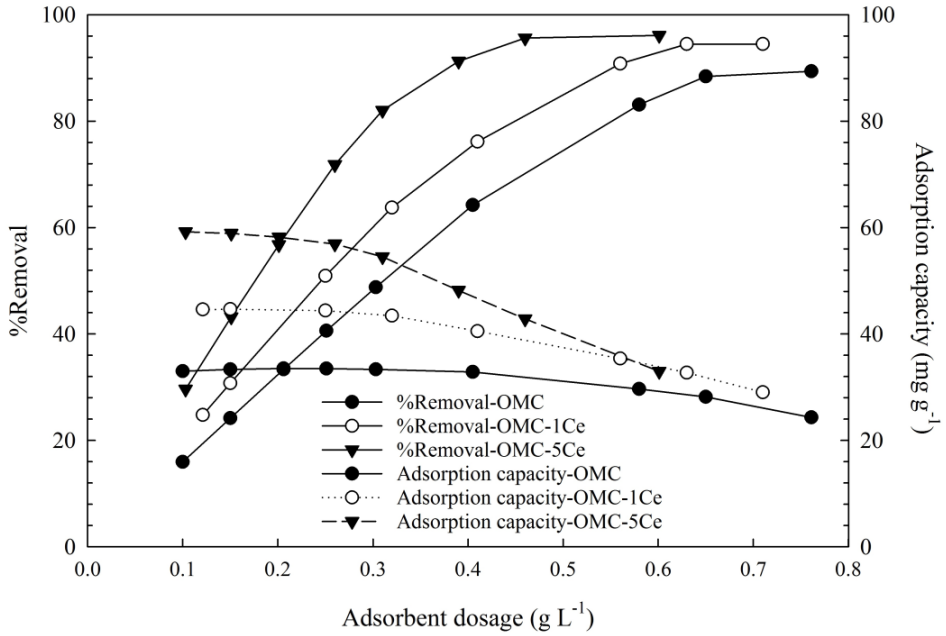

Figure 3.11. Effect of adsorbent dosage on %removal and adsorption capacity of resorcinol onto cerium modified OMCs.

3.4.2.3 Adsorption kinetics. The time dependence of resorcinol adsorption onto the ordered mesoporous carbons was investigated to determine the adsorption equilibrium. The results are shown in **Figure 3.12**. As it can be seen from **Figure 3.12**, the adsorption of resorcinol was accomplished in two distinct steps: a relatively faster step (steep slope) continuing up to 10 hr, followed by slower one to the equilibrium state. A contact period of 24 hr was required to reach the equilibrium for the adsorption process. The high initial uptake rate is attributed to the availability of higher number of active sites for resorcinol adsorption at the onset of the process. In addition, textual properties of OMCs allow resorcinol to penetrate though the pores, also known as intra-particle diffusion (Borah et al., 2009), and prompt the adsorption process at the active sites on the pore surfaces.

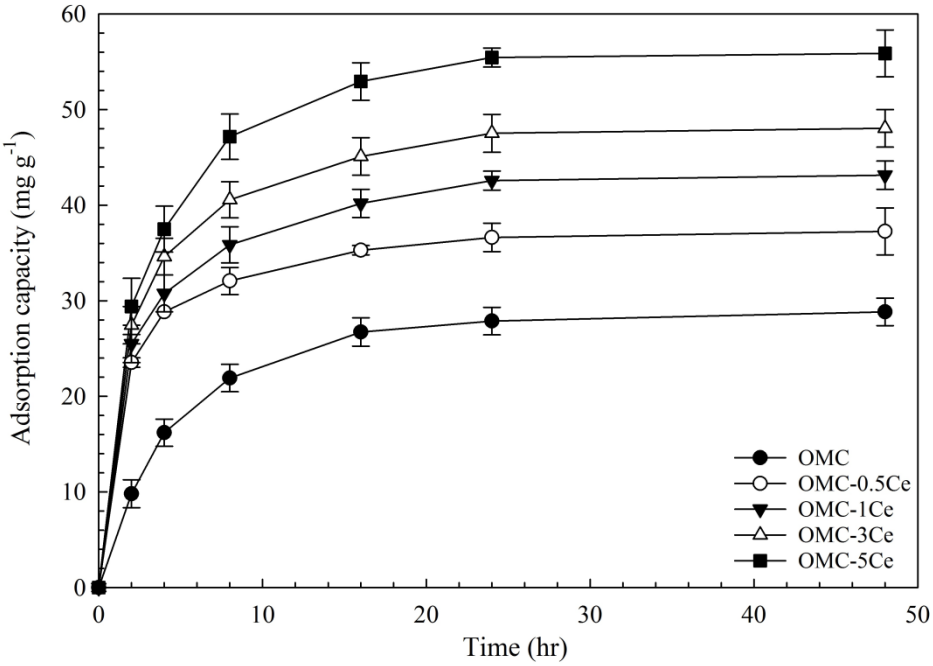

Figure 3.12. Effect of contact time on resorcinol uptake by OMCs (C_0: 20 mg L^{-1}, T: 25 ºC, pH: 6.5, Adsorbent dosage: 0.1 g L^{-1}).

3.4.2.4 Adsorption kinetics models. Data generated from the batch experiment study were fitted to the Pseudo-First-Order, Pseudo-Second-Order, Elovich and Intra-Particle Diffusion Models. The fitted data are presented in **Figure 3.13(a)-(d)**. The kinetic parameters are listed and compared in **Table 3.3**. All these data suggest that resorcinol adsorption could be better represented by the Pseudo-Second-Order kinetic model in terms of its higher correlation coefficients compared to Pseudo-First-Order kinetic and Elovich models, implying that the resorcinol adsorption on cerium modified OMCs is likely to be chemisorption (Chen et al., 2011). In addition, the adsorption capacity calculated from Pseudo- Second-Order kinetic model fitting data was found to be closer to the experimental observations. Similar observations were reported by Ding et al. (2017) for the adsorption of resorcinol onto cellulose functionalized with magnetic polydopamine.

Table 3.3. Coefficients of Pseudo-First-Order, Pseudo-Second-Order, Elovich Kinetic and Weber-Morris Intra-particle Diffusion Models for resorcinol adsorption onto OMCs.

Models	Parameters	OMC	OMC-0.5Ce	OMC-1Ce	OMC-3Ce	OMC-5Ce
Pseudo-First-Order	$q_{e(exp)}$ (mg g^{-1})	28.85	37.25	43.14	48.04	55.88
	$q_{e(cal)}$ (mg g^{-1})	22.06	18.25	24.38	27.98	39.21
	k_1 (hr^{-1})	0.136	0.140	0.150	0.160	0.180
	R^2	0.9890	0.9975	0.9848	0.9850	0.9888
Pseudo-Second-Order	$q_{e(cal)}$ (mg g^{-1})	31.34	38.49	44.84	50.00	58.48
	k_2 (g mg^{-1} hr^{-1})	0.0090	0.0170	0.0130	0.0119	0.0110
	R^2	0.9986	0.9998	0.9997	0.9998	0.9996
Elovich	α (mg g^{-1} hr^{-1})	0.5258	15.8680	8.1280	6.0565	2.0940
	β (g mg^{-1})	6.2265	4.7750	5.8658	6.7179	8.8392
	R^2	0.9374	0.9470	0.9569	0.9404	0.9279
Intra-Particle Diffusion	K_{diff} (mg g^{-1} $hr^{-1/2}$)	2.9850	2.5377	3.1350	3.5504	4.6450
	I (mg g^{-1})	10.590	22.457	24.804	27.490	29.307
	R^2	0.7063	0.8044	0.822	0.7900	0.7706

Furthermore, intra-particle diffusion may have contribution to the high initial uptake rate. Since neither Pseudo-First-Order nor Pseudo-Second-Order can determine the rate limiting step and diffusion mechanism, the data obtained from the batch experiment study were further subjected to analysis following the Intra-particle diffusion model as shown in **Figure 3.13(d)**. As can be seen in **Figure 3.13(d)**, the plot of q_t vs $t^{1/2}$ shows multi-linearity over the entire range of reaction time, implying that intra-particle diffusion was not the only rate determining step. The high initial uptake rate from 0 to 4 $hr^{1/2}$ due to higher concentration gradient between the adsorbent and the adsorbate on the external surface was controlled by surface adsorption. Once reached the saturation, resorcinol began to enter the

pores of OMC and was adsorbed by the interior surface, where intra-particle diffusion is the rate limiting step. As the intra-particle diffusion started to slow down the adsorption equilibrium was achieved. Therefore, both the surface adsorption as well as intra-particle diffusion contributed to the rate-determining step during the adsorption of resorcinol by cerium modified OMCs.

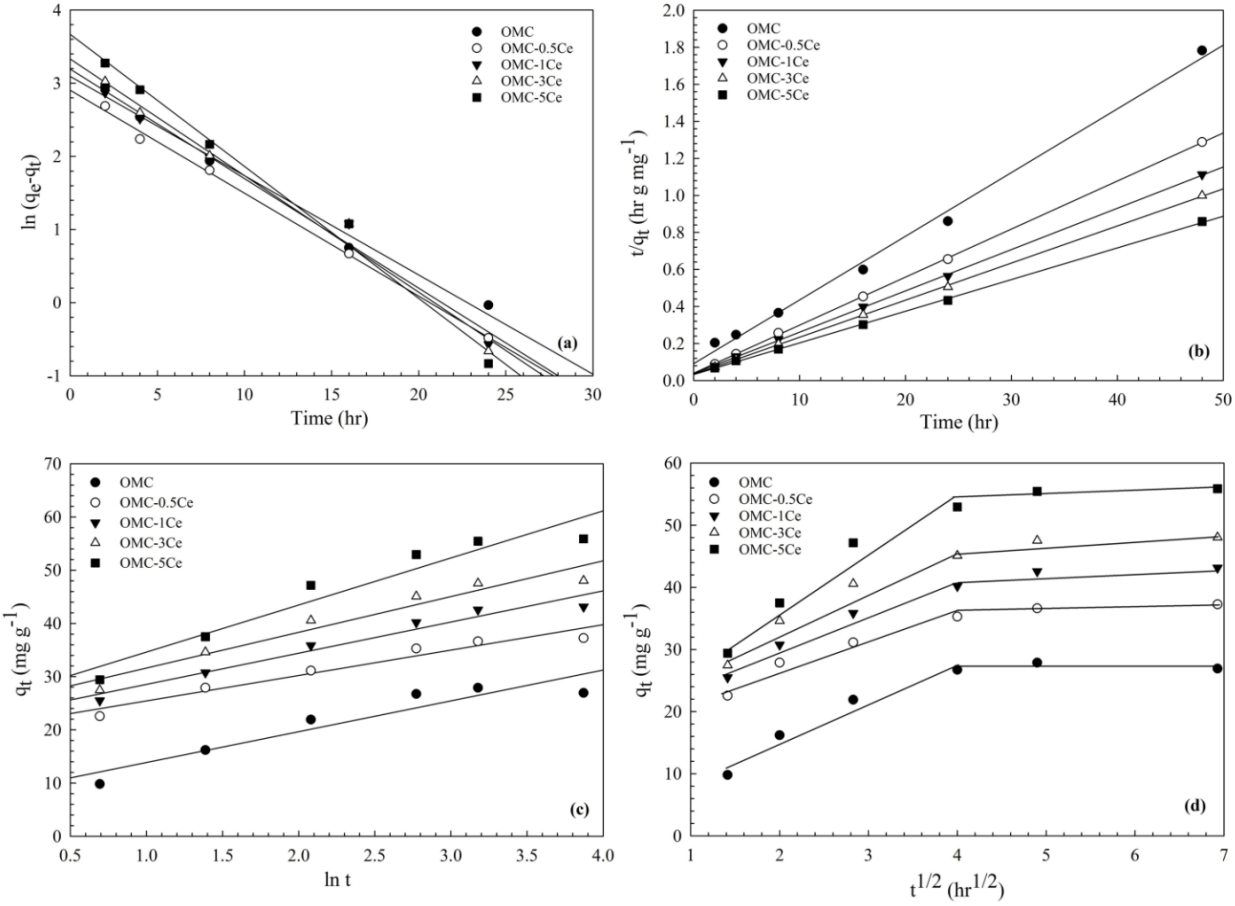

Figure 3.13. Adsorption kinetic models of Resorcinol adsorption onto OMCs (a) Pseudo-First-Order; (b) Pseudo-Second-Order; (c) Elovich; (d) Intra-Particle Diffusion Model.

3.4.2.5 Adsorption isotherms. The efficiency of cerium modified OMCs on the equilibrium adsorption capacity of resorcinol were examined as a function of equilibrium concentration and are depicted in **Figure 3.14**. The amount of adsorbed resorcinol onto the

cerium modified OMCs decreases in the following sequence: OMC-5Ce (60.98 mg g^{-1}) > OMC-3Ce (54.05 mg g^{-1}) > OMC-1Ce (46.08 mg g^{-1}) > OMC-0.5Ce (39.4 mg g^{-1}) > OMC (34.5 mg g^{-1}). This could be attributed to the increased content of cerium doped on the surface of OMC (Goscianska et al., 2014; Goscianska et al., 2015).

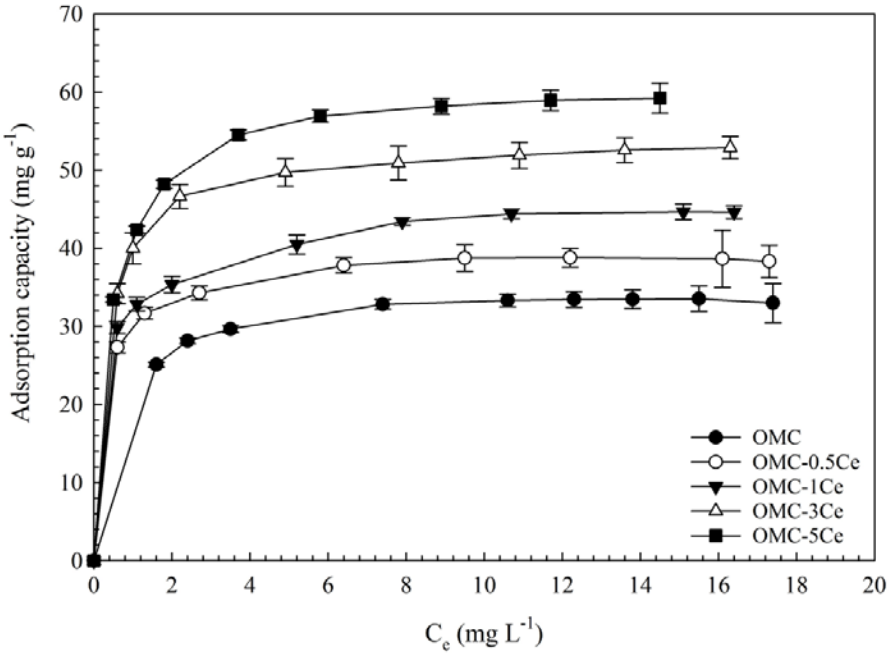

Figure 3.14. Adsorption isotherms of resorcinol onto ordered mesoporous carbon (C_0: 20 mg L^{-1}, T: 25 ºC, pH: 6.5, Contact time: 24 hr).

The adsorption isotherm, also known as equilibrium data, reveals the mechanism of interaction between adsorbent and adsorbate and the adsorption capacity of the adsorbent. Hence, the correlation of equilibrium data with a theoretical or empirical equation is essential for the interpretation of adsorption process. The equilibrium data for the adsorption of resorcinol onto OMCs were fitted to linear Langmuir and Freundlich Isotherm Models as illustrated in **Figure 3.15(a)-(b)**. The isotherm modeling data are listed and compared in **Table 3.4**. **Table 3.4** shows that the Langmuir Model fitted well with the experimental data with a higher correlation coefficient (R^2). The Langmuir monolayer adsorption capacity

(q_{max}) increased from 34.5 mg g^{-1} to 61 mg g^{-1} as the cerium content increased from 0.5% to 5%. The separation factors, R_L, were found to be in the range of 0.016-0.029 implying that the adsorption of resorcinol onto OMCs is favorable.

Table 3.4. Parameters calculated from adsorption isotherm of resorcinol onto parent OMC and modified OMCs.

Models	Parameters	OMC	OMC-0.5Ce	OMC-1Ce	OMC-3Ce	OMC-5Ce
Langmuir	q_{max} (mg g^{-1})	34.5	39.4	46.08	54.05	60.98
	K_L (L mg^{-1})	1.98	3.57	2.04	2.64	2.21
	R_L	0.028	0.016	0.029	0.023	0.031
	R^2	0.9994	0.9997	0.9996	0.9996	0.9999
Freundlich	K_F (mg g^{-1})(L $mg^{-1})^{1/n}$)	25.106	30.200	32.400	39.300	41.030
	1/n	0.1115	0.0991	0.126	0.1204	0.1619
	R^2	0.8997	0.9231	0.981	0.9049	0.9114
D-R	q_m (mg g^{-1})	33.38	37.86	42.51	51.40	56.73
	β (mol^2 J^{-2})	3×10^{-8}	1×10^{-8}	0.9×10^{-8}	0.8×10^{-8}	0.7×10^{-8}
	E (kJ mol^{-1})	4.082	7.071	7.453	7.905	8.451
	R^2	0.9862	0.9549	0.9052	0.9855	0.964

The values of K_F and $1/n$ were calculated from the intercept and slope of the plot of $lnQe$ vs. $lnCe$ as shown in **Figure 3.15(b)**. K_F was found to be 25.1, 30.2, 32.4, 39.3, and 41.03 for OMC, OMC-0.5Ce, OMC-1Ce, OMC-3Ce, and OMC-5Ce, respectively. The n constant describe the ability of the adsorbate to be adsorbed on the surface. The calculated values of n are 8.9, 10.1, 7.9, 8.3, and 6.2 for OMC, OMC-0.5Ce, OMC-1Ce, OMC-3Ce, and OMC-5Ce, respectively. The values of n were larger than 1 indicating a favorable adsorption of resorcinol onto the prepared OMCs (Chen et al., 2011). In addition, the mean free energy of adsorption, E, obtained from D-R Model was in the range of 7.07 to 8.45 kJ mol^{-1} suggesting the chemical adsorption to be the dominating mechanism with minimum

physiosorption (Konggidinata et al., 2017a). The theoretical adsorption capacity calculated based on D-R Model was close to the Langmuir monolayer adsorption capacity (q_{max}).

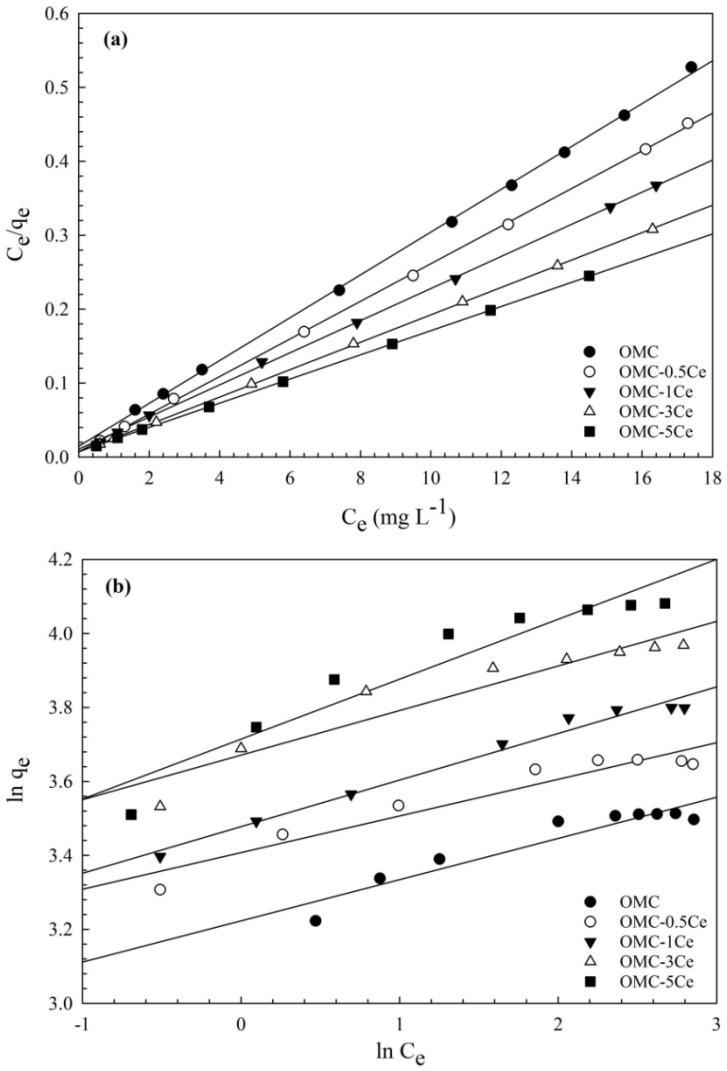

Figure 3.15. Adsorption Isotherm of OMC (a) Langmuir Model; (b) Freundlich Model.

3.5 Conclusion

Ordered mesoporous carbon COK-19 was synthesized by the hard template method employing COK-19 silica template for the first time and then doped with cerium(III) chloride. The synthesized materials were used for the adsorption of resorcinol from synthetic wastewater as a model compound. The ordered mesoporous carbons modified with cerium

showed better adsorption capacities than the parent OMC towards resorcinol which can be attributed to the physiochemical properties. The adsorption capacities of different ordered mesoporous adsorbents decrease in the following sequence: OMC-5Ce (60.98 mg g^{-1}) > OMC-3Ce (54.05 mg g^{-1}) > OMC-1Ce (46.08 mg g^{-1}) > OMC-0.5Ce (39.4 mg g^{-1}) > OMC (34.5 mg g^{-1}). Fitting the equilibrium data to different adsorption isotherm models revealed that Langmuir Model was more suitable to represent the adsorption of resorcinol onto OMC materials. Adsorption kinetics was found to follow closely the Pseudo-Second-Order kinetic model.

Acknowledgements

This work was supported by Louisiana Board of Regents (*LEQSF(2015-16)-ENH-TR-32 and LEQSF(2016-17)-RD-C-15*) and University of Louisiana at Lafayette. All the support provided by all the staff of the Energy Institute of Louisiana is also acknowledged for carrying out this research work.

Chapter 4: Neodymium Embedded Ordered Mesoporous Carbon (OMC) for Enhanced Adsorptive Removal of Sunset Yellow: Characterizations, Adsorption Study and Adsorption Mechanism

This work has been published as:

Ahmad, Z.U., Yao, L., Wang, J., Gang, D.D., Islam, F., Lian, Q., Zappi, M.E., 2019. "Neodymium embedded ordered mesoporous carbon (OMC) for enhanced adsorption of sunset yellow: Characterizations, adsorption study and adsorption mechanism", *Chemical Engineering Journal*, 359, 814–826. https://doi.org/10.1016/j.cej.2018.11.174.

Abstract

Discharging coloring products in the natural streams has degraded water quality irreversibly over the past several decades. Order mesoporous carbon (OMC) was modified by embedding neodymium(III) chloride for the first time onto the surface of OMC to alleviate these contaminants. The modified OMCs were characterized using nitrogen adsorption-desorption isotherm, scanning electron microscopy (SEM), transmission electron microscopy (TEM), fourier transform infrared (FT-IR) spectra, X-ray photoelectron spectroscopy (XPS). TEM images of neodymium modified OMCs revealed ordered structure. Analysis of FT-IR and XPS spectra revealed the formation of hydroxides coordinated with neodymium(III). In the lower pH region, the modified OMCs have positively charged sites for adsorption of anionic sunset yellow. Adsorption kinetics displayed the adsorption of sunset yellow were better fitted with Pseudo-Second-Order kinetic model than Pseudo-First-Order kinetic model. The adsorption isotherms were well fitted with Langmuir model depicting the formation of monolayer adsorbates onto the surface of OMC-Nd. The maximum monolayer adsorption capacity of 285.7 mg g^{-1} was observed for OMC-2Nd. The overall adsorption capacity was increased by 40% compared to the virgin OMC. The interaction mechanism involved ligand exchange between Nd-modified OMC and sunset yellow.

4.1 Introduction

The widespread application of synthetic dyes in various manufacturing process such as rubber, textiles, cosmetics, leather, paper and food processing industries has led to serious environmental problems and created global concern (Liu et al., 2011; Gupta, 2009). It has been estimated that 1.6 million tons of dyes are produced on an annual basis and 10-15% of this volume is discharged into the watercourses (Tan et al., 2015). Most of the dyes with

synthetic origin and complex aromatic structure are resistant to light, heat and oxidizing agents and usually non-biodegradable (Kono, 2015; Buthelezi et al., 2012). The discharge of colored substances into the aquatic ecosystems limits the process of photosynthesis by hindering with the transmission of sunlight to the benthic organisms (Ghaedi et al., 2015). The presence of these coloring substances also reduces the aesthetic value of an aquatic system and contributes to higher chemical oxygen demand (COD) (Yagub et al., 2014; Ngulube et al., 2017). In addition, these dyes have detrimental effects on human health as their metabolites are mutagenic and carcinogenic (Koupaie et al., 2011; Alver and Metin, 2012). Therefore, it is of paramount importance to remove these dyes from industrial wastewater by selecting an appropriate method to ensure safe disposal of treated effluent into natural streams.

Various treatment technologies have been developed and employed to remove pollutants from wastewaters before discharging into the environment. The techniques employed for treating wastewater include coagulation-flocculation process (Chafi et al., 2011), chemical precipitation (Kurniawan et al., 2006), ion exchange (Xing et al., 2007), membrane filtration (Alventosa-de Lara et al., 2012; Omi et al., 2017), electrochemical decolorization (Körbahti et al., 2011), photocatalytic degradation (Rajamanickam and Shanthi, 2014; Rajamanickam et al., 2015), chemical oxidation (Ghoneim et al., 2011; Sultana et al., 2018), biodegradation (Pajootan et al., 2012) and adsorption (Zhang et al., 2014; Varaprasad et al., 2017; Ahmad et al., 2019a; Ahmad et al., 2019b). These methods have several shortcomings, although these methods have been applied extensively, for example, high initial cost of setting, operation costs, generation of excess amount of sludge during chemical coagulation, inactivation of microorganism due to high toxicity of dyes

during biodegradation, production of toxic organochlorine compounds during oxidation (Tan et al., 2015; Ngulube et al., 2017). Knowing the shortcoming associated with these methods, adsorption is the most favorable wastewater treatment technique in terms of the low initial costs, simplicity of design and operation, and production of non-toxic compounds (Tang et al., 2014a; Sivashankar et al., 2014).

Researchers have focused on the synthesis and modification of different adsorbents for dye removal, such as activated carbon (Kumar et al., 2018), carbon nanotubes or CNTs (Gupta et al., 2013), nano-Fe_3O_4 encapsulated CNTs (Madrakian et al., 2011), Fe_3O_4 and hydrophilic guar gum-grafted CNTs (Yan et al., 2012), silica gel (Escobar et al., 2015), metallic nanomaterials (Salehi et al., 2010) and clay materials (Yan et al., 2015). The adsorption capacity of stevensite-rich clay for methyl violet removal was 625 mg g^{-1} (Elass et al., 2011). Magnetic multi-walled CNT-Fe_3C nanocomposite was synthesized to study the adsorption process of Direct Red 23 (DR23) from aqueous solution (Konicki et al., 2012). The maximum adsorption capacity was found to be 172.4 mg g^{-1} for DR23 and adsorption kinetics was found to follow pseudo-second-order kinetic model. Chitosan was modified by Kyzas et al. (2011) to increase the adsorption of real effluents from dyeing reactor. The imino grafted chitosan with a dosage of 5 g L^{-1} brought the residual dye content below the acceptable level. Activated carbon based adsorption has been extensively used for discoloration of wastewater. Wide pore size distribution and a majority of micropores (< 2 nm) are often attributed to the low adsorption capacity (Walker and Weatherly, 2001; Ahmad et al., 2018).

This study is focused on ordered mesoporous carbon (OMC), a relatively new member of carbonaceous family, with high BET surface area (up to 2000 m^2 g^{-1}), tunable

pore size, large pore volume, high thermo-mechanical stability (Guo et al., 2013; Ren et al., 2016; Shou et al., 2016; Chao et al., 2017). Tian et al. (2011) modified CMK-5 with 4-acetophenone oxime to increase the adsorptive removal of uranium(VI) which yielded maximum U(VI) adsorption capacity of 65.2 mg g^{-1}. Galán et al. (2013) synthesized mesoporous carbon MCSG60 to study the adsorption behavior of three reactive dyes (Naphthol Blue Black, NBB; Reactive Black 5, RB5; and Remazol Brilliant Blue R, RBBR). The maximum adsorption capacity was 270 mg g^{-1}, 270 mg g^{-1}, and 280 mg g^{-1} for NBB, RB5, RBBR, respectively.

Tang et al. (2014) introduced cobalt nanoparticles onto OMC to enhance rhodamine B (RB) removal. Dong et al. (2012) reported ferromagnetic OMC for removal of rhodamine B with an adsorption capacity of 768 mg g^{-1}. The incorporation of metals into ordered mesoporous carbon for enhanced adsorption performance is gaining rapidly growing interest. It has been reported that the lanthanide ions possess affinity towards organic compounds through the interaction of f-orbitals (Goscianska et al., 2014; Goscianska et al., 2015). Neodymium, a rare earth metal from lanthanum group, was used to modify chitosan to remove fluoride anionic species through ligand exchange mechanism (Yao et al., 2009). In this study, neodymium(III) chloride ($NdCl_3$) was incorporated into OMC through an incipient wetness technique to enhance sunset yellow (SY) removal. After comprehensive characterization of modified adsorbents, OMCs were used as adsorbents to remove anionic sunset yellow from aqueous solution. The adsorption capacities were estimated by batch adsorption experiments and adsorption kinetics and adsorption isotherms were used to evaluate the adsorption mechanism.

4.2 Materials and Methods

4.2.1 Chemicals. The triblock copolymer surfactant, Pluronic P123 (MW = 5800, $EO_{20}PO_{70}EO_{20}$, EO = ethylene oxide, PO = propylene oxide), silica source tetraethyl orthosilicate (TEOS, 98%) and hydrofluoric acid (48%) were purchased from Sigma-Aldrich. Hydrochloric acid (37%), sucrose, and sulfuric acid (98%) were purchased from Fisher Scientific. Neodymium(III) chloride (anhydrous powder, ≥99.99%) was also purchased from Sigma-Aldrich for surface modification.

4.2.2 Preparation of SBA-15. The mesostructured SBA-15 silica template was synthesized following conventional hydrothermal method under acidic condition using Pluronic P123 as the surfactant and tetraethyl orthosilicate (TEOS, 98%) as the silica source as reported in the literature with modification of reaction temperature and time (Zhao et al., 1998). Typically, 100 mL of concentrated hydrochloride acid (HCl, 37%) was added into the 525 mL of distilled water. 20 g of triblock copolymer Pluronic P123 was added into the aqueous solution. The solution was stirred for approximately 2 h until all the P123 was completely dissolved. Next, 46.5 mL of TEOS was added to the homogenous solution with vigorous stirring for 10 min. The resulting mixture was placed in a constant temperature water bath for 4 h at 40 °C, followed by aging for 24 h at 90 °C. After the aging was done, the solid product was washed with 80-90 °C hot distilled water, and dried in an oven at 105 °C overnight. After drying, the product was calcined in a muffle furnace at 550 °C for 8 h. The white silica template SBA-15 was obtained and stored in the desiccator for the next preparation of OMC.

4.2.3 Preparation of OMC. OMC was synthesized following traditional nanocasting method or hard template method as reported previously (Konggidinata et al., 2017).

Typically, 1.5 g of sucrose, 4 drops of concentrated H_2SO_4 were mixed with 20 mL of water. After dissolved, 2.0 g of SBA-15 was added to the solution and stirred for 2 h. The resulting mixture was heated in an oven at 100 ºC for 6 h and then 160 ºC for another 6 h. Then, an additional 0.51 g of sucrose, 4 drops of concentrated H_2SO_4, and 10 mL of water were added to the composite and stirred for 2 h. Following the same heat treatment as the previous step, the resulting composite was carbonized at 700 ºC for 8 h under N_2 flow of 100 mL min^{-1}. Afterwards, the silica template was removed using 150 mL of 48% HF solution at room temperature. The obtained product was filtered and washed with 4,000 mL of DI water and finally OMC was obtained.

4.2.4 Preparation of Nd embedded OMC. Incipient wetness method was employed to impregnate ordered mesoporous carbon with an aqueous solution of neodymium(III) chloride ($NdCl_3$) in an amount to obtain 0.5, 1, 1.5, 2, 2.5 wt% metal loading. The samples were dried at 100 °C for 5 h and heated in nitrogen for another 3 h at 400 °C. The samples obtained were denoted as OMC, OMC-0.5Nd, OMC-1Nd, OMC-1.5Nd, OMC-2Nd, OMC-2.5Nd, respectively. The details of synthesis procedure are shown in **Figure 4.1**.

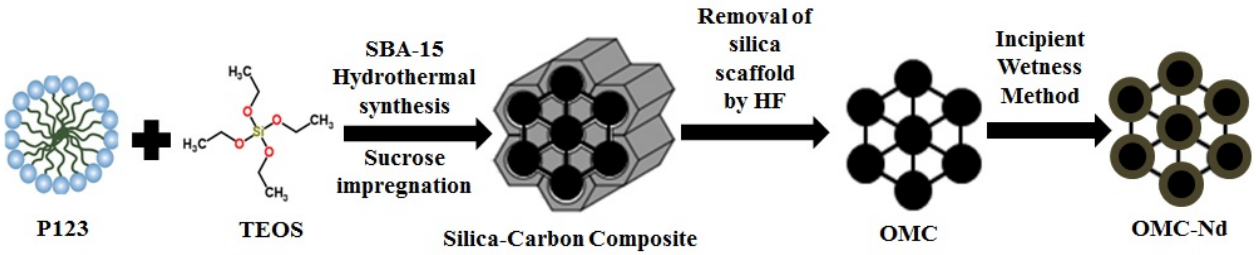

Figure 4.1. Step by step synthesis of OMC-Nd.

4.2.5 Characterization. Nitrogen sorption isotherms were recorded on Micromeritics ASAP 2020 (Accelerated Surface Area and Porosimetry System). Specific surface areas of the samples were calculated using the BET equation, while pore size distribution curves were

calculated by the BJH Method using the adsorption branch. Prior to measurement, OMC was degassed at 300 °C for 6 h under reduced pressure. The total pore volume was obtained from the amount adsorbed at a relative pressure (P/P_0) of 0.99, where P and P_0 are equilibrium and saturation pressure of adsorbate.

TEM images were obtained using a Hitachi 7600 Transmission Electron Microscope. The acceleration voltage used was 100 kV. The samples were prepared by dispersing large number of particles in ethanol with an ultrasonic bath for 45 min and a few drops of the resulting suspension were placed on a 400 mesh Cu grid.

Fourier Transform Infrared (FT-IR) Spectra was obtained in a transmission mode from KBr pellets at room temperature on a Jasco 4700 spectrometer with a resolution of 4 cm^{-1}, using 32 scans per spectrum in the region of 400-4000 cm^{-1}. The mass ratio of OMC to KBr (Potassium Bromide) was kept constant at 1:100.

Energy dispersive X-ray Spectroscopy (EDS) was used to determine the elemental composition of the prepared OMCs. EDS measurements were conducted on a JEOL 6300 Field Emission Scanning Electron Microscope (JEOL Ltd., Tokyo, Japan) using imaging techniques at 15 kV. SEM images were also obtained using the same operating conditions.

4.2.6 Batch adsorption experiments. Batch adsorption experiments were conducted to evaluate the adsorption capacity of sunset yellow FCF onto the OMCs. For that purpose, 100 mL of sunset yellow solution with a concentration of 50 mg L^{-1} was placed in 250 mL conical flasks for both control (without OMC labeled as blank) and experimental (with OMCs and adsorbate) conditions. All the samples were placed in an E24 incubator shaker (New Brunswick Scientific). The shaking speed was maintained at 250 rpm. After adsorption, the conical flasks were removed from the shaker and the solution was filtered

using 0.45 μm glass filter paper. The blank solution was used as a reference to establish the initial concentration for the solutions containing OMCs. The concentration of dye was determined using a Cary 50 UV-visible spectrophotometer (Varian) set at a wavelength of 482 nm. The amount of dye adsorbed by OMCs was determined by subtracting the final concentration from the initial concentration using the following formula:

$$\boldsymbol{Q_e = \frac{(C_o - C_e) \times V}{M}} \quad \textbf{(4.1)}$$

Where Q_e is the adsorption capacity (mg g^{-1}) of the adsorbent at equilibrium, C_o is the initial concentration of resorcinol in the solution (mg L^{-1}), C_e is the final concentration of resorcinol in the treated solution (mg L^{-1}), V is the volume of the solution taken (L), and M is the weight of the adsorbent OMC (g).

4.3 Results and Discussion

4.3.1 Characterization of OMCs. The N_2 adsorption-desorption isotherm of SBA-15 behaved like the representative type IV curve which is typical for the mesoporous materials (Chao et al., 2017). A sharp capillary condensation step was observed in the relative pressure range of 0.65-0.80 as shown in **Figure 4.2(a)**. The sharp capillary condensation step observed in the smaller relative pressure range can be translated to narrow pore size distribution which was further confirmed by the pore size distribution as shown in **Figure 4.2(b)**. N_2 adsorption-desorption isotherm of OMCs were also recorded to investigate the presence of mesoporous structure. The synthesized OMCs exhibited representative type IV isotherm with H2 hysteresis loops depicting the presence of uniform mesoporous structure as shown in **Figure 4.3** (Tang et al., 2014a). Relatively broader pore size distributions were observed for parent OMC and modified OMCs as shown in **Figure 4.4**. These pore size distributions were centered around 7-8 nm for all the synthesized OMCs.

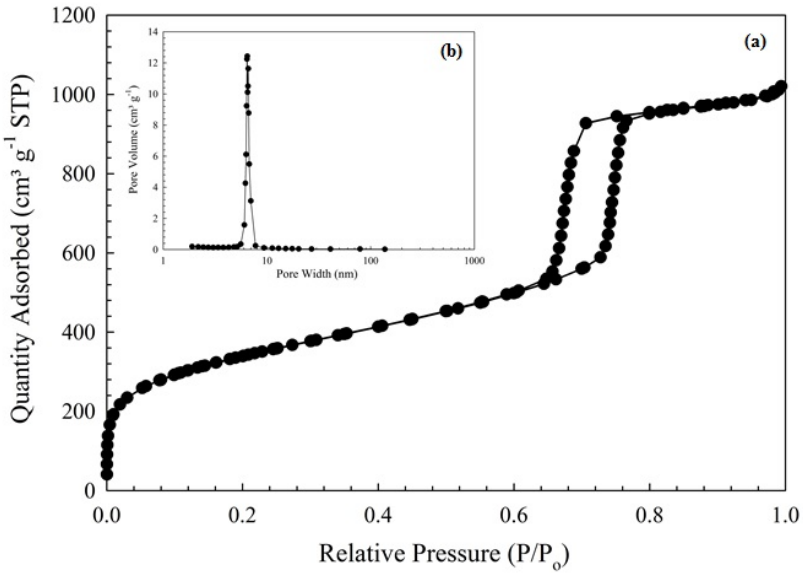

Figure 4.2. (a) Nitrogen adsorption-desorption isotherm of SBA-15 (b) corresponding pore size distribution.

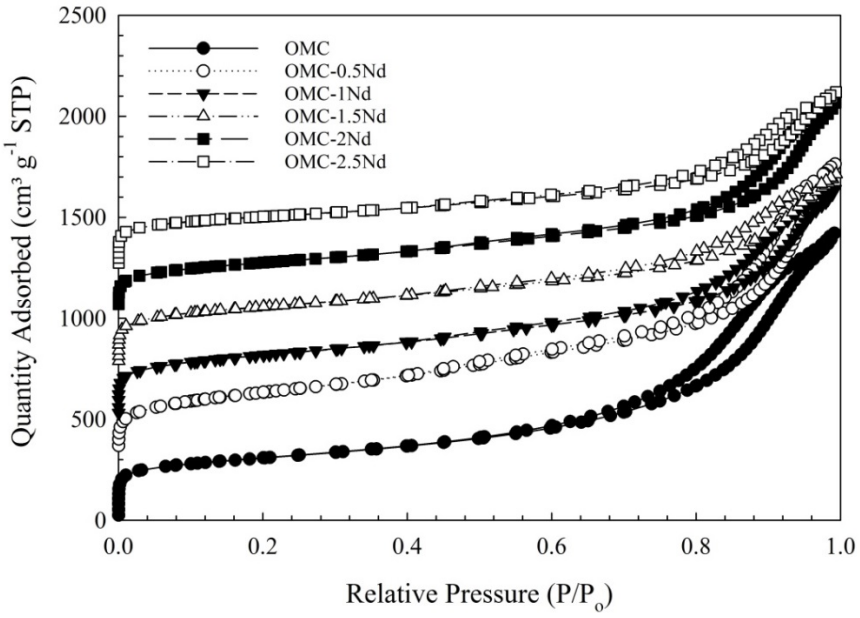

Figure 4.3. N_2 adsorption-desorption isotherms of OMCs. The sorption isotherms for the OMC-0.5Nd, OMC-1Nd, OMC-1.5Nd, OMC-2Nd, OMC-2.5Nd have been vertically shifted by 250, 500, 750, 1000 and 1250 $cm^3\ g^{-1}$, respectively.

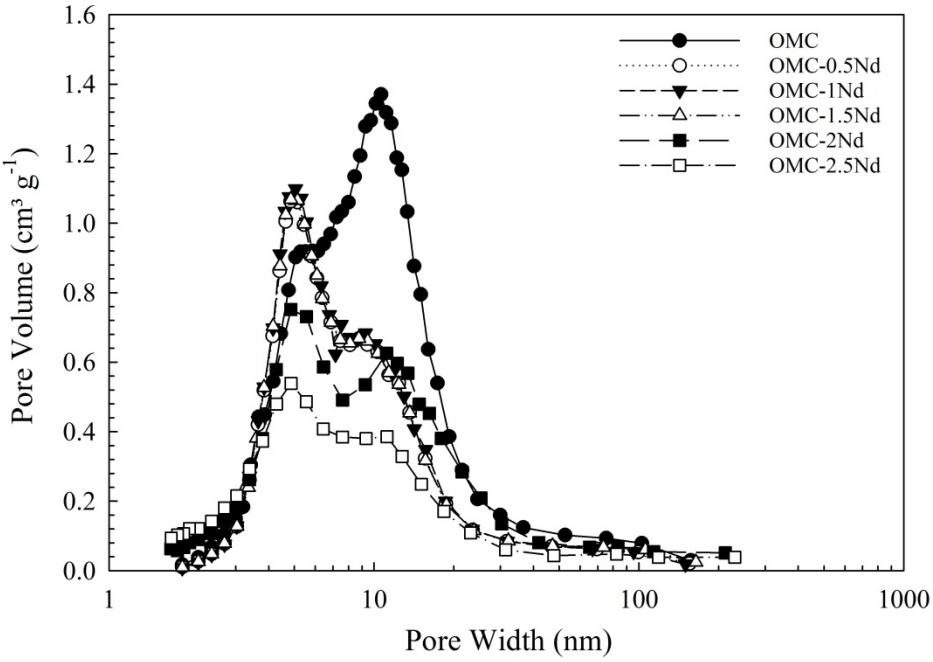

Figure 4.4. Pore size distribution of OMCs.

Table 4.1 summarized the corresponding textual parameters of parent OMC and modified OMCs. The parent OMC exhibited the largest BET surface area of 1396.20 m^2 g-1, with pore size of 8.2 nm and pore volume of 1.89 cm^3 g^{-1}. The incorporation of $NdCl_3$ led to a significant decrease in BET surface area (from 1396.20 m^2 g^{-1} to 881.91 m^2 g^{-1}) and pore volume (from 1.89 cm^3 g^{-1} to 1.29 cm^3 g^{-1}). The decrease in BET surface area for OMC-2.5Nd was 37% in comparison to that of the parent OMC. This phenomenon is attributable to the pore blocking. Furthermore, the increased amount of $NdCl_3$ nanoparticles introduced on the surface caused the pore size to decrease from 8.1 nm of OMC-0.5Nd to 7.05 nm of OMC-2.5Nd. Similar observations were reported in the literature (Tang et al., 2014a; Goscianska et al., 2014).

Table 4.1. Textual parameters of OMCs modified with Neodymium(III) Chloride.

Sample	BET Surface Area (m^2 g^{-1})	Total Pore Volume (cm^3 g^{-1})	Average Pore Size (nm)
OMC	1396.2	1.89	8.22
OMC-0.5Nd	1349.61	1.85	8.12
OMC-1Nd	1114.31	1.71	7.65
OMC-1.5Nd	1072.65	1.44	7.44
OMC-2Nd	971.68	1.35	7.27
OMC-2.5Nd	881.91	1.29	7.05

The surface morphology of parent OMC and modified OMCs was revealed by the SEM images as shown in **Figure 4.5(a)** to **Figure 4.5(f)**. After introducing neodymium on the support surface, smooth surfaces were produced with reduced number of cracks on the carbon surface as the metal content increased from 0.5% to 2.5%. All these observations were in the agreement with the decrease in BET surface area and reduced pore volume (Zhang et al., 2008). Combined with the EDS map scanning of OMC and modified OMCs as shown in **Figure 4.6(a)** to **Figure 6(e)**, Neodymium was found to be distributed on the support surface.

TEM images of parent OMC and modified OMCs are shown in **Figure 4.7(a)** to **Figure 4.7(e)**. Parent OMC has highly ordered structure compared to the modified OMCs. OMCs modified with neodymium(III) chloride showed less ordered structure. As the metal content increased from 0 to 2.5%, more neodymium was deposited on the surface and pores were further clogged, resulting in smooth surfaces. All these observations were in good agreement with the decrease in BET surface area and pore volume (Goscianska et al., 2015).

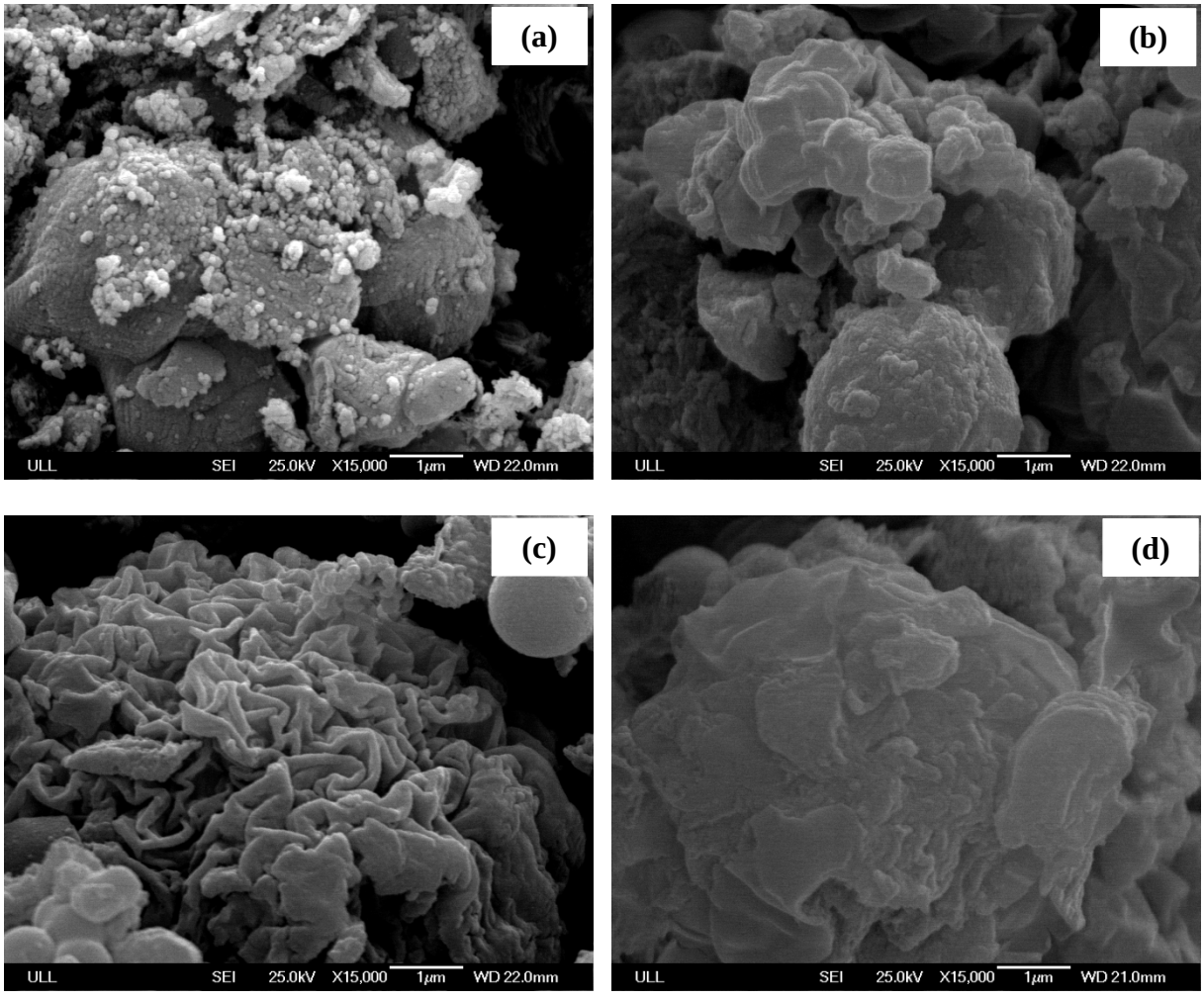

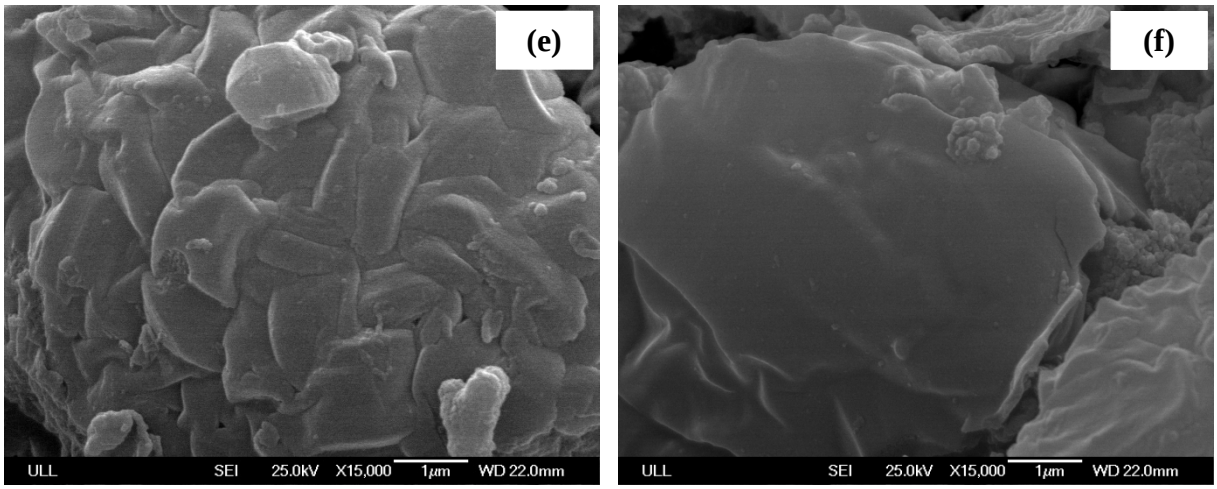

Figure 4.5. SEM micrographs of (a) OMC (b) OMC-0.5Nd (c) OMC-1Nd (d) OMC-1.5Nd (e) OMC-2Nd (f) OMC-2.5Nd.

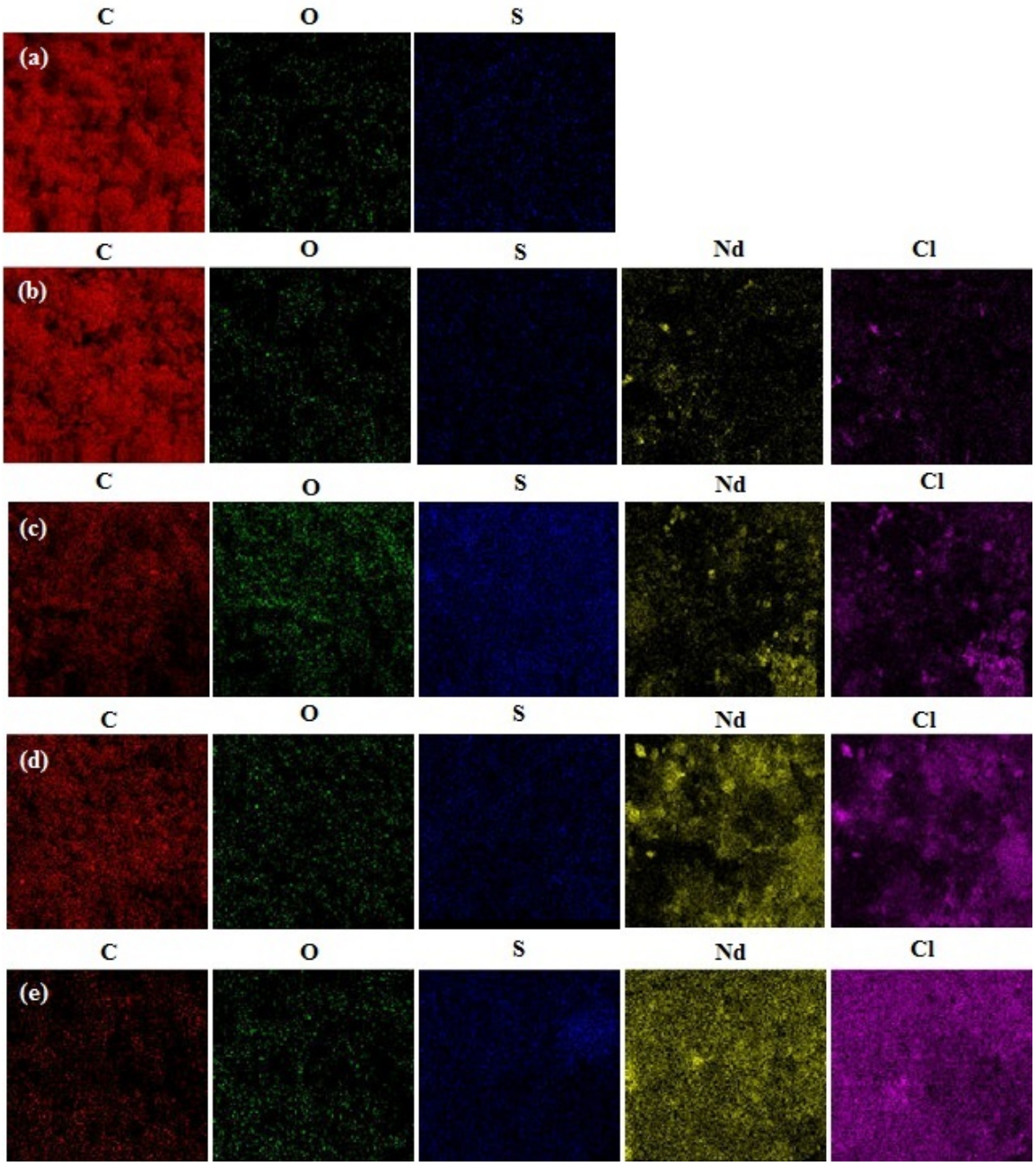

Figure 4.6. EDS map scanning of (a) OMC (b) OMC-0.5Nd (c) OMC-1Nd (d) OMC-1.5Nd (e) OMC-2Nd.

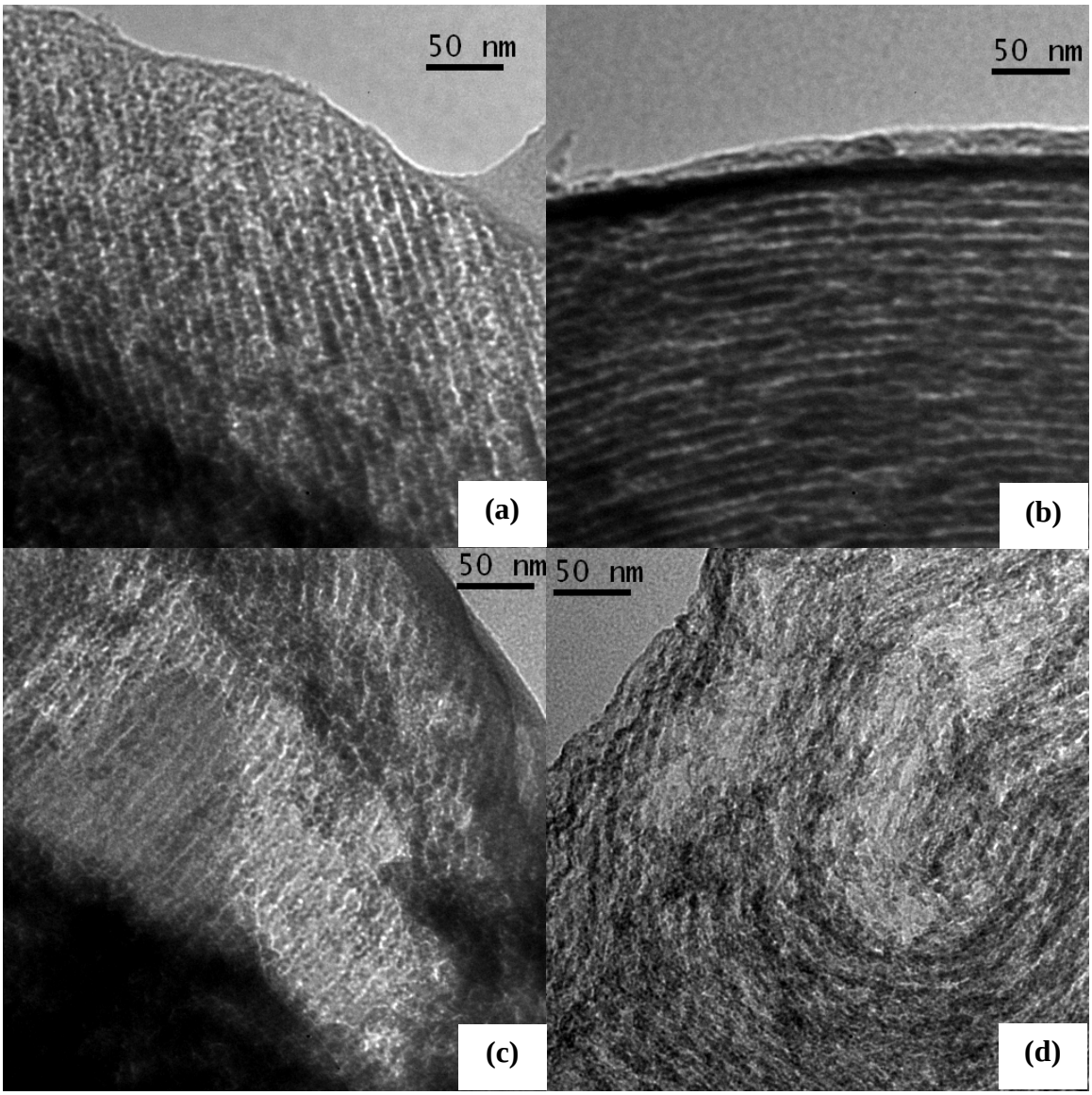

Figure 4.7. TEM micrographs of (a) OMC (b) OMC-0.5Nd (c) OMC-1.5Nd (d) OMC-2Nd.

The functional groups present on the surface of OMC and modified OMCs were investigated by FT-IR analysis as shown in **Figure 4.8**. FT-IR spectra revealed that the modification of OMC affected type of functions groups present on the OMCs. The broad peak around 3462 cm^{-1} can be attributed to the surface adsorbed water and hydroxyl groups (Viswanathan and Meenakshi, 2008). The decrease in the intensities of these bands in the FT-IR spectra of modified OMCs could be attributed to increased content of neodymium

introduced on the support surface. The small peak observed at 1080 cm^{-1} could be attributed to Nd(III) coordinated with hydroxide atom (Yao et al., 2009). The incorporation of neodymium is partly responsible for the depletion of physically-adsorbed water or surface hydroxyl groups in modified OMCs. The peaks appeared at ~540 cm^{-1} can be ascribed to formation of Nd-O in the OMC matrix (Vijayaprasath et al., 2015). A small peak observed at 2346 cm^{-1} could be credited to S–H function group due to the addition of sulfuric acid as a catalyst during the synthesis of OMC (Guo et al., 2013). The peaks around 1620 cm^{-1} could be assigned to C=O stretching in the carboxylic groups (-COOH) (Wang et al., 2010). The small peak observed around 1405 cm^{-1} corresponds to C-H group (Cansado et al., 2012).

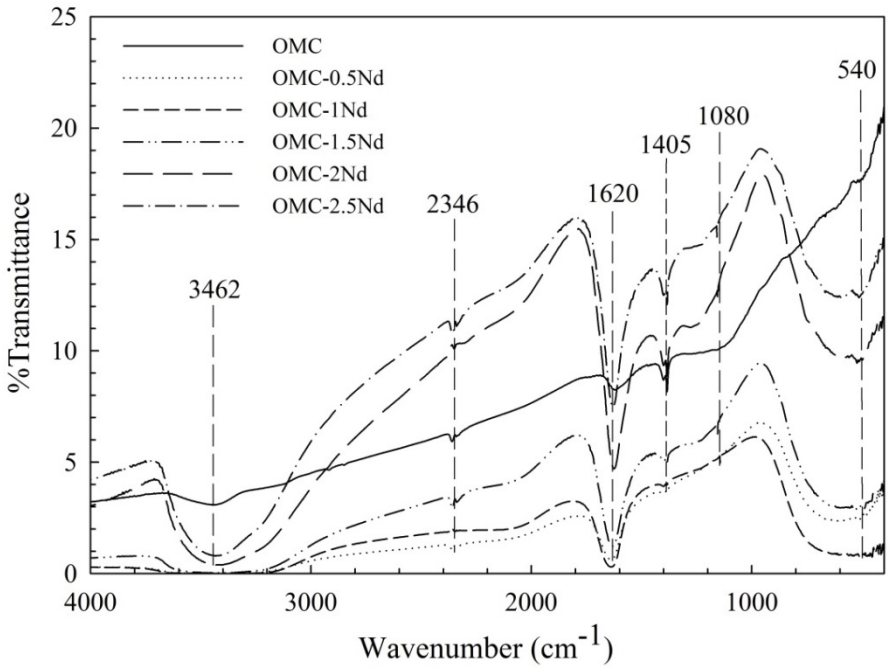

Figure 4.8. FT-IR Spectra of OMC and modified OMCs.

The XPS spectra of OMC-2Nd are shown in the following Figure. The binding energy (BE) was calibrated with carbon C1s peak (284.8 eV). The elements C, O and Nd were identified in the spectra obtained from the survey scan (**Figure 4.9a**). The shifting of signal maxima of C1s was observed after the incorporation of Nd onto OMC. The

deconvolution of C1s peak indicated the presence of surface function groups (C-C, C-O, and C=O at 284.5 eV, 286.0 eV, and 288.5 eV, respectively) which was in good agreement with the FT-IR analysis (**Figure 4.9b and Figure 4.9c**) (Wang and Zhu, 2007). The peaks of Neodymium Nd (3d) usually appears in the range of 980-1010 eV. The peaks at the location of 984.0 eV and 1006.7 eV can be ascribed to Nd $3d_{5/2}$ and Nd $3d_{3/2}$ levels, respectively as can be seen in **Figure 4.9e** which indicate that Nd ions exist as +3 oxidation states in Nd-embedded OMC (Vijayaprasath et al., 2015). Based on the XPS data combined with FT-IR spectra, it can be concluded that Nd had been successfully incorporated in the matrix of OMC. The deconvolution of O_{1s} peak revealed peak centered at 531.8 eV which can be attributed to the formation of Nd(III) coordinated with hydroxides on the surface of OMC as depicted in **Figure 4.9d** (Vijayaprasath et al., 2015). The energy level of O_{1s} at 532.3 eV and 533.8 eV can be attributed with the loosely bound oxygen on the OMC surface due to adsorbed O_2 or H_2O (Coppa and Davis, 2003).

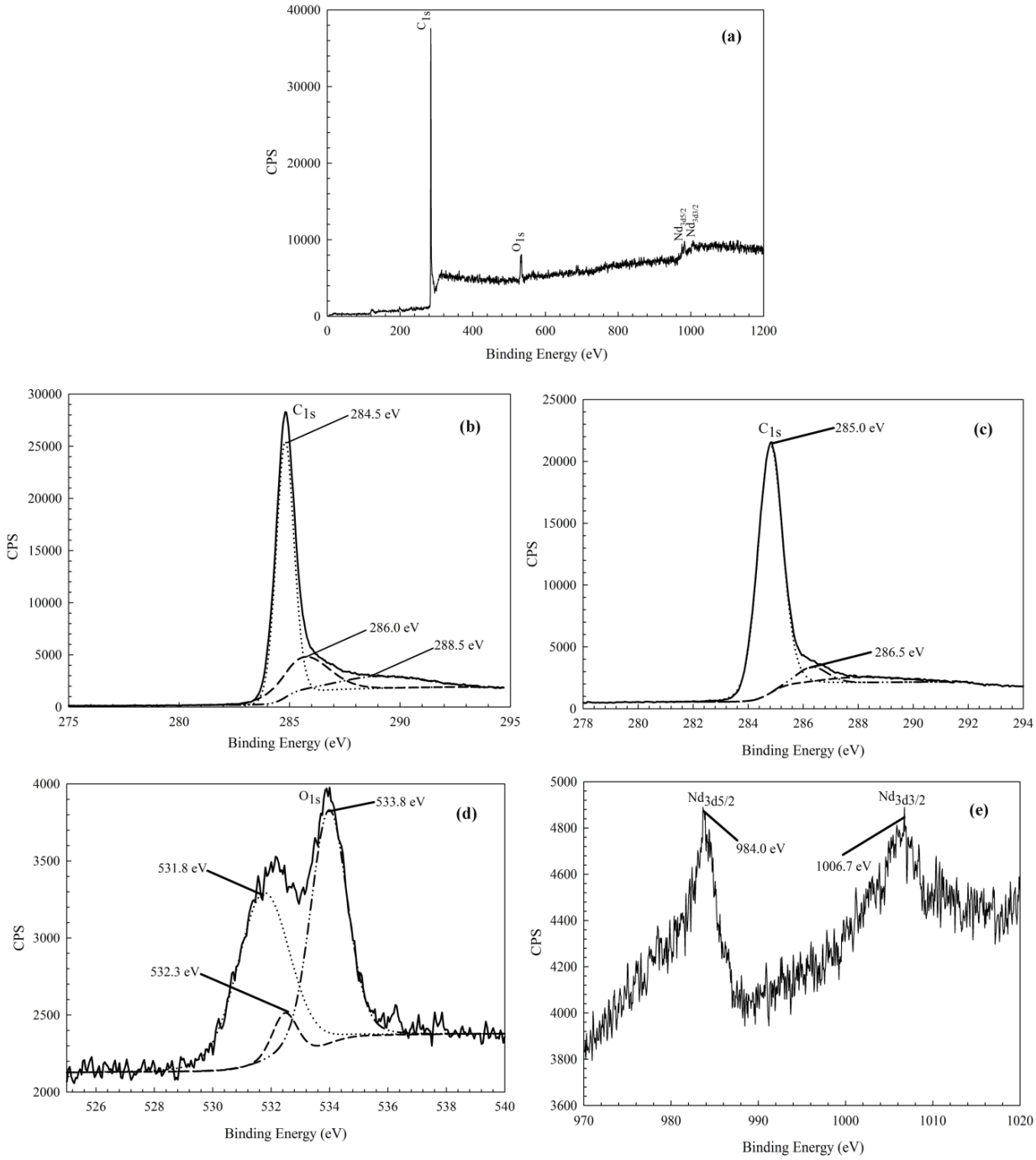

Figure 4.9. XPS Spectra of OMC-2Nd (a) Survey scan of OMC-2Nd (b) C_{1s} of OMC (c) C_{1s} of OMC-2Nd (d) O_{1s} of OMC-2Nd (e) Nd_{3d} of OMC-2Nd.

The results of elemental analysis are represented in **Table 4.2**. The analysis results showed that carbon was the principal element, followed by neodymium. The induced neodymium loading of 0.5%, 1%, 1.5%, 2% and 2.5% caused an increment of neodymium from 11.024% to 45.736%, which further confirmed that Nd particles were successfully embedded into the OMC materials. This was also further confirmed by the EDS spectra as depicted in **Figure 4.10**. The EDS spectra affirmed the presence of all the elements as determined by the elemental analysis.

Table 4.2. Results of Elemental Analysis of OMC-0.5Nd to OMC-2.5Nd.

Sample	%C	%O	%S	%Cl	%Nd
OMC-0.5Nd	66.913	19.809	1.059	1.195	11.024
OMC-1Nd	64.517	9.281	1.322	3.748	21.132
OMC-1.5Nd	51.452	4.77	0.836	9.181	33.76
OMC-2Nd	45.273	4.559	0.805	10.256	39.106
OMC-2.5Nd	35.755	3.455	0.759	14.295	45.736

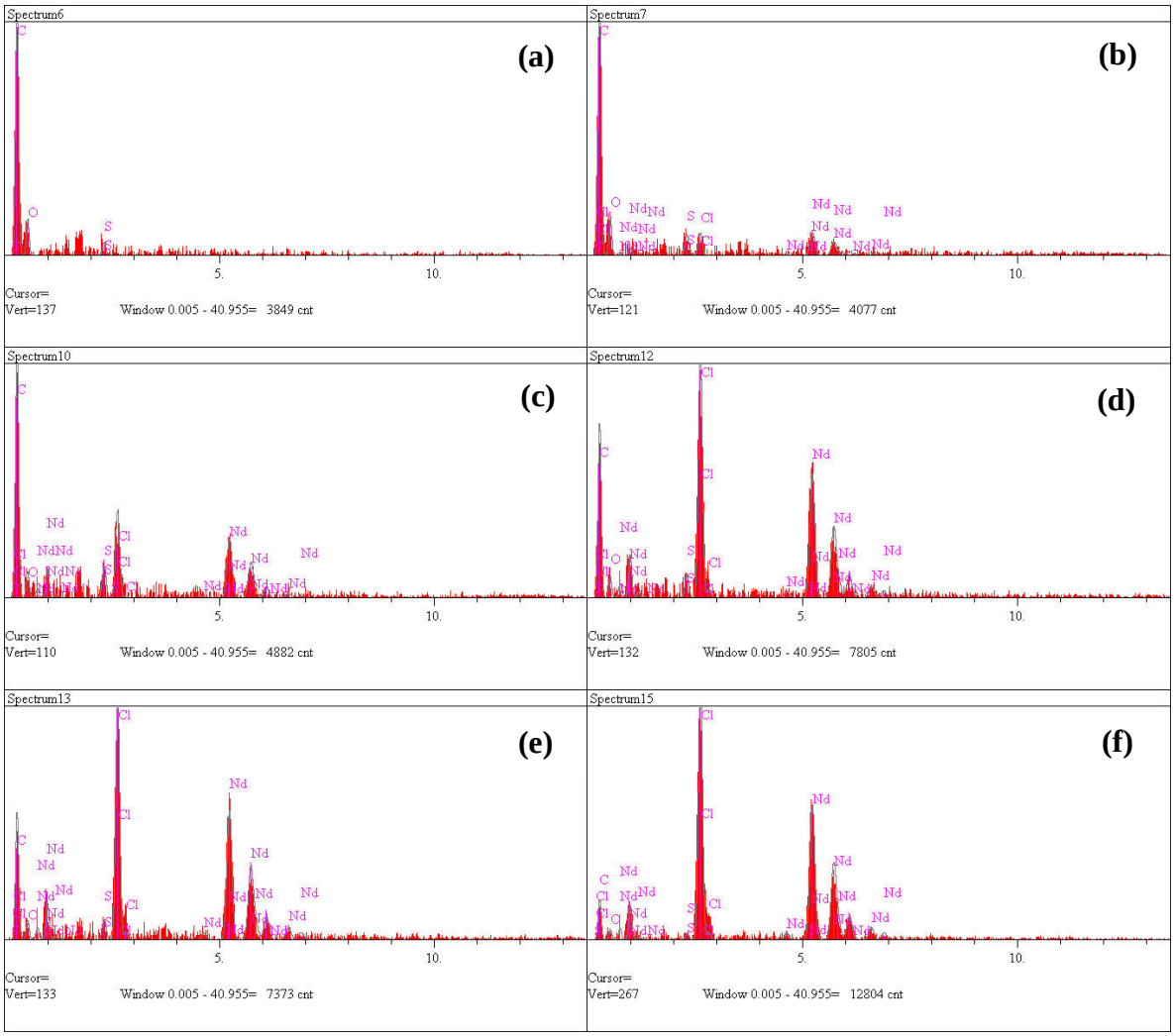

Figure 4.10. Elemental composition of surface modified OMC samples with Neodymium(III) Chloride (a) OMC-0 (b) OMC-0.5Nd (c) OMC-1Nd (d) OMC-1.5Nd (e) OMC-2Nd (f) OMC-2.5Nd.

4.3.2 Adsorption behavior.

4.3.2.1 Effects of neodymium loading on sunset yellow removal efficiency. **Figure 4.11** shows the effects of neodymium dosage on sunset yellow removal efficiency. The highest removal efficiency was obtained at 2 wt% neodymium loading. Then, a slight reduction in the removal efficiency for 2.5 wt% neodymium loading was found, followed by a dramatic decrease in the removal efficiency for 3 wt% neodymium loading. This could be attributed to decreased BET surface area at high Nd loading (881.91 $m^2 g^{-1}$ and 541.94 $m^2 g^{-1}$ for OMC-2.5Nd and OMC-3Nd, respectively) (Zhang et al., 2008).

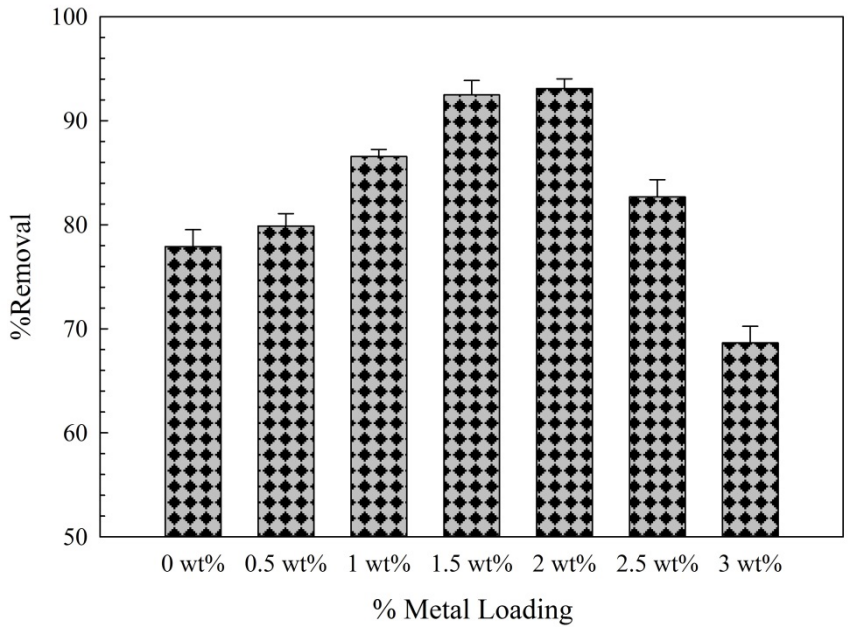

Figure 4.11. Effects of neodymium loading on sunset yellow removal (C_0: 50 mg L^{-1}, T: 25 ºC, pH: 6.5, Contact time: 240 min).

4.3.2.2 Effects of initial pH. The surface charge and protonation of adsorbent can be significantly influenced by the solution pH which could be characterized by the point of zero charge as shown in **Figure 4.12**. The acid-base titration curve gave an estimated value of pHpzc at 7.9. The surface of Nd-modified OMC was positively charged when the solution

pH was below 7.9 and became negatively charged with increasing pH of solution. When pH was in the range of 2-7, the electrostatic attraction was favorable for the adsorption of anionic species sunset yellow. The pH range of 8-10 was not favorable due to the presence of electrostatic repulsion which was against the adsorptive removal of sunset yellow. To have better insight on the influence of pH on adsorptive removal of sunset yellow, the adsorption experiments were conducted at various pH values as shown in **Figure 4.13**. The adsorption capacity was higher at lower pH value which was in accordance with the result of point of zero charge experiment. In the pH range of 2 to 7, the surface of modified OMC became protonated and provided positively charged binding sites for negatively charged sunset yellow and subsequently resulted into higher adsorption capacity. As the pH increased from 8 to 10, the surface became deprotonated and the adsorption capacity decreased due to repulsion. Similar observations were reported by Goscianska et al. (2014).

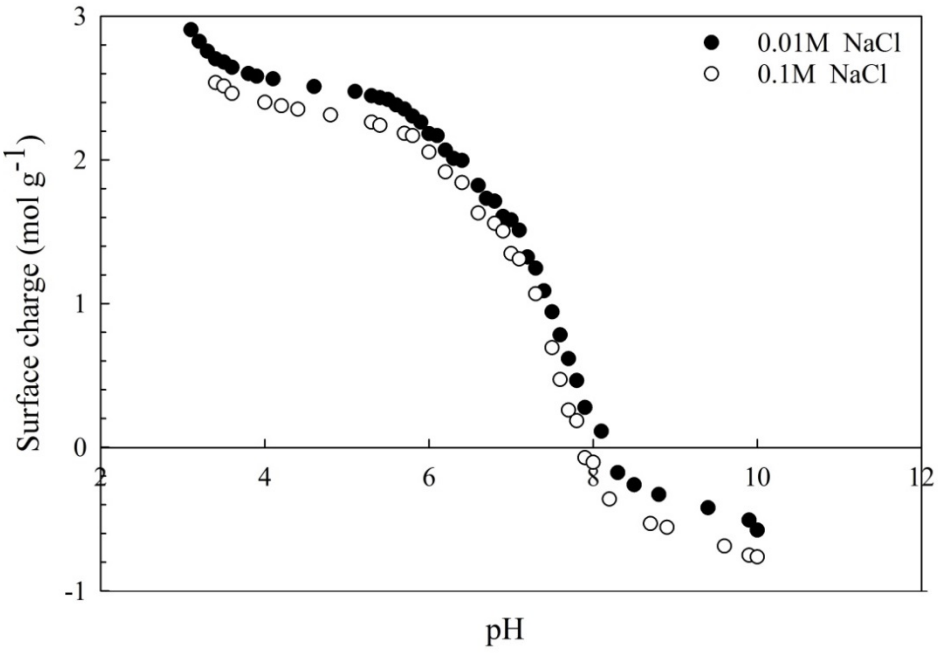

Figure 4.12. Acid-base titration curve for OMC-2Nd under ionic strengths of 0.01M and 0.1M NaCl (solid loading rate: 2 g L^{-1}).

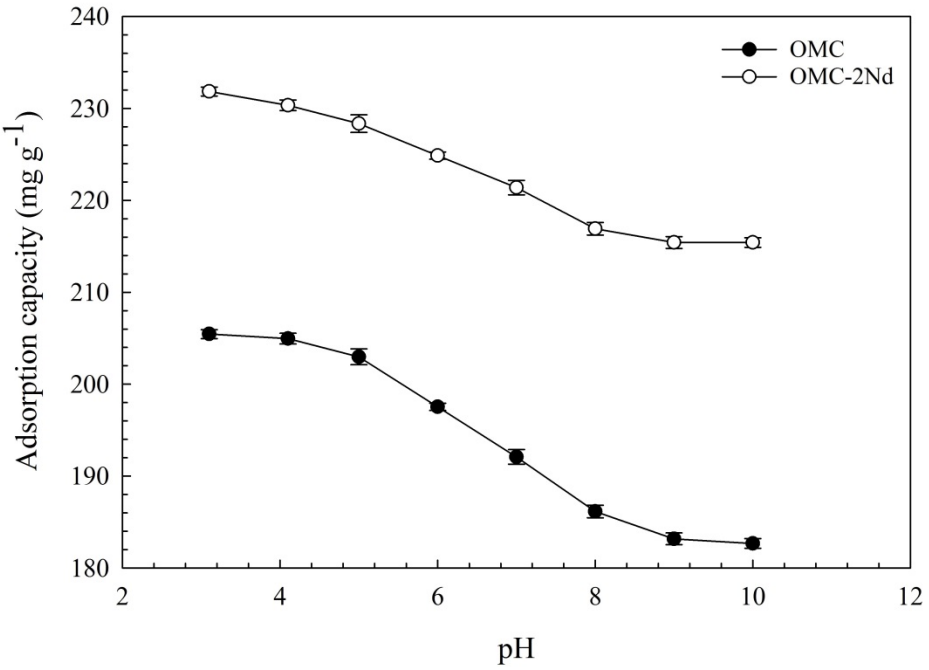

Figure 4.13. Effects of pH on sunset yellow adsorption by modified OMCs (C_0: 50 mg L^{-1}, T: 25 ºC, Adsorbent dosage: 0.2 g L^{-1}, Contact time: 240 min).

4.3.2.3 Adsorption kinetics. The time dependence of sunset yellow adsorption onto the virgin and modified OMCs was investigated to determine the adsorption equilibrium. The results are shown in **Figure 4.14**. The adsorption of sunset yellow was accomplished in two distinct steps: a relatively faster step (steep slope) continuing up to 80 min, followed by slower one to the equilibrium state. The high initial uptake rate is attributed to the availability of higher number of active sites for sunset yellow adsorption at the onset of the process. In addition, textual properties of OMCs allow sunset yellow to penetrate though the pores, also known as intra-particle diffusion and prompt the adsorption process at the active sites on the pore surfaces.

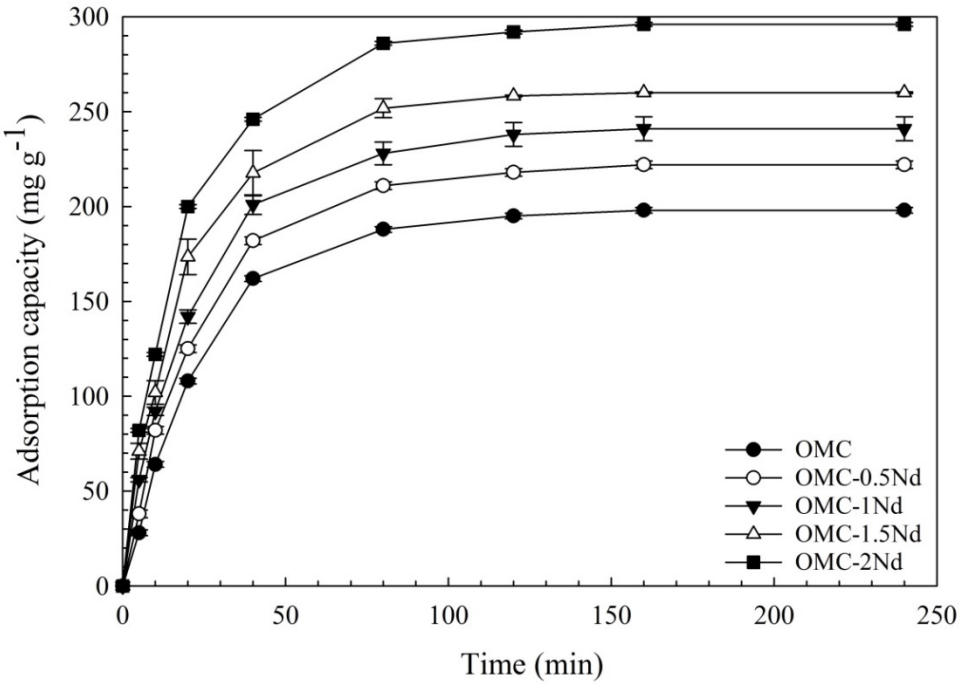

Figure 4.14. Effects of contact time on sunset yellow adsorption by modified OMCs (C_0: 50 mg L^{-1}, T: 25 ºC, pH: 6.5, Adsorbent dosage: 0.1 g L^{-1}, Contact time: 240 min).

4.3.2.4 Adsorption kinetics models. Three kinetic models namely Pseudo-First-Order, Pseudo-Second-Order, and Elovich model were employed to investigate the mechanism involved in the adsorption process. The linear form of these kinetic models can be expressed as follows (Wu et al., 2009; Li et al., 2010; Tang et al., 2014b):

Pseudo-First-Order Kinetic Model: $\boldsymbol{ln(q_e - q_t) = ln(q_e) - k_1 t}$ **(4.2)**

Pseudo-Second-Order Kinetic Model: $\boldsymbol{\frac{t}{q_t} = \frac{1}{k_2 q_e^2} + \frac{t}{q_e}}$ **(4.3)**

Elovich Model: $\boldsymbol{q_t = \beta \ln(\alpha\beta) + \beta ln t}$ **(4.4)**

Where, q_e is the amount of adsorbed sunset yellow at equilibrium (mg g^{-1}); q_t is the amount of adsorbed sunset yellow at any time t (mg g^{-1}); k_1 and k_2 are the adsorption rate constant of Pseudo-First-Order and Pseudo-Second-Order reactions; α and β are the initial adsorption rate (mg g^{-1} min^{-1}) and desorption constant (g mg^{-1}), respectively.

Since Pseudo-First-Order, Pseudo-Second-Order, and Elovich model cannot illuminate on the diffusion mechanism and rate limiting step, Intra-Particle Diffusion model was also employed for investigation. The model developed by Weber and Moris (Borah et al., 2009) is expressed as follows:

$$q_t = K_{diff} t^{1/2} + I \quad \textbf{(4.5)}$$

Where qt is the amount of adsorbate adsorbed on the adsorbent at any time t (mg g^{-1}); K_{diff} is the intra-particle diffusion rate constant (mg g^{-1} $min^{-1/2}$); I is the term that is proportional to the boundary layer thickness (mg g^{-1}).

Data generated from the batch experiment study were fitted to the Pseudo-First-Order, Pseudo-Second-Order, Elovich and Weber-Moris Intra-Particle Diffusion Models. The fitted data are presented in **Figure 4.15(a)-(d)** and the kinetic parameters are listed and compared in **Table 4.3**. The theoretical adsorption capacity calculated from Pseudo-Second-Order kinetic model fitting data were closer to the experimental observations implying that the sunset yellow adsorption onto neodymium modified OMCs is likely to be chemisorption (Tang et al., 2014a).

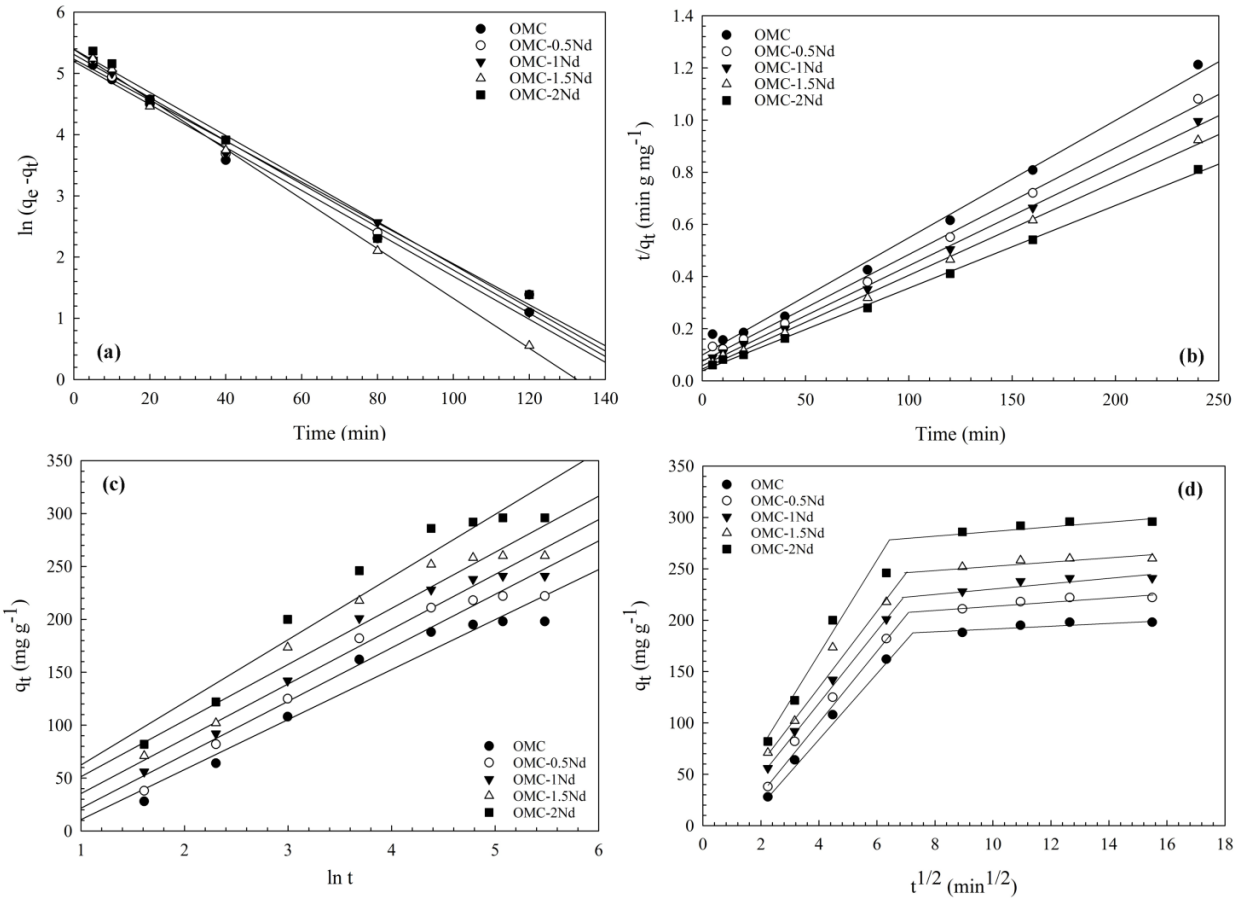

Figure 4.15. Adsorption kinetics models sunset yellow adsorption onto virgin and modified OMCs (a) Pseudo-First-Order; (b) Pseudo-Second-Order; (c) Elovich; (d) Weber-Moris Intra-Particle Diffusion model.

Table 4.3. Coefficients of Pseudo-First-Order, Pseudo-Second-Order, Elovich kinetic and Weber-Moris Intra-particle Diffusion models for adsorption of sunset yellow onto OMCs.

Models	Parameter	OMC	OMC-0.5Nd	OMC-1Nd	OMC-1.5Nd	OMC-2Nd
Pseudo-First-Order	$q_{e(exp)}$ (mg g^{-1})	198.04	222.24	241.52	262.32	296.42
	$q_{e(cal)}$ (mg g^{-1})	191.87	202.33	219.47	187.3	220.24
	k_1 (min^{-1})	0.0356	0.0352	0.0407	0.0334	0.0362
	R^2	0.9960	0.9953	0.9985	0.9897	0.9862
Pseudo-Second-Order	$q_{e(cal)}$ (mg g^{-1})	208.33	227.27	243.9	270.27	294.12
	k_2 (g mg^{-1} min^{-1})	0.0002	0.0003	0.0003	0.0003	0.0004
	R^2	0.9927	0.9962	0.9983	0.9984	0.9989
Elovich	α (mg g^{-1} min^{-1})	102.33	89.65	71.04	54.65	62.42
	β (g mg^{-1})	47.26	50.52	51.78	53.01	59.2
	R^2	0.9449	0.9471	0.9371	0.9332	0.9367
Intra-Particle Diffusion	K_{diff} (mg g^{-1} $min^{-1/2}$)	12.56	13.43	13.79	14.02	15.65
	I (mg g^{-1})	41.75	54.65	69.11	86.78	101.82
	R^2	0.7897	0.7919	0.795	0.7713	0.7746

Furthermore, intra-particle diffusion may have contribution to the high initial uptake rate. The kinetics data obtained from the batch experiment study were further analyzed using the Intra-particle diffusion model as shown in **Figure 4.15(d)**. The plot of q_t vs $t^{1/2}$ shows multi-linearity over the entire range of reaction time, implying that intra-particle diffusion was not the only rate determining step. The high initial uptake rate from 0 to 9 $min^{1/2}$ due to higher concentration gradient between the adsorbent and the adsorbate on the external surface was controlled by surface adsorption. Once reached the saturation, sunset yellow began to enter the pores of OMC and was adsorbed by the interior surface, where intra-particle diffusion is the rate limiting step. As the intra-particle diffusion started to slow down the adsorption equilibrium was achieved. Therefore, both the surface adsorption as well as intra-particle diffusion contributed to the rate-determining step during the adsorption of sunset yellow by neodymium modified OMCs.

4.3.2.5 Adsorption isotherms. The efficiency of neodymium modified OMCs on the equilibrium adsorption capacity of sunset yellow was examined as a function of equilibrium concentration and is depicted in **Figure 4.16**. The amount of adsorbed dye on the modified OMCs decreases in the following order: OMC-2Nd (285.71 mg g^{-1}) > OMC-1.5Nd (263.16 mg g^{-1}) > OMC-1Nd (243.9 mg g^{-1}) > OMC-0.5Nd (222.22 mg g^{-1}) > OMC (204.08 mg g^{-1}). The adsorption capacity increases with the increased content of neodymium(III) chloride for the modified OMCs although they have smaller BET surface area and reduced pore volume which indicates the formation of metal-organic complexes (Ökte and Yilmaz, 2009).

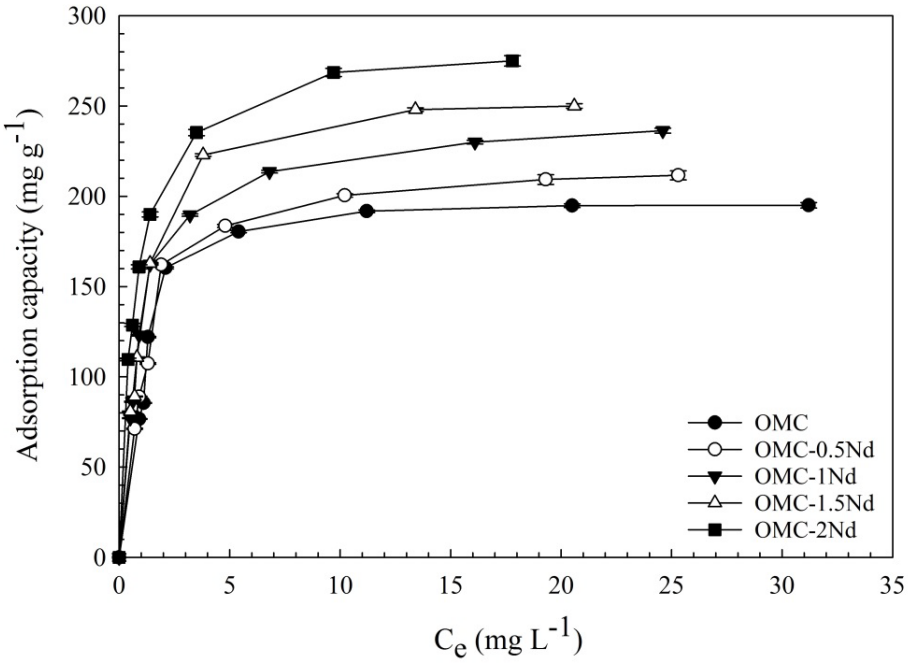

Figure 4.16. Adsorption isotherms of Sunset Yellow onto ordered mesoporous carbon (C_0: 50 mg L^{-1}, T: 25 ºC, Contact time: 240 min).

In order to understand the adsorption process and investigate the adsorption mechanism, four different isotherm models were investigated and correlated with the experimental data namely, Langmuir, Freundlich, Dubinin-Radushkevich, and Temkin model. The Langmuir isotherm model is based on the assumption that formation of a

monolayer adsorbate on the adsorbent surface can be ascribed to maximum adsorption capacity with constant energy (Kaveeshwar et al., 2018). The Freundlich isotherm model is based on multi-layer adsorption and involves the interaction between adsorbed molecules (Niazi et al., 2018). The Dubinin-Radushkevich (D-R) model is also applied to have better understanding of adsorption process. The D-R model involves the adsorption of adsorbate on heterogeneous surface with a non-uniform (Gaussian) distribution of energy (Amosa et al., 2016). Temkin model assumes that the heat of adsorption decreases linearly in the adsorbate-adsorbent interactions layer and uniform distribution of energy (Ali et al., 2017). The linear form of these isotherm models can be expressed as follows:

Langmuir Model: $\frac{C_e}{Q_e} = \frac{1}{Q_{max}K_L} + \frac{C_e}{Q_{max}}$ **(4.6)**

Freundlich Model: $\boldsymbol{lnQ_e = lnK_F + \frac{1}{n} lnC_e}$ **(4.7)**

Dubinin-Radushkevich Model: $\boldsymbol{lnq_e = lnq_m - \beta\varepsilon^2}$ **(4.8)**

Temkin Model: $\boldsymbol{q_e = Bln(A_T) + Bln(C_e)}$ **(4.9)**

Where q_e is the equilibrium adsorption amount on OMC (mg g^{-1}); q_{max} is the maximum monolayer adsorption capacity of OMC (mg g^{-1}); C_e is the equilibrium solute concentration (mg L^{-1}); K_L is Langmuir isotherm constant related to the affinity of binding sites (L mg^{-1}); K_F and n are Freundlich constant and intensity factor, respectively; q_m is the theoretical adsorption capacity (mg g-1); β is model constant (mol^2 J^{-2}); ε is the Polanyi potential (J mol^{-1}); AT is Temkin isotherm equilibrium binding constant (L g^{-1}).

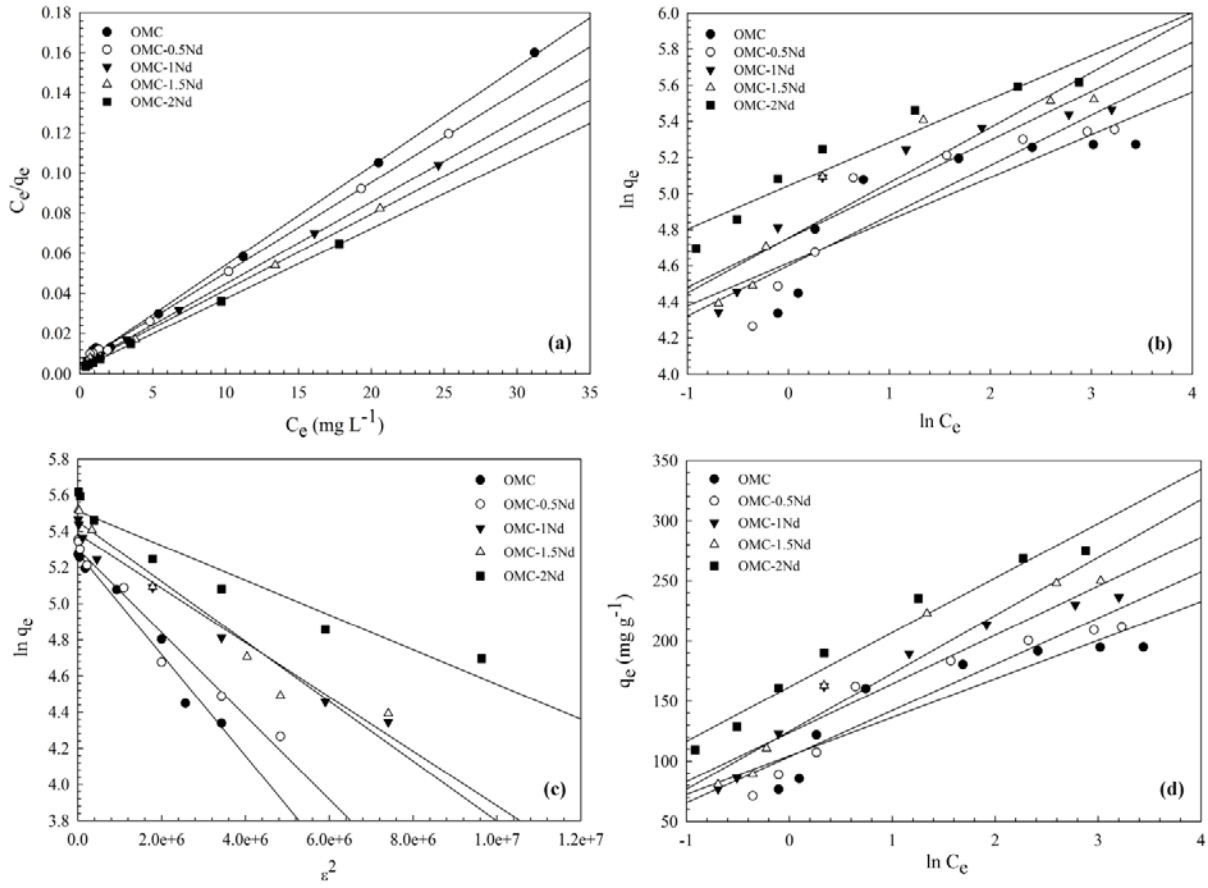

Figure 4.17. Adsorption isotherm models. (a) Langmuir (b) Freundlich (c) Dubinin-Radushkevich (D-R) (d) Temkin model.

The adsorption isotherm or equilibrium data were fitted to Langmuir, Freundlich, D-R, and Temkin isotherm models as illustrated in **Figure 4.17(a)-(d)**. The calculated coefficients are presented and compared in **Table 4.4**. Comparison of R^2 values shows that Langmuir isotherm model fitted well with the experimental data with a higher correlation coefficient (R^2 = 0.999-1.000) than other models. The maximum adsorption capacity of sunset yellow onto modified OMCs was found to be 204.08, 222.22, 243.90, 263.16, 285.72 mg g^{-1} for OMC, OMC-0.5Nd, OMC-1Nd, OMC-1.5Nd, OMC-2Nd, respectively.

The dimensionless Langmuir parameter or separation factor, R_L, can be used to predict the nature of adsorption and can be defined as follows:

$$\boldsymbol{R_L = \frac{1}{1+K_L C_e}} \quad \textbf{(4.10)}$$

The RL value can represent the nature of adsorption (irreversible if $R_L = 0$; favorable if $0 < R_L < 1$; linear if $R_L = 1$; unfavorable if $R_L > 1$) (Belhamdi et al., 2016). All the values of R_L were found to be between 0 and 1 depicting favorable adsorption.

The values of K_F and $1/n$ were calculated from the intercept and slope of the plot of lnq_e vs. lnC_e as shown in **Figure 4.17(b)**. Values of K_F were 101.11, 103.67, 115.93, 116.19, 154.97 mg g^{-1} (L mg^{-1})1/n, respectively. The n values of 4.2, 3.6, 3.7, 3.3, and 3.2 were observed for OMC, OMC-0.5Nd, OMC-1Nd, OMC-1.5Nd, OMC-2Nd, respectively. All these n values represent favorable adsorption since n value of 2-10 indicates favorable adsorption (Chen et al., 2011).

The values of β and q_m of D-R model were calculated from the slope and intercept of lnq_e vs. ε^2 plot as shown in **Figure 4.17(c)**. The mean free energy of adsorption, E, can be calculated from the constant β as follows:

$$\boldsymbol{E = \frac{1}{\sqrt{2\beta}}} \quad \textbf{(4.11)}$$

Where E provides information regarding the adsorption mechanism (if E < 8 kJ mol^{-1}, the process is physical adsorption in nature; if 8 kJ mol^{-1} < E < 16 kJ mol^{-1} the process involves ion exchange and diffusion) (Konggidinata et al., 2017a). The mean free energy obtained for sunset yellow was less than 8 kJ mol^{-1} depicting that physical adsorption was also involved in combination with chemical adsorption. Similarly, the values of B and A_T of Temkin model were calculated from the slope and intercept of q_e vs. lnC_e as depicted in

Figure 4.17(d). The values of B and A_T ranged from 32.02-45.25 J mol^{-1} and 26.2-35.7 L g^{-1}, respectively indicating that the adsorption occurred via chemisorption (Araújo et al., 2018).

Table 4.4. Comparison of the coefficients of isotherm for sunset yellow adsorption onto modified OMCs.

Models	Parameters	OMC	OMC-0.5Nd	OMC-1Nd	OMC-1.5Nd	OMC-2Nd
Langmuir	q_{max} (mg g^{-1})	204.08	222.22	243.90	263.16	285.72
	K_L (L mg^{-1})	1.021	0.849	1.051	0.974	1.458
	R_L	0.0304	0.0445	0.0372	0.0475	0.0371
	R^2	0.9998	0.9993	0.9998	0.9992	1
Freundlich	K_F [mg g^{-1}(L $mg^{-1})^{1/n}$]	101.11	103.67	115.93	116.19	154.97
	1/n	0.2368	0.2776	0.271	0.3051	0.3145
	R^2	0.7435	0.8294	0.8459	0.8675	0.9145
D-R	q_m (mg g^{-1})	196.232	200.798	218.416	233.621	247.819
	β (mol^2 J^{-2})	3.0×10^{-7}	2.5×10^{-8}	2.0×10^{-8}	1.5×10^{-8}	1.0×10^{-8}
	E (kJ mol^{-1})	1.29	4.47	5.00	5.77	7.10
	R^2	0.9758	0.9672	0.9808	0.9482	0.9258
Temkin	B (J mol^{-1})	32.023	38.343	40.622	48.142	45.249
	b_T	77.369	64.616	60.991	51.464	54.754
	A_T (L g^{-1})	26.184	15.029	21.023	13.4	35.714
	R^2	0.8127	0.8937	0.925	0.9245	0.9624

Table 4.5 shows the adsorption capacities of previously reported adsorbents for the removal of sunset yellow. The synthesized modified OMCs showed their potential in terms of adsorption capacity compared to other adsorbent reported in the literature.

Table 4.5. Comparison of sunset yellow adsorption capacity for various adsorbents.

Adsorbent	Q_e (mg g^{-1})	Conditions	Reference
OMC[a]	204.08	T: 25ºC, C_0: 50 mg L^{-1}, pH: 6.5	This study
OMC-0.5Nd[a]	222.22		
OMC-1Nd[a]	243.9		
OMC-1.5Nd[a]	263.16		
OMC-2Nd[a]	285.71		
Alligator weed activated carbon[a]	271	T: 25ºC, C_0: 250 mg L^{-1}, adsorbent dosage: 1.2 g L^{-1}	Kong et al., 2017
$Cd(OH)_2$-NW-AC[a]	80.6	T: 25ºC, C_0: 10-25 mg L^{-1}	Ghaedi and Mosallanejad, 2014
CdTN-AC[a]	181.81	T: 25ºC, C_0: 25-150 mg L^{-1}	Ghaedi et al., 2012
Fe_3O_4-MNPs-AC[a]	76.37	T: 25ºC, C_0: 15 mg L^{-1}	Bagheri et al., 2017
Cu doped ZnS-NPs-AC	67.3-85.4	T: 25ºC, C_0: 5-40 mg L^{-1}, adsorbent dosage: 0.01-0.02 g	Agarwal et al., 2016
PPy/MWCNTs[b]	98.5	C_0: 50 mg L^{-1}	Aliabadi and Mahmoodi, 2018

Note: *superscript a = maximum monolayer adsorption capacity calculated from Langmuir model. b = equilibrium adsorption capacity.*

4.3.2.6 Adsorption mechanism of SY onto Nd-modified OMC. The adsorption process could be interpreted in the terms of ligand exchange mechanism between anionic sunset yellow and hydroxide ions coordinated with Nd(III) on the OMC surface according to the following reactions:

$$R - Nd(H_2O)_3^{3+} \rightarrow R - Nd(H_2O)_{3-m}(OH)_m^{3-m} + mH^+, m = 1,2,3 \quad \textbf{(4.12)}$$

$$SY \rightarrow Na^+ + SY^- (\textit{After being dissolved in solution}) \quad \textbf{(4.13)}$$

$$R - Nd(H_2O)_{3-m}(OH)_m^{3-m} + qSY^- \rightarrow R - Nd(H_2O)_{3-m}(OH)_{m-q}^{3-m+q}(SY)_q^{3-m-q} + qOH^- \quad \textbf{(4.14)}$$

$$q = 1,2$$

$R = Nd\ incoporated\ OMC\ matrix$

When OMC was modified with Nd^{3+}, the Nd^{3+} was coordinated with H_2O to form $Nd(H_2O)_3^{3+}$. The water molecules coordinated with Nd^{3+} were deprotonated to release H^+ to form OH^- coordinated on Nd^{3+} according to **Equation (4.12)**. When anionic site of sunset yellow approached to the Nd-modified OMC, OH^- was substituted by sunset yellow according to ligand exchange mechanism proposed according to **Equation (4.14)**. **Fig. 4.18** depicts the proposed adsorption mechanism coupled with XPS and FT-IR analysis.

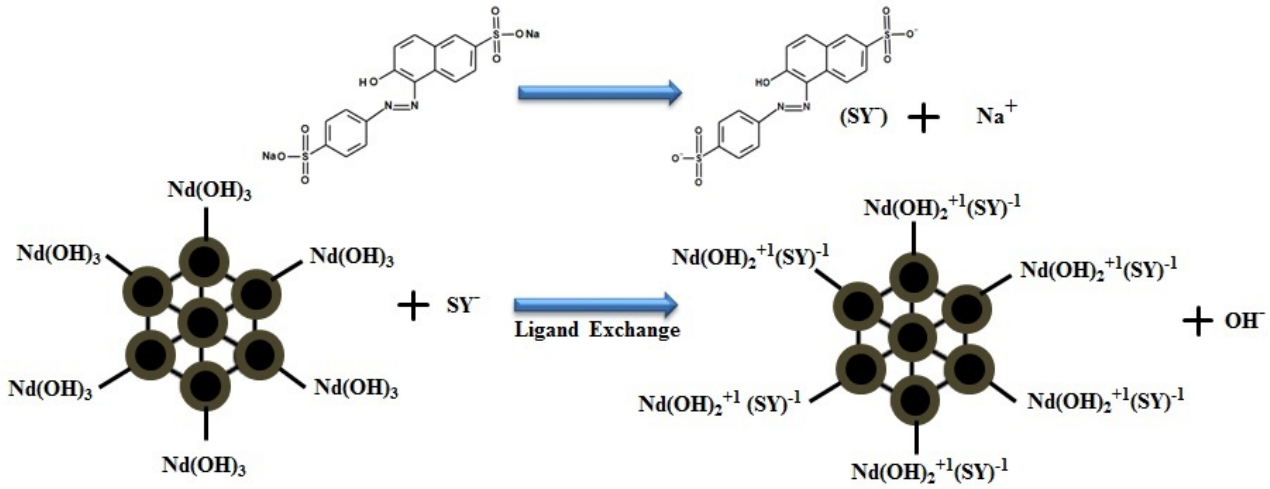

Figure 4.18. An example of the proposed adsorption mechanism of sunset yellow onto Nd-modified OMC when *m = 3 and q =1*.

4.4 Conclusion

In this work, incipient wetness impregnation method was employed to synthesize neodymium embedded ordered mesoporous carbons for the adsorptive removal of sunset yellow. The Nd-modified OMCs were characterized using N_2 adsorption-desorption isotherm, SEM, TEM, EDS, FT-IR, and XPS. BET surface area and pore volume decreased from 1349.6 to 881.9 $m^2\ g^{-1}$ and 1.85 to 1.29 $cm^3\ g^{-1}$, respectively with the increment of metal loading from 0.5% to 2.5% onto the OMC support surfaces. TEM images of OMCs

modified with neodymium showed less ordered structure than the virgin OMC. XPS data revealed the oxidation state of Nd as +3 in the OMC matrix and the formation of Nd^{3+} coordinated with hydroxide ion. Kinetics study revealed that the adsorption process achieved the equilibrium within 80 min and followed Pseudo-Second-Order reaction. The adsorption capacity of the modified OMCs decreases in the sequence of OMC-2Nd > OMC-1.5Nd > OMC-1Nd > OMC-0.5Nd > OMC. The adsorption isotherm data were better correlated with Langmuir model than Freundlich model with higher correlation coefficient (R^2> 0.999). The maximum monolayer adsorption capacity of Nd-modified OMCs towards sunset yellow was in the range of 204.1-285.7 mg g^{-1}. The Nd-modified OMCs showed better potential than most of the other adsorbents previously reported in the literature.

Acknowledgements

This work was supported by Louisiana Board of Regents (*LEQSF(2015-16)-ENH-TR-32 and LEQSF(2016-17)-RD-C-15*) and University of Louisiana at Lafayette. The authors would like to appreciate all the support provided by the Department of Chemistry and the Energy Institute of Louisiana.

Chapter 5: Economic Analysis and Environmental Applications

5.1 Economic Analysis

The use of ordered mesoporous carbon for water treatment is currently limited to exploring their potential to act as an effective adsorbent although they show promise for bench scale water treatment and environmental remediation. The majority of water purification studies employing ordered mesoporous carbon still remain at the proof of concept stage. Some roadblocks to the advancements in the use of OMC for water treatment and environmental remediation are technical hurdles, regulatory challenges, public perception, and the dearth of detailed cost-benefit analyses compared to the existing technologies (Savage and Diallo, 2005; Karn et al., 2009; Adeleye et al., 2016). In order to address this last obstacle, the costs of preparation of OMCs have been calculated in order to provide an up-to-date reference on the state of water treatment techniques for researchers, industry, and policy makers.

An economic analysis was performed to evaluate the cost of modified OMCs in comparison to the commercially available granular activated carbon (Norit GAC 1240W). The costs of chemicals for OMC production are given in **Table 5.1** and the costs to produce OMC-B-*a* are presented in **Table 5.2**. The cost to produce 1 kg of OMC-B-0, OMC-B-1, OMC-B-2, and OMC-B-4 was calculated to be $441.02, $441.416, $441.812, and $442.604, respectively while the cost to purchase 1 kg of GAC (Norit GAC 1240W) is $178.00. The cost breakdowns for the OMCs are tabulated in **Table 5.3**. It could be observed that the major material contributions were from COK-19, sucrose, and hydrofluoric acid, which accounted for 81.6%, 4.1%, and 13.0% of the total costs, respectively.

Table 5.1. Cost of chemicals for OMCs production.

Name	Price per unit
Triblock copolymer pluronic P-123	$0.225/kg
Triblock copolymer pluronic F-127	$165.00/kg
Citric acid monohydrate (99%)	$0.825/kg
Trisodium citrate dihydrate	$1.00/kg
Sodium silicate solution (26.5%)	$0.65/kg
Sucrose	$4.50/kg
Sulfuric Acid (98%)	$0.40/kg
Hydrofluoric Acid (48%)	$0.50/kg
Cerium(III) Chloride (Anhydrous, 99.5%)	$50.00/kg
Boric Acid (≥99.5 %)	$0.55/kg
Neodymium(III) chloride (Anhydrous, 99.5%)	$75.00/kg
Hydrochloric Acid	$0.10/kg
Tetraethyl Orthosilicate (TEOS)	$10.00/kg
Deionized (DI) water	$0.00185/gal

Table 5.2. Cost comparison for OMC-B-*a* and GAC.

Sample	GAC	OMC-B-0	OMC-B-1	OMC-B-2	OMC-B-4
Cost ($/kg)	178.00	441.020	441.416	441.812	442.604

Table 5.3. Cost contribution analysis for OMC-B-*a*.

Sample	COK-19 ($/kg)	Sucrose ($/kg)	Sulfuric acid ($/kg)	Boric acid ($/kg)	Hydrofluoric acid ($/kg)	DI Water ($/kg)
OMC-B-0	360.00	18.00	1.60	0.0000	57.50	3.92
OMC-B-1	360.00	18.00	1.60	0.3960	57.50	3.92
OMC-B-2	360.00	18.00	1.60	0.7920	57.50	3.92
OMC-B-4	360.00	18.00	1.60	1.5840	57.50	3.92

The costs to produce OMC-Ce are presented in **Table 5.4**. The cost to produce 1 kg of OMC-0.5Ce, OMC-1Ce, OMC-3Ce, and OMC-5Ce was calculated as $491.02, $542.02,

$750.02, and $967.32, respectively. The cost breakdowns for the OMC-Ce are tabulated in **Table 5.5**. It was discernable that one of the major material contributions was due to cerium(III) chloride which accounted for 10.2%, 18.64%, 41.2%, and 54.4% for OMC-0.5Ce, OMC-1Ce, OMC-3Ce, and OMC-5Ce, respectively.

Table 5.4. Cost comparison for OMC-Ce and GAC.

Sample	GAC	OMC	OMC-0.5Ce	OMC-1Ce	OMC-3Ce	OMC-5Ce
Cost ($/kg)	178.00	441.02	491.02	542.02	750.02	967.32

Table 5.5. Cost contribution analysis for OMC-Ce.

Sample	COK-19 ($/kg)	Sucrose ($/kg)	Sulfuric acid ($/kg)	Hydrofluoric acid ($/kg)	Cerium(III) chloride ($/kg)	DI Water ($/kg)
OMC	360.00	18.00	1.60	57.50	0.00	3.92
OMC-0.5Ce	360.00	18.00	1.60	57.50	50.00	3.92
OMC-1Ce	360.00	18.00	1.60	57.50	101.00	3.92
OMC-3Ce	360.00	18.00	1.60	57.50	309.00	3.92
OMC-5Ce	360.00	18.00	1.60	57.50	526.30	3.92

The costs to produce OMC-Nd are presented in **Table 5.6**. The cost to produce 1 kg of OMC-0.5Nd, OMC-1Nd, OMC-1.5Nd, and OMC-2Nd was calculated as $363.57, $371.07, $378.87, and $394.47, respectively. The cost breakdowns for the OMC-Nd are tabulated in **Table 5.7**. It was discernable that major costs could be attributed to SBA-15 (40.5-44.9%) and hydrofluoric acid (43.73-47.45%) in the preparation of Nd-modified OMC. The costs of neodymium(III) chloride accounted for 2.06%, 4.05%, 6.02%, and 7.75% for OMC-0.5Nd, OMC-1Nd, OMC-1.5Nd, and OMC-2Nd, respectively.

Table 5.6. Cost comparison for OMC-Nd and GAC.

Sample	GAC	OMC	OMC-0.5Nd	OMC-1Nd	OMC-1.5Nd	OMC-2Nd
Cost ($/kg)	178.00	356.07	363.57	371.07	378.87	394.47

Table 5.7. Cost contribution analysis for OMC-Nd.

Sample	SBA-15 ($/kg)	Sucrose ($/kg)	Sulfuric acid ($/kg)	Hydrofluoric acid ($/kg)	Neodymium(III) chloride ($/kg)	DI Water ($/kg)
OMC	160.00	18.00	1.60	172.5	0.00	4.00
OMC-0.5Nd	160.00	18.00	1.60	172.5	7.50	4.00
OMC-1Nd	160.00	18.00	1.60	172.5	15.00	4.00
OMC-1.5Nd	160.00	18.00	1.60	172.5	22.80	4.00
OMC-2Nd	160.00	18.00	1.60	172.5	30.60	4.00

The yield of OMC produced from one batch can significantly affect the production cost. A more controlled experimental setup, such as a completely inert environment during the carbonization step, can reduce the loss of carbon that is converted to CO_2 and H_2O and subsequently reduce production cost. In addition to this, modified OMCs produced in this research work are most suitable for specific or target pollutants. The cost of modified OMCs is higher than the traditional GAC, but this cost can be reduced within industrial settings. Future industrial application can reduce the cost of OMCs. In addition to this, these OMCs have higher adsorption capacity if compared to traditional GAC, which has very limited capacity. These OMCs can remove higher pollutant load from the industrial wastewater.

Table 5.8. Cost for various modified OMCs for pollutant removal.

Pollutant	Adsorbent	Removal cost ($/mg)	Pollutant removal (lb) by 1 kg of adsorbent
Resorcinol	GAC (Norit GAC 1240W)	0.0064	0.0627
	OMC-B-0	0.0120	0.0892
	OMC-B-1	0.0070	0.1418
	OMC-B-2	0.0084	0.1174
	OMC-B-4	0.0101	0.0983
Resorcinol	GAC (Norit GAC 1240W)	0.0064	0.0627
	OMC	0.0130	0.0773
	OMC-0.5Ce	0.0125	0.0883
	OMC-1Ce	0.0120	0.1032
	OMC-3Ce	0.0140	0.1211
	OMC-5Ce	0.0160	0.1366
Sunset Yellow	GAC (Norit GAC 1240W)	0.01300	0.0314
	OMC	0.00174	0.4571

OMC-0.5Nd	0.00164	0.4978
OMC-1Nd	0.00152	0.5464
OMC-1.5Nd	0.00144	0.5900
OMC-2Nd	0.00138	0.6400

On the basis of the removal efficiency and removal cost, adsorption process is the most cost-effective method for phenolic compounds and dyes. The removal cost per milligram of pollutant is $0.0064 for GAC. The removal cost per milligram of pollutant is $0.012, $0.007, $0.0084, and $0.010 for OMC-B-0, OMC-B-1, OMC-B-2 and OMC-B-4, respectively. The pollutant removal by 1 kg of adsorbent was found to be 0.0627, 0.0892, 0.1418, 0.1174, and 0.0983 lb for GAC (Norit GAC 1240W), OMC-B-0, OMC-B-1, OMC-B-2 and OMC-B-4, respectively.

The removal cost per milligram of pollutant is $0.0064 for GAC, whereas the removal cost per milligram of pollutant is $0.013, $0.0125, $0.012, $0.014, and $0.016 for virgin OMC, OMC-0.5Ce, OMC-1Ce, OMC-3Ce, and OMC-5Ce, respectively. The pollutant removal by 1 kg of adsorbent was found to be 0.0773, 0.0883, 0.1032, 0.1211, and 0.1366 lb for virgin OMC, OMC-0.5Ce, OMC-1Ce, OMC-3Ce, and OMC-5Ce, respectively.

The removal cost per milligram of pollutant is $0.013 for GAC, whereas the removal cost per milligram of pollutant is $0.00174, $0.00164, $0.00152, $0.00144, $0.00138 for virgin OMC, OMC-0.5Nd, OMC-1Nd, OMC-1.5Nd, OMC-2Nd, respectively, which is much cheaper than most of the currently available technologies. The pollutant removal by 1 kg of adsorbent was 0.4571, 0.4978, 0.5464, 0.5900, and 0.6400 lb for OMC, OMC-0.5Nd, OMC-

1Nd, OMC-1.5Nd, and OMC-2Nd, respectively which is much higher than GAC which is 0.0314 lb. All these improved pollutant removals can be ascribed to modifying OMCs.

5.2 Environmental Applications

Water is one of the most abundant resources on the earth's surface, but less than 1% of the fresh water supply is available and safe for human consumption. According to the World Health Organization (WHO), more than 760 million people did not have access to a drinking water supply in 2011 (Grey et al., 2013). The cost of drinkable water is ever rising due to increasing energy cost, growing populations, and other environmental or climatic factors. In addition to this, an increasing number of drinking water resources are showing high levels of contamination because of the discharge of untreated wastewater in natural streams. Traditional water and wastewater treatment methods do not efficiently remove these contaminants and do not have the capability to meet the stringent water quality standards imposed by regulatory agencies (Adeleye et al., 2016). Contaminated surface water also poses threat to ground water, which may penetrate into aquifers and pollute drinking water sources. All of these challenges create the need for alternative water treatment technologies and new innovative adsorbents to replace existing technologies (Qu et al., 2013).

The developed materials in this research work were envisaged for environmental remediation of pollutants, such as phenols and dyes. Phenols are pollutants of high priority concern because of their high level of toxicity and accumulation in the environment. Phenol is produced at an annual rate of approximately 6 million tons, a significantly increasing trend (Schmidt, 2005). The discharge of phenol in natural water without any prior treatment can lead to the formation of chlorinated phenols during the disinfection and oxidation process. The manufacturing process and transportation of phenol may excessively expose workers to

this substance (Mukherjee et al., 2013). Phenol possesses hazardous health effects that can be both acute and chronic. Long term exposure to phenol can lead to serious health effects, such as irregular breathing, muscle weakness, respiratory arrest, and coma through inhalation, ingestion, eye contact, and absorption through the skin. Anorexia, weight loss, diarrhea, vertigo, salivation, and greenish or smoky colored urine can be attributed to chronic phenol exposure (Busca et al., 2008). Chronic exposure to phenol can also lead to irritation in the gastrointestinal and central nervous systems and liver, kidney, and cardiovascular tissues in animals. Studies on animals have shown weight reduction in the fetal body, growth retardation, and abnormal development in offspring (Zhang and Li, 2014). Contamination of surface and ground water with synthetic dyes is a serious environmental problem which poses a threat to human and aquatic life. The discharge of these coloring products into the hydrosphere can give an undesirable color to water even at low concentrations as well as causing impaired visibility and reduced sunlight penetration. The degrading products are also mutagenic and carcinogenic and cause increased COD and BOD levels of aquatic sources. Some of these dyes are xenobiotic in nature and aerobically recalcitrant to biodegradation and therefore pose a threat when wastewater is disposed of in the nearest environment without being treated. The complex aromatic structure and synthetic origin of the dyes make them stable to the heat, oxidizing agents, photodegradation and biodegradation. Today more than 100,000 commercial dyes are known with an annual production of $>7\times10^5$ ton/year. The total amount of dye consumption is more than 10,000 ton/year in textile industry and approximately 100 ton/year are discharged into the natural stream (Gupta et al., 2013). The surface functionalized adsorbents can help to eliminate these pollutants, resulting in economic benefits and improved health. The aesthetic perspective of this entire

environmental cleanup is intangible, which bears a recreational value, adding worth to the tourism industry.

In addition to this, the developed adsorbent can be applied for the removal of anionic species, such as fluoride ion, from water. The presence of fluoride ion in drinking water can cause adverse health impacts. Fluorosis, an endemic public health problem existing in 22 nations around the globe, can initiate crippling disorder due to the excessive intake in the human body. Fluoride normally enters the environment and human body through water, food, industrial exposure, drugs, cosmetics, etc.; however, drinking water is the single major source of daily intake (Meenakshi and Maheshwari, 2006). The excessive ingestion of fluoride ions are attracted by positively charged calcium in teeth and bones due to its strong electronegativity nature and causes dental, skeleton, and nonskeletal forms of fluorosis in children as well as adults (Ayoob and Gupta, 2006). Excess fluoride ions in drinking water can cause human diseases, such as rickets, neurological disorder, ossification of tendons and ligaments, and dental diseases. According to the World Health Organization (WHO) the maximum permissible concentration of fluoride ions in drinking water must be below 1.5 mg L^{-1}. The Ministry of Water Resources in China proposed maximum acceptable concentration of fluoride ion in drinking water as 1.0 mg L^{-1} based on economical, practical and technical considerations (Yao et al., 2009). A strict rule from USEPA is adopted for the maximum allowable fluoride ion concentration in drinking water at 1.5 mg L^{-1} (Dong and Wang, 2016). The neodymium embedded OMCs bears a great potential for the removal of anionic species from drinking water (Ahmad et al., 2019c).

Bibliography

Adebisi, G. A., Chowdhury, Z. Z., Alaba, P. A., 2017. Equilibrium, kinetic, and thermodynamic studies of lead ion and zinc ion adsorption from aqueous solution onto activated carbon prepared from palm oil mill effluent. *Journal of Cleaner Production*, 148, 958–968. https://doi.org/10.1016/j.jclepro.2017.02.047.

Adeleye, A. S., Conway, J. R., Garner, K., Huang, Y., Su, Y., Keller, A. A., 2016. Engineered nanomaterials for water treatment and remediation: Costs, benefits, and applicability. *Chemical Engineering Journal*, 286, 640–662. https://doi.org/10.1016/j.cej.2015.10.105.

Agarwal, S., Rani, A., 2017. Adsorption of resorcinol from aqueous solution onto CTAB/NaOH/flyash composites: Equilibrium, kinetics and thermodynamics. *Journal of Environmental Chemical Engineering*, 5, 526–538. https://doi.org/10.1016/j.jece.2016.11.035.

Agarwal, S., Tyagi, I., Gupta, V. K., Dastkhoon, M., Ghaedi, M., Yousefi, F., Asfaram, A., 2016. Ultrasound-assisted adsorption of Sunset Yellow CFC dye onto Cu doped ZnS nanoparticles loaded on activated carbon using response surface methodology based on central composite design. *Journal of Molecular Liquids*, 219, 332–340. https://doi.org/10.1016/j.molliq.2016.02.100.

Aghav, R.M., Kumar, S., Mukherjee, S.N., 2011. Artificial neural network modeling in competitive adsorption of phenol and resorcinol from water environment using some carbonaceous adsorbents. *Journal of Hazardous Materials*, 188, 67–77. https://doi.org/10.1016/j.jhazmat.2011.01.067.

Aharoni, C., Tompkins, F. C. (1970) Kinetics of adsorption and desorption and the Elovich equation. *Advances in Catalysis*, 21, 1–49.

Ahmad, Z. U., Chao, B., Konggidinata, M. I., Lian, Q., Zappi, M. E., Gang, D. D., 2018. Molecular simulation and experimental validation of resorcinol adsorption on Ordered Mesoporous Carbon (OMC). *Journal of Hazardous Materials*, 354, 258–265. https://doi.org/10.1016/j.jhazmat.2018.04.072.

Ahmad, Z. U., Lian, Q., Zappi, M. E., Buchireddy, P.R., Gang, D. D., 2019a. Adsorptive removal of resorcinol on a novel ordered mesoporous carbon (OMC) employing COK-19 silica scaffold: Kinetics and equilibrium study. 75, 307–317. *Journal of Environmental Sciences*. https://doi.org/10.1016/j.jes.2018.04.014.

Ahmad, Z. U., Lian, Q., Zappi, M. E., Buchireddy, P.R., Gang, D. D., 2019b. Adsorptive Removal of Resorcinol onto Surface Modified Ordered Mesoporous Carbon: Kinetics and Equilibrium Study. Environmental Progress and Sustainable Energy. 38, S386–S397. https://doi.org/10.1002/ep.13070.

Ahmad, Z. U., Yao, L., Wang, J., Gang, D. D., Islam, F., Lian, Q., Zappi, M. E., 2019c. Neodymium embedded ordered mesoporous carbon (OMC) for enhanced adsorption

of sunset yellow: Characterizations, adsorption study and adsorption mechanism. Chemical Engineering Journal. 359, 814-826. https://doi.org/10.1016/j.cej.2018.11.174.

Ahmaruzzaman, M., 2008. Adsorption of phenolic compounds on low-cost adsorbents: A review. *Advances in Colloid and Interface Science*, 143, 46–67. https://doi.org/10.1016/j.cis.2008.07.002.

Ali, S.B., Jaouali, I., Najar, S.S., Ouederni, A., 2017. Characterization and adsorption capacity of raw pomegranate peel biosorbent for copper removal. *Journal of Cleaner Production*, 142, 3809–3821. https://doi.org/10.1016/j.jclepro.2016.10.081.

Aliabadi, R.S., Mahmoodi, N.O., 2018. Synthesis and characterization of polypyrrole, polyaniline nanoparticles and their nanocomposite for removal of azo dyes; sunset yellow and Congo red. *Journal of Cleaner Production*, 179, 235-245. https://doi.org/10.1016/j.jclepro.2018.01.035.

Alventosa-de Lara, E., Barredo-Damas, S., Alcaina-Miranda, M.I., Iborra-Clar, M.I., 2012. Ultrafiltration technology with a ceramic membrane for reactive dye removal: Optimization of membrane performance. *Journal of Hazardous Materials*, 209-210, 492–500. https://doi.org/10.1016/j.jhazmat.2012.01.065.

Alver, E., Metin, A.Ü., 2012. Anionic dye removal from aqueous solutions using modified zeolite: Adsorption kinetics and isotherm studies. *Chemical Engineering Journal*, 200–202, 59–67. https://doi.org/10.1016/j.cej.2012.06.038.

Amosa, M.K., Jami, M.S., Alkhatib, M.F.R., 2016. Electrostatic Biosorption of COD, Mn and H_2S on EFB-Based Activated Carbon Produced through Steam Pyrolysis: An Analysis Based on Surface Chemistry, Equilibria and Kinetics. *Waste and Biomass Valorization*, 7, 109–124. https://doi.org/10.1007/s12649-015-9435-7.

Arafat, A.A., Franz, M., Pinto, N.G., 1999. Effect of Salt on the Mechanism of Adsorption of Aromatics on Activated Carbon. *Langmuir*, 15(18), 5997–6003. https://doi.org/10.1021/la9813331.

Arana, J., Melian, E.P., López, V.R., Alonso, A.P., Rodríguez, J.D., Díaz, O.G., et al., 2007. Photocatalytic degradation of phenol and phenolic compounds: Part I. Adsorption and FTIR study. *Journal of Hazardous Materials*, 146, 520–528. https://doi.org/10.1016/j.jhazmat.2007.04.066.

Araújo, C.S.T., Almeida, I.L.S., Rezende, H.C., Marcionilio, S.M.L.O., Léon, J.J.L., Matos, T.N.de, 2018. Elucidation of mechanism involved in adsorption of Pb(II) onto lobeira fruit (*Solanum lycocarpum*) using Langmuir, Freundlich and Temkin isotherms. *Microchemical Journal*, 137, 348–354. https://doi.org/10.1016/j.microc.2017.11.009.

Aydın, H., Bulut, Y., Yerlikaya, Ç. (2008). Removal of copper (II) from aqueous solution by adsorption onto low-cost adsorbents. *Journal of Environmental Management*, 87, 37–45. https://doi.org/10.1016/j.jenvman.2007.01.005.

Ayoob, S., Gupta, A. K., 2006. Fluoride in Drinking Water: A Review on the Status and Stress Effects. *Critical Reviews in Environmental Science and Technology*, 36, 433–487. https://doi.org/10.1080/10643380600678112.

Bagheri, A.R., Ghaedi, M., Asfaram, A., Bazrafshan, A.A., Jannesar, R., 2017. Comparative study on ultrasonic assisted adsorption of dyes from single system onto Fe_3O_4 magnetite nanoparticles loaded on activated carbon: Experimental design methodology. *Ultrasonics Sonochemistry*, 34, 294–304. https://doi.org/10.1016/j.ultsonch.2016.05.047.

Bashkova, S., Bagreev, A., Bandosz, T. J., 2003. Adsorption/oxidation of CH_3SH on activated carbons containing nitrogen. *Langmuir*, 19(15), 6115–6121. https://doi.org/10.1021/la0300030.

Bayram, E., Hoda, N., Ayranci, E., 2009. Adsorption/electrosorption of catechol and resorcinol onto high area activated carbon cloth. *Journal of Hazardous Materials*, 168, 1459–1466. https://doi.org/10.1016/j.jhazmat.2009.03.039.

Belhamdi, B., Merzougui, Z., Trari, M., Addoun, A., 2016. A kinetic, equilibrium and thermodynamic study of l-phenylalanine adsorption using activated carbon based on agricultural waste (date stones). *Journal of Applied Research and Technology*, 14, 354–366. https://doi.org/10.1016/j.jart.2016.08.004.

Bilgili, M. S. (2006). Adsorption of 4-chlorophenol from aqueous solutions by xad-4 resin: isotherm, kinetic, and thermodynamic analysis. *Journal of Hazardous Materials*, 137, 157–164. https://doi.org/10.1016/j.jhazmat.2006.01.005.

Boehm, H.P., 1994. Some aspects of the surface chemistry of carbon blacks and other carbons, *Carbon*, 32, 759–769. https://doi.org/10.1016/0008-6223(94)90031-0.

Borah, D., Satokawa, S., Kato, S., Kojima, T., 2009. Sorption of As(V) from aqueous solution using acid modified carbon black. *Journal of Hazardous Materials*, 162, 1269–1277. https://doi.org/10.1016/j.jhazmat.2008.06.015.

Busca, G., Berardinelli, S., Resini, C., Arrighi, L., 2008. Technologies for the removal of phenol from fluid streams: A short review of recent developments. *Journal of Hazardous Materials*, 160, 265–288. https://doi.org/10.1016/j.jhazmat.2008.03.045.

Buthelezi, S.P., Olaniran, A.O., Pillay, B., 2012. Textile Dye Removal from Wastewater Effluents Using Bioflocculants Produced by Indigenous Bacterial Isolates. *Molecules*, 17, 14260–14274. https://doi.org/10.3390/molecules171214260.

Cansado, I.P., Mourão, P.A., Falcão, A.I., Carrott, M.R., Carrott, P.J., 2012. The influence of the activated carbon post-treatment on the phenolic compounds removal. *Fuel Processing Technology*, 103, 64–70. https://doi.org/10.1016/j.fuproc.2011.10.015.

Ceyhan, O., Baybas, D., 2001. Adsorption of some textile dyes by hexade-cyltrimethylammonium bentonite. *Turkish Journal of Chemistry*, 25, 193–200.

Chafi, M., Gourich, B., Essadki, A.H., Vial, C., Fabregat, A., 2011. Comparison of electrocoagulation using iron and aluminium electrodes with chemical coagulation for the removal of a highly soluble acid dye. *Desalination*, 281, 285–292. https://doi.org/10.1016/j.desal.2011.08.004.

Chai, G.S., Yoon, S.B., Yu, J.S., Choi, J.H., Sung, Y.E., 2004. Ordered porous carbons with tunable pore sizes as catalyst supports in direct methanol fuel cell. *Journal of Physical Chemistry B*, 108, 7074–7079. https://doi.org/10.1021/jp0370472.

Chao, B., Konggidinata, M.I., Lin, L., Zappi, M., Gang, D.D., 2017. Effect of carbon precursors and pore expanding reagent on ordered mesoporous carbon for resorcinol removal. *Journal of Water Process Engineering*, 17, 256–263. https://doi.org/10.1016/j.jwpe.2017.05.002.

Chen, T., Wang, T., Wang, D.J., Xue, H.R., Zhao, J.Q., Ding, X.C., Wu, S.C., He, J.P., 2011. Synthesis of ordered large-pore mesoporous carbon for Cr(VI) adsorption. *Materials Research Bulletin*, 46, 1424–1430. https://doi.org/10.1016/j.materresbull.2011.05.009.

Choi, J. M., Jeong, D., Cho, E., Jun, B. H., Park, S., Yu, J. H., Tahir, M. N., Jung, S. (2016) Chemically functionalized silica gel with alkynyl terminated monolayers as an efficient new material for removal of mercury ions from water. *Journal of Industrial and Engineering Chemistry*, 35, 376–382. https://doi.org/10.1016/j.jiec.2016.01.020.

Chutia, P., Kato, S., Kojima, T., Satokawa, S., 2009. Adsorption of As(V) on surfactant-modified natural zeolites. *Journal of Hazardous Materials*, 162, 204–211. https://doi.org/10.1016/j.jhazmat.2008.05.024.

Coppa, B. J., Davis, R. F., 2003. Gold Schottky contacts on oxygen plasma-treated, *n*-type ZnO (000$\bar{1}$). *Applied Physics Letters*, 82, 400–402. https://doi.org/10.1063/1.1536264.

Cordova Villegas, L. G., Mashhadi, N., Chen, M., Mukherjee, D., Taylor, K. E., Biswas, N., 2016. A Short Review of Techniques for Phenol Removal from Wastewater. *Current Pollution Reports*, 2, 157–167. https://doi.org/10.1007/s40726-016-0035-3.

Dąbrowski, A., Podkościelny, P., Hubicki, Z., Barczak, M., 2005. Adsorption of phenolic compounds by activated carbon-a critical review. *Chemosphere*, 58, 1049–1070. https://doi.org/10.1016/j.chemosphere.2004.09.067.

Dai, W., Zheng, M., Zhao, Y., Liao, S., Ji, G., Cao, J., 2009. Template synthesis of three-dimensional cubic ordered mesoporous carbon with tunable pore sizes. *Nanoscale Research Letter*, 5, 103–107. https://doi.org/10.1007/s11671-009-9450-3.

Darmstadt, H., Roy, C., Kaliaguine, S., Choi, S.J., Ryoo, R., 2002. Surface chemistry of ordered mesoporous carbons. *Carbon*, 40, 2673–2683. https://doi.org/10.1016/S0008-6223(02)00187-2.

Din, A.T.M., Hameed, B.H., Ahmad, A.L., 2009. Batch adsorption of phenol onto physiochemical-activated coconut shell. *Journal of Hazardous Materials*, 161, 1522–1529. https://doi.org/10.1016/j.jhazmat.2008.05.009.

Ding, C., Sun, Y., Wang, Y., Li, J., Lin, Y., Sun, W., Luo, C., 2017. Adsorbent for resorcinol removal based on cellulose functionalized with magnetic poly(dopamine). *International Journal of Biological Macromolecules*, 99, 578–585. https://doi.org/10.1016/j.ijbiomac.2017.03.018.

Dong, S., Wang, Y., 2016. Characterization and adsorption properties of a lanthanum-loaded magnetic cationic hydrogel composite for fluoride removal. *Water Research*, 88, 852–860. https://doi.org/10.1016/j.watres.2015.11.013.

Dong, Y., Lin, H., Qu, F., 2012. Synthesis of ferromagnetic ordered mesoporous carbons for bulky dye molecules adsorption. *Chemical Engineering Journal*, 193-194, 169–177. https://doi.org/10.1016/j.cej.2012.04.024.

Duan, F., Yang, Y., Li, Y., Cao, H., Wang, Y., Zhang, Y., 2014. Heterogeneous Fenton-like degradation of 4-chlorophenol using iron/ordered mesoporous carbon catalyst. *Journal of Environmental Sciences*, 26, 1171–1179.

Dursun, A.Y., Kalayci, C.S., 2005. Equilibrium, kinetic and thermodynamic studies on the adsorption of phenol onto chitin. *Journal of Hazardous Materials*, 123, 151–157. https://doi.org/10.1016/j.jhazmat.2005.03.034.

Elass, K., Laachach, A., Alaoui, A., Azzi, M., 2011. Removal of methyl violet from aqueous solution using a stevensite-rich clay from Morocco. *Applied Clay Science*, 54, 90–96. https://doi.org/10.1016/j.clay.2011.07.019.

El-Naas, M.H., Al-Zuhair, S., Alhaija, M.A., 2010. Removal of phenol from petroleum refinery wastewater through adsorption on date-pit activated carbon. *Chemical Engineering Journal*, 162(3), 997–1005. https://doi.org/10.1016/j.cej.2010.07.007.

Escobar, C., Fisch, A., Santos, J.H.Z., 2015. Effect of a Sol–Gel Route on the Preparation of Silica-Based Sorbent Materials Synthesized by Molecular Imprinting for the Adsorption of Dyes. *Industrial and Engineering Chemistry Research*, 54, 254–262. https://doi.org/10.1021/ie503993d.

Fang, B., Zhou, H., Honma, I., 2006. Ordered porous carbon with tailored pore size for electrochemical hydrogen storage application. *Journal of Physical Chemistry B*, 110, 4875–4880. https://doi.org/10.1021/jp056063r.

Freundlich, H., 1907. Über die adsorption in lösungen, *Zeitschrift für physikalische Chemie*. 57, 385–470.

Fuertes, A.B., Sonia, A., 2004. Graphitic mesoporous carbons synthesized through mesostructured silica templates. *Carbon*, 42, 3049–3055. https://doi.org/10.1016/j.carbon.2004.06.020.

Fytianos, K., Voudrias, E., Kokkalis, E., 2000. Sorption–desorption behaviour of 2, 4-dichlorophenol by marine sediments. *Chemosphere*, 40, 3–6. https://doi.org/10.1016/S0045-6535(99)00214-3.

Galán, J., Rodríguez, A., Gómez, J.M., Allen, S.J., Walker, G.M., 2013. Reactive dye adsorption onto a novel mesoporous carbon. *Chemical Engineering Journal*, 219, 62–68. https://doi.org/10.1016/j.cej.2012.12.073.

Gattrell, M., Kirk, D.W., 1990. The electrochemical oxidation of aqueous phenol at a glassy carbon electrode. *The Canadian Journal of Chemical Engineering*, 68, 997–1003. https://doi.org/10.1002/cjce.5450680615.

Ghaedi, M., Daneshfar, A., Ahmadi, A., Momeni, M.S., 2015. Artificial neural network-genetic algorithm based optimization for the adsorption of phenol red (PR) onto gold and titanium dioxide nanoparticles loaded on activated carbon. *Journal of Industrial and Engineering Chemistry*, 21, 587–598. https://doi.org/10.1016/j.jiec.2014.03.024.

Ghaedi, M., Hajjati, S., Mahmudi, Z., Tyagi, I., Agarwal, S., Maity, A., Gupta, V. K. (2015). Modeling of competitive ultrasonic assisted removal of the dyes–methylene blue and safranin-O using Fe_3O_4 nanoparticles. *Chemical Engineering Journal*, 268, 28–37. https://doi.org/10.1016/j.cej.2014.12.090.

Ghaedi, M., Jah, A.H., Khodadoust, S., Sahraei, R., Daneshfar, A., Mihandoost, A., Purkait, M.K., 2012. Cadmium telluride nanoparticles loaded on activated carbon as adsorbent for removal of sunset yellow. *Spectrochimica Acta Part A: Molecular and Biomolecular Spectroscopy*, 90, 22–27. https://doi.org/10.1016/j.saa.2011.12.064.

Ghaedi, M., Mosallanejad, N., 2014. Study of competitive adsorption of malachite green and sunset yellow dyes on cadmium hydroxide nanowires loaded on activated carbon. *Journal of Industrial and Engineering Chemistry*, 20, 1085–1096. https://doi.org/10.1016/j.jiec.2013.06.046.

Ghoneim, M. M., El-Desoky, H. S., Zidan, N. M., 2011. Electro-Fenton oxidation of Sunset Yellow FCF azo-dye in aqueous solutions. *Desalination*, 274, 22–30. https://doi.org/10.1016/j.desal.2011.01.062.

Goscianska, J., Fathy, N. A., Aboelenin, R. M. M., 2017. Adsorption of solophenyl red 3BL polyazo dye onto amine-functionalized mesoporous carbons. *Journal of Colloid and Interface Science*, 505, 593–604. https://doi.org/10.1016/j.jcis.2017.06.052.

Goscianska, J., Marciniak, M., Pietrzak, R., 2014. Mesoporous carbons modified with lanthanum (III) chloride for methyl orange adsorption. *Chemical Engineering Journal*, 247, 258–264. https://doi.org/10.1016/j.cej.2014.03.012.

Goscianska, J., Marciniak, M., Pietrzak, R., 2015. Ordered mesoporous carbons modified with cerium as effective adsorbents for azo dyes removal. *Separation and Purification Technology*, 154, 236–245. https://doi.org/10.1016/j.seppur.2015.09.042.

Goscianska, J., Olejnik, A., 2018. Dispersion stability of the aminosilane-grafted mesoporous carbons in different solvents. *Microporous and Mesoporous Materials*, 265, 149–161. https://doi.org/10.1016/j.micromeso.2018.02.009.

Goscianska, J., Pietrzak, R., Matos, J., 2018. Catalytic performance of ordered mesoporous carbons modified with lanthanides in dry methane reforming. *Catalysis Today*, 301, 204–216. https://doi.org/10.1016/j.cattod.2017.05.014.

Grey, D., Garrick, D., Blackmore, D., Kelman, J., Muller, M., Sadoff, C., 2013. Water security in one blue planet: twenty-first century policy challenges for science. *Philosophical Transactions of the Royal Society A: Mathematical, Physical and Engineering Sciences*, 371: 20120406. http://dx.doi.org/10.1098/rsta.2012.0406.

Guo, R., Guo, J., Yu, F., Gang, D.D., 2013. Synthesis and surface functional group modifications of ordered mesoporous carbons for resorcinol removal. *Microporous and Mesoporous Materials*, 175, 141–146. https://doi.org/10.1016/j.micromeso.2013.03.028.

Gupta, V.K., 2009. Application of low-cost adsorbents for dye removal–A review. *Journal of Environmental Management*, 90, 2313–2342. https://doi.org/10.1016/j.jenvman.2008.11.017.

Gupta, V.K., Kumar, R., Nayak, A., Saleh, T.A., Barakat, M.A., 2013. Adsorptive removal of dyes from aqueous solution onto carbon nanotubes: a review. *Advances in Colloid and Interface Science*, 193, 24–34. https://doi.org/10.1016/j.cis.2013.03.003.

Huang, J., Huang, K., Yan, C., 2009. Application of an easily water-compatible hypercrosslinked polymeric adsorbent for efficient removal of catechol and resorcinol in aqueous solution. *Journal of Hazardous Materials*, 167, 69–74. https://doi.org/10.1016/j.jhazmat.2008.12.120.

Jaroniec, M., 2008. Incorporation of inorganic nanoparticles into mesoporous carbons synthesized by soft templating. *The Journal of Physical Chemistry C*, 112, 11657–11660. https://doi.org/10.1021/jp803367p.

Joo, J.B., Kim, P., Kim, W., Kim, J., Yi, J., 2006. Preparation of mesoporous carbon templated by silica particles for use as a catalyst support in polymer electrolyte membrane fuel cells. *Catalysis Today*, 111, 171–175. https://doi.org/10.1016/j.cattod.2005.10.021.

Joo, S.H., Jun, S., Ryoo, R., 2001. Synthesis of ordered mesoporous carbon molecular sieves CMK-1. *Microporous and Mesoporous Materials*, 44, 153–158. https://doi.org/10.1016/S1387-1811(01)00179-2.

Karn, B., Kuiken, T., 2009. Nanotechnology and in Situ Remediation: A Review of the Benefits and Potential Risks. *Environmental Health Perspectives*, 117, 1813-1831. https://dx.doi.org/10.1289%2Fehp.0900793.

Katsoulidis, A.P., Kanatzidis, M.G., 2011. Phloroglucinol based microporous polymeric organic frameworks with −OH functional groups and high CO_2 capture capacity. *Chemistry of Materials*, 23, 1818–1824. https://doi.org/10.1021/cm103206x.

Kaveeshwar, A. R., Kumar, P. S., Revellame, E. D., Gang, D. D., Zappi, M. E., Subramaniam, R. (2018). Adsorption properties and mechanism of barium (II) and strontium (II) removal from fracking wastewater using pecan shell based activated carbon. *Journal of Cleaner Production*, 193, 1-13. https://doi.org/10.1016/j.jclepro.2018.05.041.

Kaveeshwar, A.R., Ponnusamy, S.K., Revellame, E.D., Gang, D.D., Zappi, M.E., Subramaniam, R., 2018. Pecan shell based activated carbon for removal of iron(II) from fracking wastewater: Adsorption kinetics, isotherm and thermodynamic studies. *Process Safety and Environmental Protection*, 114, 107–122. https://doi.org/10.1016/j.psep.2017.12.007.

Kazemi, P., Peydayesh, M., Bandegi, A., Mohammadi, T., Bakhtiari, O., 2014. Stability and extraction study of phenolic wastewater treatment by supported liquid membrane using tributyl phosphate and sesame oil as liquid membrane. *Chemical Engineering Research and Design*, 92, 375–383. https://doi.org/10.1016/j.cherd.2013.07.023.

Kerkhofs, S., Willhammar, T., Van Den Noortgate, H., Kirschhock, C.E., Breynaert, E., Van Tendeloo, G., et al., 2015. Self-assembly of Pluronic F127–silica spherical coreshell nanoparticles in cubic close-packed structures. *Chemistry of Materials*, 27, 5161–5169. https://doi.org/10.1021/acs.chemmater.5b01772.

Kim, C.H., Lee, D.K., Pinnavaia, T.J., 2004. Graphitic mesostructured carbon prepared from aromatic precursors. *Langmuir*, 20, 5157–5159. https://doi.org/10.1021/la049602c.

Kim, D.J., Lee, H.I., Yie, J.E., Kim, S.J., Kim, J.M., 2005. Ordered mesoporous carbons: Implication of surface chemistry, pore structure and adsorption of methyl mercaptan. *Carbon*, 43, 1868–1873. https://doi.org/10.1016/j.carbon.2005.02.035.

Kim, S.S., Karkamkar, A., Pinnavaia, T.J., Kruk, M., Jaroniec, M., 2001. Synthesis and characterization of ordered, very large pore MSU-H silicas assembled from water-soluble silicates. *Journal of Physical Chemistry B*, 105, 7663–7670. https://doi.org/10.1021/jp010773p.

Kobya, M., Demirbas, E., Senturk, E., Ince, M., 2005. Adsorption of heavy metal ions from aqueous solutions by activated carbon prepared from apricot stone. *Bioresource Technology*, 96(13), 1518–1521. https://doi.org/10.1016/j.biortech.2004.12.005.

Kong, Q., Liu, Q., Miao, M.S., Liu, Y.Z., Chen, Q.F., Zhao, C.S., 2017. Kinetic and equilibrium studies of the biosorption of sunset yellow dye by alligator weed activated carbon. *Desalination and Water Treatment*, 66, 281–290. https://doi.org/10.5004/dwt.2017.20223.

Konggidinata, M.I., 2017b. Application and Modifications of Ordered Mesoporous Carbon (OMC) for BTEX Removal: Characterization, Adsorption Mechanisms, and Kinetic Studies (Master Dissertation). University of Louisiana at Lafayette.

Konggidinata, M.I., Chao, B., Lian, Q., Subramaniam, R., Zappi, M., Gang, D.D., 2017a. Equilibrium, kinetic and thermodynamic studies for adsorption of BTEX onto Ordered Mesoporous Carbon (OMC). *Journal of Hazardous Materials*, 336, 249–259. https://doi.org/10.1016/j.jhazmat.2017.04.073.

Konicki, W., Pełech, I., Mijowska, E., Jasińska, I., 2012. Adsorption of anionic dye Direct Red 23 onto magnetic multi-walled carbon nanotubes-Fe_3C nanocomposite: Kinetics, equilibrium and thermodynamics. *Chemical Engineering Journal*, 210, 87–95. https://doi.org/10.1016/j.cej.2012.08.025.

Kono, H., 2015. Preparation and Characterization of Amphoteric Cellulose Hydrogels as Adsorbents for the Anionic Dyes in Aqueous Solutions. *Gels*, 1, 94–116. http://dx.doi.org/10.3390/gels1010094.

Körbahti, B.K., Artut, K., Geçgel, C., Özer, A., 2011. Electrochemical decolorization of textile dyes and removal of metal ions from textile dye and metal ion binary mixtures. *Chemical Engineering Journal*, 173, 677–688. https://doi.org/10.1016/j.cej.2011.02.018.

Koupaie, E.H., Moghaddam, M.R.A., Hashemi, S.H., 2011. Post-treatment of anaerobically degraded azo dye Acid Red 18 using aerobic moving bed biofilm process: Enhanced removal of aromatic amines. *Journal of Hazardous Materials*, 195, 147–154. https://doi.org/10.1016/j.jhazmat.2011.08.017.

Kresge, C.T., Leonowicz, M.E., Roth, W.J., Vartuli, J.C., Beck, J.S., 1992. Ordered mesoporous molecular sieves synthesized by a liquid-crystal template mechanism. *Nature*, 359, 710–712. http://dx.doi.org/10.1038/359710.

Ku, Y., Lee, K. C. (2000). Removal of phenols from aqueous solution by XAD-4 resin. *Journal of Hazardous Materials*, 80, 59–68. https://doi.org/10.1016/S0304-3894(00)00275-2.

Kumar, A., Kumar, S., Kumar, S., 2003. Adsorption of resorcinol and catechol on granular activated carbon: equilibrium and kinetics. *Carbon*, 41, 3015–3025. https://doi.org/10.1016/S0008-6223(03)00431-7.

Kumar, P.S., Varjani, S.J., Suganya, S., 2018. Treatment of dye wastewater using an ultrasonic aided nanoparticle stacked activated carbon: Kinetic and isotherm modelling. *Bioresource Technology*, 250, 716–722. https://doi.org/10.1016/j.biortech.2017.11.097.

Kumar, S., Zafar, M., Prajapati, J.K., Kumar, S., Kannepalli, S., 2011. Modeling studies on simultaneous adsorption of phenol and resorcinol onto granular activated carbon from

simulated aqueous solution. *Journal of Hazardous Materials*, 185, 287–294. https://doi.org/10.1016/j.jhazmat.2010.09.032.

Kurniawan, T.A., Chan, G.Y.S., Lo, W.H., Babel, S., 2006. Physico–chemical treatment techniques for wastewater laden with heavy metals. *Chemical Engineering Journal*, 118, 83–98. https://doi.org/10.1016/j.cej.2006.01.015.

Kyzas, G.Z., Kostoglou, M., Vassiliou, A.A., Lazaridis, N.K., 2011. Treatment of real effluents from dyeing reactor: Experimental and modeling approach by adsorption onto chitosan. *Chemical Engineering Journal*, 168, 577–585. https://doi.org/10.1016/j.cej.2011.01.026.

Lagergren, S., 1898. Zur theorie der sogenannten adsorption geloster stoffe. Kungliga svenska vetenskapsakademiens. *Handlingar*. 24, 1–39.

Lee, H.I., Kim, J.H., You, D.J., Lee, J.E., Kim, J.M., Ahn, W.S., et al., 2008. Rational Synthesis Pathway for Ordered Mesoporous Carbon with Controllable 30- to 100-Angstrom Pores. *Advanced Materials*, 20, 757–762. https://doi.org/10.1002/adma.200702209.

Lee, J.S., Joo, S.H., Ryoo, R., 2002. Synthesis of mesoporous silicas of controlled pore wall thickness and their replication to ordered nanoporous carbons with various pore diameters. *Journal of American Chemical Society*, 124, 1156–1157. https://doi.org/10.1021/ja012333h.

Lee, W.H., Reucroft, P.J., 1999. Vapor adsorption on coal- and wood-based chemically activated carbons: (I) Surface oxidation states and adsorption of H_2O. *Carbon*, 37(1), 7–14. https://doi.org/10.1016/S0008-6223(98)00181-X.

Lettow, J.S., Han, Y.J., Schmidt-Winkel, P., Yang, P., Zhao, D., Stucky, G.D., et al., 2000. Hexagonal to mesocellular foam phase transition in polymer-templated mesoporous silicas. *Langmuir*, 16, 8291–8295. https://doi.org/10.1021/la000660h.

Li, L., Liu, S., Zhu, T., 2010. Application of activated carbon derived from scrap tires for adsorption of Rhodamine B. *Journal of Environmental Science*, 22, 1273–1280. https://doi.org/10.1016/S1001-0742(09)60250-3.

Liang, C., Li, Z., Dai, S., 2008. Mesoporous carbon materials: synthesis and modification. *Angewandte Chemie International Edition*, 47, 3696–3717. https://doi.org/10.1002/anie.200702046.

Liao, Q., Sun, J., Gao, L., 2008. The adsorption of resorcinol from water using multi-walled carbon nanotubes. *Colloids and Surfaces A: Physicochemical and Engineering Aspects*, 312, 160–165. https://doi.org/10.1016/j.colsurfa.2007.06.045.

Lin, S.H., Juang, R.S., 2009. Adsorption of phenol and its derivatives from water using synthetic resins and low-cost natural adsorbents: a review. *Journal of Environmental Management*, 90, 1336–1349. https://doi.org/10.1016/j.jenvman.2008.09.003.

Liu, J., Guo, D., Zhou, Y., Wu, Z., Li, W., Zhao, F., Zheng, X., 2011. Identification of ancient textiles from Yingpan, Xinjiang, by multiple analytical techniques. *Journal of Archeological Science*, 38, 1763–1770. https://doi.org/10.1016/j.jas.2011.03.017.

Liu, L., Deng, Q.F., Ma, T.Y., Lin, X.Z., Hou, X.X., Liu, Y.P., et al., 2011. Ordered mesoporous carbons: citric acid-catalyzed synthesis, nitrogen doping and CO_2 capture. *Journal of Materials Chemistry*, 21, 16001–16009. https://doi.org/10.1039/C1JM12887F.

Liu, Q. S., Zheng, T., Wang, P., Jiang, J. P., Li, N., 2010. Adsorption isotherm, kinetic and mechanism studies of some substituted phenols on activated carbon fibers. *Chemical Engineering Journal*, 157, 348–356. https://doi.org/10.1016/j.cej.2009.11.013.

Lu, A.H., Li, W.C., Schmidt, W., Schüth, F., 2005. Template synthesis of large pore ordered mesoporous carbon. *Microporous and Mesoporous Materials*, 80(1-3), 117–128. https://doi.org/10.1016/j.micromeso.2004.12.007.

Madrakian, T., Afkhami, A., Ahmadi, M., Bagheri, H., 2011. Removal of some cationic dyes from aqueous solutions using magnetic-modified multi-walled carbon nanotubes. *Journal of Hazardous Materials*, 196, 109–114. https://doi.org/10.1016/j.jhazmat.2011.08.078.

Mangrulkar, P.A., Kamble, S.P., Meshram, J., Rayalu, S.S., 2008. Adsorption of phenol and o-chlorophenol by mesoporous MCM-41. *Journal of Hazardous Materials*, 160, 414–421. https://doi.org/10.1016/j.jhazmat.2008.03.013.

Mckay, G., Otterburn, M.S., Sweeney, A.G., 1980. The removal of colour from effluent using various adsorbents-III. Silica: rate processes. *Water Research*, 14, 15–20. https://doi.org/10.1016/0043-1354(80)90037-8.

Meenakshi, Maheshwari, R.C., 2006. Fluoride in drinking water and its removal. *Journal of Hazardous Materials*, 137, 456–463. https://doi.org/10.1016/j.jhazmat.2006.02.024.

Mezohegyi, G., van der Zee, F. P., Font, J., Fortuny, A., Fabregat, A., 2012. Towards advanced aqueous dye removal processes: A short review on the versatile role of activated carbon. *Journal of Environmental Management*, 102, 148–164. https://doi.org/10.1016/j.jenvman.2012.02.021.

Mohammadi, S., Kargari, A., Sanaeepur, H., Abbassian, K., Najafi, A., Mofarrah, E., 2015. Phenol removal from industrial wastewaters: a short review. *Desalination and Water Treatment*, 53, 2215–2234. https://doi.org/10.1080/19443994.2014.883327.

Mokaya, R., 1999. Improving the stability of mesoporous MCM-41 silica via thicker more highly condensed pore walls. *Journal of Physical Chemistry B*, 103, 10204–10208. https://doi.org/10.1021/jp992233m.

Mukherjee, S., Basak, B., Bhunia, B., Dey, A., Mondal, B., 2013. Potential use of polyphenol oxidases (PPO) in the bioremediation of phenolic contaminants containing industrial

wastewater. *Reviews in Environmental Science and Bio/Technology*, 12, 61–73. https://doi.org/10.1007/s11157-012-9302-y.

Mukherjee, S., Kumar, S., Misra, A.K., Fan, M., 2007. Removal of phenols from water environment by activated carbon, bagasse ash and wood charcoal. *Chemical Engineering Journal*, 129, 133–142. https://doi.org/10.1016/j.cej.2006.10.030.

Ngulube, T., Gumbo, J. R., Masindi, V., Maity, A., 2017. An update on synthetic dyes adsorption onto clay based minerals: A state-of-art review. *Journal of Environmental Management*, 191, 35–57. https://doi.org/10.1016/j.jenvman.2016.12.031.

Niazi, L., Lashanizadegan, A., Sharififard, H., 2018. Chestnut oak shells activated carbon: Preparation, characterization and application for Cr(VI) removal from dilute aqueous solutions. *Journal of Cleaner Production*, 185, 554–561. https://doi.org/10.1016/j.jclepro.2018.03.026.

Ökte, A. N., Yılmaz, Ö., 2009a. Characteristics of lanthanum loaded TiO_2-ZSM-5 photocatalysts: Decolorization and degradation processes of methyl orange. *Applied Catalysis A: General*, 354, 132–142. https://doi.org/10.1016/j.apcata.2008.11.022.

Ökte, A. N., Yılmaz, Ö., 2009b. La and Ce loaded TiO_2-ZSM-5 catalysts: Comparative characterization and photocatalytic activity investigations. *Microporous and Mesoporous Materials*, 126, 245–252. https://doi.org/10.1016/j.micromeso.2009.06.013.

Omi, F.R., Choudhury, M.R., Anwar, N., Bakr, A.R., Rahaman, M.S., 2017. Highly Conductive Ultrafiltration Membrane via Vacuum Filtration Assisted Layer-by-Layer Deposition of Functionalized Carbon Nanotubes. *Industrial and Engineering Chemistry Research*, 56, 8474–8484. https://doi.org/10.1021/acs.iecr.7b00847.

Pajootan, E., Arami, M., Mahmoodi, N.M., 2012. Binary system dye removal by electrocoagulation from synthetic and real colored wastewaters. *Journal of the Taiwan Institute of Chemical Engineers*, 43, 282–290. https://doi.org/10.1016/j.jtice.2011.10.014.

Qu, X., Brame, J., Li, Q., Alvarez, P. J. J., 2013. Nanotechnology for a Safe and Sustainable Water Supply: Enabling Integrated Water Treatment and Reuse. *Accounts of Chemical Research*, 46, 834-843. https://doi.org/10.1021/ar300029v.

Rajamanickam, D., Dhatshanamurthi, P., Shanthi, M., 2015. Preparation and characterization of SeO_2/TiO_2 composite photocatalyst with excellent performance for sunset yellow azo dye degradation under natural sunlight illumination. *Spectrochimica Acta Part A: Molecular and Biomolecular Spectroscopy*, 138, 489–498. https://doi.org/10.1016/j.saa.2014.11.070.

Rajamanickam, D., Shanthi, M., 2014. Photocatalytic degradation of an azo dye Sunset Yellow under UV-A light using TiO_2/CAC composite catalysts. *Spectrochimica Acta*

Part A: Molecular and Biomolecular Spectroscopy, 128, 100–108. https://doi.org/10.1016/j.saa.2014.02.126.

Rêgo, T., Cadaval Jr, T., Dotto, G., Pinto, L., 2013. Statistical optimization, interaction analysis and desorption studies for the azo dyes adsorption onto chitosan films. *Journal of Colloid and Interface Science*, 411, 27–33. https://doi.org/10.1016/j.jcis.2013.08.051.

Ren, H., Shou, W., Ren, C., Gang, D.D., 2016. Preparation and post-treatments of ordered mesoporous carbons (OMC) for resorcinol removal. *International Journal of Environmental Science and Technology*, 13, 1505–1514. https://doi.org/10.1007/s13762-016-0990-7.

Ryoo, R., Joo, S. H., Jun, S. (1999). Synthesis of highly ordered carbon molecular sieves via template-mediated structural transformation. *The Journal of Physical Chemistry B*, 103, 7743–7746. https://doi.org/10.1021/jp991673a.

Ryoo, R., Joo, S.H., Jun, S., 1999. Synthesis of highly ordered carbon molecular sieves via template-mediated structural transformation. *The Journal of Physical Chemistry B*, 103, 7743–7746. https://doi.org/10.1021/jp991673a.

Ryoo, R., Joo, S.H., Kruk, M., Jaroniec, M., 2001. Ordered mesoporous carbons. *Advanced Materials*, 13, 677–681. https://doi.org/10.1002/1521-4095(200105)13:9%3C677::AID-ADMA677%3E3.0.CO;2-C.

Salehi, R., Arami, M., Mahmoodi, N.M., Bahrami, H., Khorramfar, S., 2010. Novel biocompatible composite (Chitosan–zinc oxide nanoparticle): Preparation, characterization and dye adsorption properties. *Colloids and Surfaces B: Biointerfaces*, 80, 86–93. https://doi.org/10.1016/j.colsurfb.2010.05.039.

Sari, A., Tuzen, M., Citak, D., Soylak, M., 2007. Equilibrium, kinetic and thermodynamic studies of adsorption of Pb(II) from aqueous solution onto Turkish kaolinite clay. *Journal of Hazardous Materials*, 149, 283–291. https://doi.org/10.1016/j.jhazmat.2007.03.078.

Savage, N., Diallo, M. S., 2005. Nanomaterials and Water Purification: Opportunities and Challenges. *Journal of Nanoparticle Research*, 7, 331-342. https://doi.org/10.1007/s11051-005-7523-5.

Sayari, A., Liu, P., Kruk, M., Jaroniec, M., 1997. Characterization of large-pore MCM-41 molecular sieves obtained via hydrothermal restructuring. *Chemistry of Materials*, 9, 2499–2506. https://doi.org/10.1021/cm970128o.

Schmidt, R. J., 2017. Industrial catalytic processes—phenol production. *Applied Catalysis A: General*, 280, 89–103. https://doi.org/10.1016/j.apcata.2004.08.030.

Shen, W., Li, Z., Liu, Y., 2008. Surface chemical functional groups modification of porous carbon. *Recent Patents on Chemical Engineering*, 1, 27–40.

Shon, J. K., Jin, X., Choi, Y. S., Won, J. G., Hwang, Y. K., You, D. J., Li, C., Kim, J. M., 2016. Effect of acid catalysts on carbonization temperatures for ordered mesoporous carbon materials. *Carbon Letters*, 20, 66–71. http://dx.doi.org/ DOI:10.5714/CL.2016.20.066.

Shou, W., Chao, B., Ahmad, Z.U., Gang, D.D., 2016. Ordered mesoporous carbon preparation by the in situ radical polymerization of acrylamide and its application for resorcinol removal. *Journal of Applied Polymer Science*, 133, 43426–43436. https://doi.org/10.1002/app.43426.

Sivashankar, R., Sathya, A.B., Vasantharaj, K., Sivasubramanian, V., 2014. Magnetic composite an environmental super adsorbent for dye sequestration–A review. *Environmental Nanotechnology, Monitoring & Management*, 1-2, 36–49. https://doi.org/10.1016/j.enmm.2014.06.001.

Soler-Illia, GJ de AA., Louis, A., Sanchez, C. (2002) Synthesis and characterization of mesostructured titania-based materials through evaporation-induced self-assembly. *Chemistry of Materials*, 14, 750–759. https://doi.org/10.1021/cm011217a.

Soto, M. L., Moure, A., Domínguez, H., Parajó, J. C. (2011). Recovery, concentration and purification of phenolic compounds by adsorption: A review. *Journal of Food Engineering*, 105, 1–27. https://doi.org/10.1016/j.jfoodeng.2011.02.010.

Sultana, S., Choudhury, M.R., Bakr, A.R., Anwar, N., Rahaman, M.S., 2018. Effectiveness of electro-oxidation and electro-Fenton processes in removal of organic matter from high-strength brewery wastewater. *Journal of Applied Electrochemistry*, 48, 519–528. https://doi.org/10.1007/s10800-018-1185-3.

Sun, T., Feng, L., Gao, X., Jiang, L., 2005. Bioinspired Surfaces with Special Wettability. *Accounts of Chemical Research*, 38(8), 644–652. https://doi.org/10.1021/ar040224c.

Sun, X., Wang, C., Li, Y., Wang, W., Wei, J., 2015. Treatment of phenolic wastewater by combined UF and NF/RO processes. *Desalination*, 355, 68–74. https://doi.org/10.1016/j.desal.2014.10.018.

Swiatkowski, A., Pakula, M., Biniak, S., Walczyk, M., 2004. Influence of the surface chemistry of modified activated carbon on its electrochemical behaviour in the presence of lead(II) ions. *Carbon*, 42, 3057–3069. https://doi.org/10.1016/j.carbon.2004.06.043.

Tan, K.B., Vakili, M., Horri, B.A., Poh, P.E., Abdullah, A.Z., Salamatinia, B., 2015. Adsorption of dyes by nanomaterials: Recent developments and adsorption mechanisms. *Separation and Purification Technology*, 150, 229–242. https://doi.org/10.1016/j.seppur.2015.07.009.

Tang, L., Cai, Y., Yang, G., Liu, Y., Zeng, G., Zhou, Y., Li, S., Wang, J., Zhang, S., Fang, Y., He, Y., 2014a. Cobalt nanoparticles-embedded magnetic ordered mesoporous

carbon for highly effective adsorption of rhodamine B. *Applied Surface Science*, 314, 746–753. https://doi.org/10.1016/j.apsusc.2014.07.060.

Tang, L., Yang, G.D., Zeng, G.M., Cai, Y., Li, S., Zhou, Y.Y., Pang, Y., Liu, Y.Y., Zhang, Y., Luna, B., 2014b. Synergistic effect of iron doped ordered mesoporous carbon on adsorption-coupled reduction of hexavalent chromium and the relative mechanism study. *Chemical Engineering Journal*, 239, 114–122. https://doi.org/10.1016/j.cej.2013.10.104.

Thommes, M., Kaneko, K., Neimark, A.V., Olivier, J.P., Rodriguez-Reinoso, F., Rouquerol, J., et al., 2015. Physisorption of gases, with special reference to the evaluation of surface area and pore size distribution (IUPAC Technical Report). *Pure and Applied Chemistry*, 87, 1051–1069. https://doi.org/10.1515/pac-2014-1117.

Tian, G., Geng, J., Jin, Y., Wang, C., Li, S., Chen, Z., Wang, H., Zhao, Y., Li, S. (2011). Sorption of uranium(VI) using oxime-grafted ordered mesoporous carbon CMK-5. *Journal of Hazardous Materials*, 190, 442–450. https://doi.org/10.1016/j.jhazmat.2011.03.066.

Tian, G., Geng, J., Jin, Y., Wang, C., Li, S., Chen, Z., Wang, H., Zhao Y., Li, S., 2011. Sorption of uranium(VI) using oxime-grafted ordered mesoporous carbon CMK-5. *Journal of Hazardous Materials*, 190, 442–450. https://doi.org/10.1016/j.jhazmat.2011.03.066.

USEPA, 1985. Technical Support Document for Water Quality-based Toxics Control, EPA/440/485032, Washington, DC, USA: *United States Environmental Protection Agency*.

Vakili, M., Rafatullah, M., Salamatinia, B., Abdullah, A. Z., Ibrahim, M. H., Tan, K. B., Gholami, Z., Amouzgar, P., 2014. Application of chitosan and its derivatives as adsorbents for dye removal from water and wastewater: A review. *Carbohydrate Polymers*, 113, 115-130. https://doi.org/10.1016/j.carbpol.2014.07.007.

Varaprasad, K., Jayaramudu, T., Sadiku, E.R., 2017. Removal of dye by carboxymethyl cellulose, acrylamide and graphene oxide via a free radical polymerization process. *Carbohydrate Polymers*, 164, 186–194. https://doi.org/10.1016/j.carbpol.2017.01.094.

Vijayaprasath, G., Murugan, R., Palanisamy, S., Prabhu, N. M., Mahalingam, T., Hayakawa, Y., Ravi, G., 2015. Structural, optical and antibacterial activity studies of neodymium doped ZnO nanoparticles. *Journal of Materials Science: Materials in Electronics*, 26, 7564–7576. https://doi.org/10.1007/s10854-015-3393-5.

Viswanathan, N., Meenakshi, S., 2008. Enhanced fluoride sorption using La(III) incorporated carboxylated chitosan beads. *Journal of Colloid and Interface Science*, 322, 375–383. https://doi.org/10.1016/j.jcis.2008.03.007.

Walker, G.M., Weatherley, L.R., 2001. Adsorption of dyes from aqueous solution-the effect of adsorbent pore size distribution and dye aggregation. *Chemical Engineering Journal*, 83, 201–206. https://doi.org/10.1016/S1385-8947(00)00257-6.

Wang, C.J., Li, Z., Jiang, W.T., Jean, J.S., Liu, C.C., 2010. Cation exchange interaction between antibiotic ciprofloxacin and montmorillonite. *Journal of Hazardous Materials*, 183, 309–314. https://doi.org/10.1016/j.jhazmat.2010.07.025.

Wang, S., Zhu, Z. H., 2007. Effects of acidic treatment of activated carbons on dye adsorption. *Dyes and Pigments*, 75, 306–314. https://doi.org/10.1016/j.dyepig.2006.06.005.

Weber, W. J., Morris, J. C. (1964). Equilibria and capacities for adsorption on carbon. *Journal of the Sanitary Engineering Division*, 90, 79–108.

Wu, F.C., Tseng, R.L., Juang, R.S., 2009. Characteristics of Elovich equation used for the analysis of adsorption kinetics in dye-chitosan systems. *Chemical Engineering Journal*, 150, 366–373. https://doi.org/10.1016/j.cej.2009.01.014.

Xia, Y., Mokaya, R., 2007. Ordered mesoporous carbon monoliths: CVD nanocasting and hydrogen storage properties. *The Journal of Physical Chemistry C*, 111, 10035–10039. https://doi.org/10.1021/jp071936y.

Xiao, J., Peng, T., Li, R., Peng, Z., Yan, C., 2006. Preparation, phase transformation and photocatalytic activities of cerium-doped mesoporous Titania nanoparticles. *Journal of Solid State Chemistry*, 179, 1161–1170. https://doi.org/10.1016/j.jssc.2006.01.008.

Xing, Y., Chen, X., Wang, D., 2007. Electrically Regenerated Ion Exchange for Removal and Recovery of Cr(VI) from Wastewater. *Environmental Science and Technology*, 41, 1439–1443. https://doi.org/10.1021/es061499l.

Xu, J., Wu, F., Wu, H.T., Xue, B., Li, Y.X., Cao, Y., 2014. Three-dimensional ordered mesoporous carbon nitride with large mesopores: Synthesis and application towards base catalysis. *Microporous and Mesoporous Materials*, 198, 223–229. https://doi.org/10.1016/j.micromeso.2014.07.042.

Yagub, M.T., Sen, T.K., Afroze, S., Ang, H.M., 2014. Dye and its removal from aqueous solution by adsorption: A review. *Advances in Colloid and Interface Science*, 209, 172–184. https://doi.org/10.1016/j.cis.2014.04.002.

Yan, L., Chang, P.R., Zheng, P., Ma, X., 2012. Characterization of magnetic guar gum-grafted carbon nanotubes and the adsorption of the dyes. *Carbohydrate Polymers*, 87, 1919–1924. https://doi.org/10.1016/j.carbpol.2011.09.086.

Yan, L.G., Qin, L.L., Yu, H.Q., Li, S., Shan, R.R., Du, B., 2015. Adsorption of acid dyes from aqueous solution by CTMAB modified bentonite: Kinetic and isotherm modeling. *Journal of Molecular Liquids*, 211, 1074–1081. https://doi.org/10.1016/j.molliq.2015.08.032.

Yang, J., Yu, M., Chen, W., 2015. Adsorption of hexavalent chromium from aqueous solution by activated carbon prepared from longan seed: Kinetics, equilibrium and thermodynamics. *Journal of Industrial and Engineering Chemistry*, 21, 414–422. https://doi.org/10.1016/j.jiec.2014.02.054.

Yao, R., Meng, F., Zhang, L., Ma, D., Wang, M., 2009. Defluoridation of water using neodymium-modified chitosan. *Journal of Hazardous Materials*, 165, 454–460. https://doi.org/10.1016/j.jhazmat.2008.10.052.

Zhang, A., Li, Y., 2014. Removal of phenolic endocrine disrupting compounds from waste activated sludge using UV, H_2O_2, and UV/H_2O_2 oxidation processes: Effects of reaction conditions and sludge matrix. *Science of The Total Environment*, 493, 307–323. https://doi.org/10.1016/j.scitotenv.2014.05.149.

Zhang, G., Yi, L., Deng, H., Sun, P., 2014. Dyes adsorption using a synthetic carboxymethyl cellulose-acrylic acid adsorbent. *Journal of Environmental Sciences*, 26, 1203–1211. https://doi.org/10.1016/S1001-0742(13)60513-6.

Zhang, N., Lin, L.S., Gang, D., 2008. Adsorptive selenite removal from water using iron-coated GAC adsorbents. *Water Research*, 42, 3809–3816. https://doi.org/10.1016/j.watres.2008.07.025.

Zhao, D., Huo, Q., Feng, J., Chmelka, B.F., Stucky, G.D., 1998. Nonionic Triblock and Star Diblock Copolymer and Oligomeric Surfactant Syntheses of Highly Ordered, Hydrothermally Stable, Mesoporous Silica Structures. *Journal of the American Chemical Society*, 120, 6024–6036. https://doi.org/10.1021/ja974025i.

Zhuang, X., Wan, Y., Feng, C., Shen, Y., Zhao, D., 2009. Highly efficient adsorption of bulky dye molecules in wastewater on ordered mesoporous carbons. *Chemistry of Materials*, 21, 706–716. https://doi.org/10.1021/cm8028577.

Ahmad, Zaki Uddin. Bachelor of Science, Bangladesh University of Engineering and Technology (BUET), 2011; Master of Science, Bangladesh University of Engineering and Technology (BUET), 2015; Master of Science, University of Louisiana at Lafayette, Fall 2017; Doctor of Philosophy, University of Louisiana at Lafayette, Spring 2019
Major: Systems Engineering
Title of Dissertation: Synthesis and Characterization of Novel Functionalized Ordered Mesoporous Carbon (OMC) for Resorcinol and Sunset Yellow Removal
Dissertation Director: Dr. Daniel Dianchen Gang
Pages in Dissertation: 143; Words in Abstract: 179

Abstract

Phenolic compounds and their derivatives are major water pollutants because of their wide usage in industry and agriculture. The widespread application of synthetic dyes in various manufacturing processes has been found responsible for degraded water quality. Ordered Mesoporous Carbon (OMC) has attracted much attention due to its unique features, such as high BET surface area, uniform pore size, large pore volume, and high thermo-mechanical stability. The virgin OMC was modified, employing pore size modification and surface modification using boric acid, cerium(III) chloride, and neodymium(III) chloride. The modified OMCs were characterized using nitrogen adsorption-desorption isotherm, scanning electron microscopy (SEM), transmission electron microscopy (TEM), Fourier transform infrared (FT-IR) spectra, and X-ray photoelectron spectroscopy (XPS). The adsorption capacity of all modified OMCs was evaluated by conducting batch adsorption experiments. The adsorption kinetics and adsorption isotherm data were fitted with different models. The maximum adsorption capacity was calculated and compared with materials reported in the available literature. The modification of OMC with cerium(III) chloride improved the adsorption capacity by 76.8%. The modification of OMC using neodymium(III) chloride increased the adsorption capacity by 40%.

Biographical Sketch

Zaki Uddin Ahmad was born on December 16, 1987, in Dhaka, Bangladesh. He received his Bachelor of Science in Water Resources Engineering in 2011 from Bangladesh University of Engineering and Technology (BUET). He also received his Master of Science in Civil (Environmental) Engineering from Bangladesh University of Engineering and Technology (BUET) in 2015. Later on, he moved to United States in August 2015 and started pursuing his PhD in Systems Engineering (with a concentration in Civil Engineering) at the University of Louisiana at Lafayette. On his way to his PhD, he received another Master of Science in Civil (Environmental) Engineering in December 2017. He graduated with a PhD in Systems Engineering (with a concentration in Civil Engineering) in Spring 2019.